AN ABSTRACT OF THE THESIS OF

Thana Sornchamni for the degree of Master of Science in Chemical Engineering presented on November 22, 2000. Title: The Prediction of Voidage Distribution in a Non-uniform Magnetically Assisted Fluidized Bed: Theory and Experiment.

Abstract approved: _____ Goran Jovanovic _____

Previous studies in Magnetically Stabilized Fluidized Bed (MSFB) are well known for conventional two-phase, gas-solid or liquid-solid fluidization. Many researchers have investigated the fluid dynamic behavior of the MSFB, however, all of these studies are based on a uniform magnetic field that is constant throughout the bed column. Currently, there are no references in the open literature indicating either fundamental or applied research with a magnetically fluidized bed where a non-uniform magnetic field is used in a two-phase liquid-solid fluidization.

In this study, the fluid dynamic behavior of a Magnetically Assisted Fluidized Bed (MAFB) in a non-uniform magnetic field is experimentally observed. In the MAFB, a magnetic force, F_m, is created which acts on the ferromagnetic particles (20% ferrite) by varying the magnetic field intensity from the top to the bottom of the fluidization column. However, the field gradient is kept constant throughout the bed. Because of the differences in the magnetic field intensity at any location in the bed, the particle

holdup, or inversely the bed voidage, has to change to accommodate the equilibrium of forces acting on the particles (drag force, gravitational force, buoyancy force, and magnetic force).

In the laboratory experiments, performed magnetic field gradient, ($\frac{dH_z}{dz}$ = -14,663 A/m/m, -18,289 A/m/m, –20,543 A/m/m and –33,798 A/m/m) and fluid flow rate (U_0 = 0.0153 m/s, 0.0176 m/s, 0.0199 m/s and 0.0222 m/s) are varied. These experiments show that the increase in the magnetic field gradient and the magnetic field intensity results in the decrease in the height of the bed, and therefore, in the decrease of the bed voidage. The dynamic pressure drop, $\Delta P_{f(d)}$, is also experimentally measured, then converted to a corresponding voidage. The relationship between the dynamic pressure drop and the bed voidage is given by the following equation:

$$\varepsilon = 1 - \left(\frac{-\frac{\Delta P_{f(d)}}{\Delta z}}{(\rho_p - \rho_f)g + \mu_0 \chi H_z \frac{dH_z}{dz}} \right)$$

The fluid dynamic behavior of the MAFB is described by the equation of motion and the equation of continuity for both liquid and solid phases. A mathematical model is developed and used to evaluate the voidage distribution in the MAFB. The resulting expression for the voidage distribution in the MAFB is given as

$$\frac{d_p^3 \rho_f (\rho_p - \rho_f) g_z}{\mu^2} = \frac{1.75}{\varepsilon^3}\left(\frac{d_p U_0 \rho_f}{\mu}\right)^2 + \frac{150(1-\varepsilon)}{\varepsilon^3}\left(\frac{d_p U_0 \rho_f}{\mu}\right) + \frac{\mu_0 \rho_f d_p^3}{\mu^2} \chi H_z \frac{dH_z}{dz}$$

Experimentally obtained bed voidage data in both, laboratory experiments (1g) and on board of the NASA KC-135 plane (0g) fit very well the above equation which does not have any adjustable parameter.

The Prediction of Voidage Distribution in a Non-uniform Magnetically Assisted Fluidized Bed: Theory and Experiment

by

Thana Sornchamni

A THESIS

Submitted to

Oregon State University

in partial fulfillment of
the requirements for the
degree of

Master of Science

Presented November 22, 2000
Commencement June 2001

Master of Science thesis of Thana Sornchamni presented on November 22, 2000

APPROVED:

Redacted for privacy

Major Professor, representing Chemical Engineering

Redacted for privacy

Head of Department of Chemical Engineering

Redacted for privacy

Dean of Graduate School

I understand that my thesis will become part of the permanent collection of Oregon State University libraries. My signature below authorizes release of my thesis to any reader upon request.

Redacted for privacy

Thana Sornchamni, Author

TABLE OF CONTENTS

	Page
CHAPTER 1 - INTRODUCTION	1
CHAPTER 2 - THEORETICAL BACKGROUND	5
2.1 - The Mass and Momentum Conservation Equations	8
2.2 - Constitutive Relationships	9
CHAPTER 3 - EXPERIMENTAL APPARATUS AND MATERIALS	15
3.1 - Fluidization Column	15
3.2 - Magnetic Field Generator (Helmholtz Rings)	17
3.3 - Water Supply System	19
3.4 - Instrumentation	20
3.5 - The Ferromagnetic Particles	23
3.6 - Fluidization Column, Magnetic Field Generator, and Rotameter (Experiments on Board The NASA KC-135 plane)	25
3.7 – The NASA KC-135 Plane	28
CHAPTER 4 - VOIDAGE DISTRIBUTION MODEL AND EXPERIMENTAL METHOD	30
4.1 - Voidage Distribution Model	30
4.2 - Experimental Method	36

TABLE OF CONTENTS (Continued)

	Page
CHAPTER 5 - EXPERIMENTAL RESULTS AND DISSCUSSION	38
5.1 - The Effect of Magnetic Force on The Magnetically Assisted Fluidized Bed (MAFB)	38
5.2 - The Voidage Distribution Model and Experimental Results	42
5.3- Experiments on Board The NASA KC-135 Plane	56
5.4 - Discussion	62
CHAPTER 6 - CONCLUSION AND RECOMMENDATIONS	64
6.1 - Conclusion	64
6.2 - Recommendations	66
BIBLIOGRAPHY	68
APPENDICES	71

LIST OF FIGURES

Figure		Page
2-1	A Balance of forces acting on a fluidized bed particles in a conventional fluidized bed (liquid media-solid particles)	6
2-2	A Balance of forces acting on a fluidized particle containing ferromagnetic material in a) magnetically assisted fluidized bed in microgravity, and b) in a fluidized bed in microgravity in the absence of the magnetic field	7
2-3	Two-dimensional fluidization column	13
3-1	Experimental apparatus used in laboratory experiments	16
3-2	A single copper wire and the magnetic induction	20
3-3	The front panel of the Gaussmeter	21
3-4	Configuration and dimension of an axial probe	22
3-5	The ferromagnetic particle	23
3-6	The Magnetically Assisted Fluidized Bed (Experiment on board the NASA KC-135 plane)	27
3-7	The magnetic coils on the magnetically assisted fluidized bed (experiments on the NASA KC-135)	28
3-8	The Trajectory of The Boeing NASA KC-135	29
5-1	Bed expansion as a function of superficial fluid velocity for the different magnetic field intensity and field gradients	40
5-2	Bed expansion as a function of the magnetic field gradients field gradient for different superficial fluid velocities	41
5-3	The voidage distribution of particle A in the MAFB ($\frac{dH}{dz}$ = -14,663 A/m/m, U_0 = 0.0176 m/s, and the bed height = 0.25 m)	44

LIST OF FIGURES (Continued)

Figure		Page
5-4	The voidage distribution of particle A in the MAFB ($\frac{dH}{dz}$ = -18,289 A/m/m, U_0 = 0.0176 m/s, and the bed height = 0.235 m)	44
5-5	The voidage distribution of particle A in the MAFB ($\frac{dH}{dz}$ = -20,543 A/m/m, U_0 = 0.0176 m/s, and the bed height = 0.220 m)	45
5-6	The voidage distribution of particle A in the MAFB ($\frac{dH}{dz}$ = -14,663 A/m/m, U_0 = 0.0222 m/s, and the bed height = 0.220 m)	45
5-7	The voidage distribution of particle A in the MAFB ($\frac{dH}{dz}$ = -18,289 A/m/m, U_0 = 0.0222 m/s, and the bed height = 0.205 m)	46
5-8	The voidage distribution of particle A in the MAFB ($\frac{dH}{dz}$ = -20,543 A/m/m, U_0 = 0.0222 m/s, and the bed height = 0.190 m)	46
5-9	The voidage distribution of particle A in the MAFB ($\frac{dH}{dz}$ = -14,663 A/m/m, U_0 = 0.0176 m/s, and the bed height = 0.130 m)	47
5-10	The voidage distribution of particle A in the MAFB ($\frac{dH}{dz}$ = -18,289 A/m/m, U_0 = 0.0176 m/s, and the bed height = 0.120 m)	48

LIST OF FIGURES (Continued)

Figure		Page
5-11	The voidage distribution of particle A in the MAFB ($\frac{dH}{dz}$ = -20,543 A/m/m, U_0 = 0.0153 m/s, and the bed height = 0.095 m)	48
5-12	The voidage distribution of particle A in the MAFB ($\frac{dH}{dz}$ = -20,543 A/m/m, U_0 = 0.0176 m/s, and the bed height = 0.110 m)	48
5-13	The voidage distribution of particle A in the MAFB ($\frac{dH}{dz}$ = -20,543 A/m/m, U_0 = 0.0199 m/s, and the bed height = 0.130 m)	49
5-14	The voidage distribution of particle A in the MAFB ($\frac{dH}{dz}$ = -33,798 A/m/m, U_0 = 0.0153 m/s, and the bed height = 0.085 m)	49
5-15	The voidage distribution of particle A in the MAFB ($\frac{dH}{dz}$ = -33,798 A/m/m, U_0 = 0.0176 m/s, and the bed height = 0.095 m)	50
5-16	The voidage distribution of particle A in the MAFB ($\frac{dH}{dz}$ = -33,798 A/m/m, U_0 = 0.0199 m/s, and the bed height = 0.115 m)	50
5-17	The voidage distribution of particle B in the MAFB ($\frac{dH}{dz}$ = -14,663 A/m/m, U_0 = 0.0222 m/s, and the bed height = 0.187 m)	51

LIST OF FIGURES (Continued)

Figure		Page
5-18	The voidage distribution of particle B in the MAFB ($\frac{dH}{dz}$ = -18,289 A/m/m, U_0 = 0.0222 m/s, and the bed height = 0.178 m)	51
5-19	The voidage distribution of particle B in the MAFB ($\frac{dH}{dz}$ = -20,543 A/m/m, U_0 = 0.0222 m/s, and the bed height = 0.165 m)	52
5-20	The voidage distribution of particle B in the MAFB ($\frac{dH}{dz}$ = -14,663 A/m/m, U_0 = 0.0222 m/s, and the bed height = 0.240 m)	52
5-21	The voidage distribution of particle B in the MAFB ($\frac{dH}{dz}$ = -18,289 A/m/m, U_0 = 0.0222 m/s, and the bed height = 0.230 m)	53
5-22	The voidage distribution of particle B in the MAFB ($\frac{dH}{dz}$ = -20,543 A/m/m, U_0 = 0.0222 m/s, and the bed height = 0.217 m)	53

LIST OF FIGURES (Continued)

Figure		Page
5-23	The comparison of the calculated mass obtained from the model and experiment with the exact mass	54
5-24	The prediction of the voidage distribution of particle C in the zero-g condition ($U_{0(bottom)}$ = 0.0000 m/s, d_p = 0.0024 m and h = 0.16 m)	57
5-25	The prediction of the voidage distribution of particle C in the zero-g condition ($U_{0(bottom)}$ = 0.0010 m/s, d_p = 0.0024 m and h = 0.16 m)	58
5-26	The prediction of the voidage distribution of particle C in the zero-g condition ($U_{0(bottom)}$ = 0.0055m/s, d_p = 0.0024 m and h = 0.202 m)	58
5-27	The prediction of the voidage distribution of particle C in the zero-g condition ($U_{0(bottom)}$ = 0.0076m/s, d_p = 0.0024 m and h = 0.197 m)	59
5-28	The prediction of the voidage distribution of particle C in the zero-g condition($U_{0(bottom)}$ = 0.0110 m/s, d_p = 0.0024 m and h = 0.189 m)	59
5-29	The prediction of the voidage distribution of particle D in the zero-g condition ($U_{0(bottom)}$ = 0.0000 m/s, d_p = 0.0015 m and h = 0.180 m)	60
5-30	The prediction of the voidage distribution of particle D in the zero-g condition($U_{0(bottom)}$ = 0.0010 m/s, d_p = 0.0015 m and h = 0.208 m)	60
5-31	The comparison between the height of the bed obtained from model and the height of the bed obtained from experimental observations	61

LIST OF FIGURES (Continued)

Figure		Page
5-32	The comparison between the predicted mass and the exact mass of particles in the bed	61

LIST OF TABLES

Table		Page
1-1	The summary of the studies of magnetically stabilized fluidized bed	2
3-1	The ferromagnetic particle properties	25
5-1	Bed height at different fluid flow rates and different magnetic field gradients for particle A and B	39

LIST OF APPENDICES

Appendix		Page
A	The Derivation of The Mass and Momentum Conservation Equations For The MAFB	72
	A.1 The Mass Conservation Equations	72
	A.1.1 The Mass Conservation Equation for The Fluid Phase	72
	A.1.2 The Mass Conservation Equation for The Particle Phase	73
	A.2 The Momentum Conservation Equations	74
	A.2.1 The Momentum Conservation Equation for The Fluid Phase	74
	A.2.2 The Momentum Conservation Equation for The Particle Phase	78
B	The Production of Ferromagnetic Particles	79
C	Properties of Materials	81
D	Calibration Curves	83
E	Magnetic Field Intensities	85
F	Magnetic Susceptibility Measurement	90
G.	Dynamic Pressure Drop and The Voidage Distribution	92

LIST OF APPENDIX FIGURES

Figure		Page
A-1	A stationary volume element $\Delta x\Delta y\Delta z$ through which a fluid and particles are flowing	72
A-2	A stationary volume element $\Delta x\Delta y\Delta z$ in which the x-momentum component is transported through the surface	74
B-1	The particle production schematic diagram	80
D-1	Flow rotameter calibration curve used in laboratory experiments	83
D-2	Flow rotameter calibration curve used on board the NASA KC-135 plane	84
D-3	Rheostat resistance calibration curve	84
E-1	The magnetic field intensity in the bed used for the laboratory experiments (voltage setting on the power supply = 1.0 volt)	85
E-2	The magnetic field intensity in the bed used for the laboratory experiments (voltage setting on the power supply = 2.0 volts)	86
E-3	The magnetic field intensity in the bed used for the laboratory experiments (voltage setting on the power supply = 3.0 volts)	87
E-4	The magnetic field intensity in the bed used for the laboratory experiments (voltage setting on the power supply = 3.5 volts)	88
E-5	The magnetic field intensity used in the experiments on board the NASA KC-135 (voltage setting on the power supply =1.0 volt)	89
F-1	The magnetic field intensity used for measuring magnetic susceptibility	90

LIST OF APPENDIX TABLES

Table		Page
C-1	The properties of sodium alginate powder	81
C-2	The compositions and properties of ferromagnetic powder	81
C-3	The physical and chemical properties of microsphere balloons	82
F-1	The calculation of magnetic susceptibility of ferromagnetic particle	91
G-1	Dynamic Pressure Drop, $\Delta P_{f(d)}$, for particle A at U_0 = 1.76 cm/s, $\frac{dH}{dz}$ = -14,663 A/m/m, hin = 13.5 cm	92
G-2	Dynamic Pressure Drop, $\Delta P_{f(d)}$, for particle A at U_0 = 1.76 cm/s, $\frac{dH}{dz}$ = -18,289 A/m/m, hin = 13.5 cm	94
G-3	Dynamic Pressure Drop, $\Delta P_{f(d)}$, for particle A at U_0 = 1.76 cm/s, $\frac{dH}{dz}$ = -20,543 A/m/m, hin = 13.5 cm	95
G-4	Dynamic Pressure Drop, $\Delta P_{f(d)}$, for particle A at U_0 = 2.22 cm/s, $\frac{dH}{dz}$ = -14,663 A/m/m, hin = 9.5 cm	96
G-5	Dynamic Pressure Drop, $\Delta P_{f(d)}$, for particle A at U_0 = 2.22 cm/s, $\frac{dH}{dz}$ = -18,289 A/m/m, hin = 9.5 cm	97
G-6	Dynamic Pressure Drop, $\Delta P_{f(d)}$, for particle A at U_0 = 2.22 cm/s, $\frac{dH}{dz}$ = -20,543 A/m/m, hin = 9.5 cm	98
G-7	Dynamic Pressure Drop, $\Delta P_{f(d)}$, for particle A at U_0 = 1.76 cm/s, $\frac{dH}{dz}$ = -14,663 A/m/m, hin = 6.5 cm	99

LIST OF APPENDIX TABLES (Continued)

Table		Page
G-8	Dynamic Pressure Drop, $\Delta P_{f(d)}$, for particle A at U_0 = 1.76 cm/s, $\frac{dH}{dz}$ = -18,289 A/m/m, hin = 6.5 cm	100
G-9	Dynamic Pressure Drop, $\Delta P_{f(d)}$, for particle A at U_0 = 1.53 cm/s, $\frac{dH}{dz}$ = -20,543 A/m/m, hin = 6.5 cm	101
G-10	Dynamic Pressure Drop, $\Delta P_{f(d)}$, for particle A at U_0 = 1.76 cm/s, $\frac{dH}{dz}$ = -20,543 A/m/m, hin = 6.5 cm	102
G-11	Dynamic Pressure Drop, $\Delta P_{f(d)}$, for particle A at U_0 = 1.99 cm/s, $\frac{dH}{dz}$ = -20,543 A/m/m, hin = 6.5 cm	103
G-12	Dynamic Pressure Drop, $\Delta P_{f(d)}$, for particle A at U_0 = 1.53 cm/s, $\frac{dH}{dz}$ = -33,798 A/m/m, hin = 6.5 cm	104
G-13	Dynamic Pressure Drop, $\Delta P_{f(d)}$, for particle A at U_0 = 1.53 cm/s, $\frac{dH}{dz}$ = -33,798 A/m/m, hin = 6.5 cm	105
G-14	Dynamic Pressure Drop, $\Delta P_{f(d)}$, for particle A at U_0 = 1.99 cm/s, $\frac{dH}{dz}$ = -33,798 A/m/m, hin = 6.5 cm	106
G-15	Dynamic Pressure Drop, $\Delta P_{f(d)}$, for particle B at U_0 = 2.22 cm/s, $\frac{dH}{dz}$ = -14,663 A/m/m, hin = 13.5 cm	107
G-16	Dynamic Pressure Drop, $\Delta P_{f(d)}$, for particle B at U_0 = 2.22 cm/s, $\frac{dH}{dz}$ = -18,289A/m/m, hin = 13.5 cm	108

LIST OF APPENDIX TABLES (Continued)

Table		Page
G-17	Dynamic Pressure Drop, $\Delta P_{f(d)}$, for particle B at U_0 = 2.22 cm/s, $\frac{dH}{dz}$ = -20,543 A/m/m, hin = 13.5 cm	109
G-18	Dynamic Pressure Drop, $\Delta P_{f(d)}$, for particle B at U_0 = 2.22 cm/s, $\frac{dH}{dz}$ = -14,663 A/m/m, hin = 17.0 cm	110
G-19	Dynamic Pressure Drop, $\Delta P_{f(d)}$, for particle B at U_0 = 2.22 cm/s, $\frac{dH}{dz}$ = -18,289 A/m/m, hin = 17.0 cm	111
G-20	Dynamic Pressure Drop, $\Delta P_{f(d)}$, for particle B at U_0 = 2.22 cm/s, $\frac{dH}{dz}$ = -20,543 A/m/m, hin = 17.0 cm	112

NOMENCLATURE

a	Radius of a single copper ring	[mm]
$\boldsymbol{B}$	Magnetic flux density	[Wb/m^2, Tesla]
c	Cohesion constant	[N/m^2]
C	A virtual mass coefficient defined in equation (2-5)	[/]
d_p	Average particle diameter	[m]
D	Thickness of two-dimensional bed	[m]
E	Elastic coefficient of the fluidized bed	[N/m^2]
$\boldsymbol{F_I}$, $\boldsymbol{F_d}$	Interface interaction force between fluid and particle	[N/m^3]
$\boldsymbol{F_b}$	Buoyancy force exerted on the particle	[N/m^3]
$\boldsymbol{F_g}$	Gravitational force exerted on the particle	[N/m^3]
$\boldsymbol{F_m}$	Magnetic force exerted on the particle	[N/m^3]
$\boldsymbol{g}$	Gravitational acceleration	[m/s^2]
h	Height of the bed	[m]
h_{in}	Initial height of the bed	[m]
$\boldsymbol{H}$	Magnetic field intensity	[A/m]
H_r	The magnitude of magnetic field intensity in r direction	[A/m]
H_z	The magnitude of magnetic field intensity in z direction	[A/m]
H_θ	The magnitude of magnetic field intensity in θ direction	[A/m]
I	Electric current intensity	[A]
L	Overall bed height	[m]

$\boldsymbol{M_b}$	Magnetization of bed medium	[A/m]
M_p	Magnetization of the particle	[A/m]
ΔP	Pressure drop between any two given points across bed	[Pa]
P_f	Total fluid pressure	[N/m^2]
P_p	Effective pressure in particle phase	[N/m^2]
t	Time	[s]
U	Velocity of fluid phase	[m/s]
U_0	Superficial fluid velocity	[m/s]
u_x, u_y, u_z	Interstitial fluid velocity in x, y and z components	[m/s]
u_{mf}	Minimum fluidizing velocity	[m/s]
V	Velocity of particle phase	[m/s]
v_x, v_y, v_z	Interstitial fluid velocity in x, y and z components	[m/s]
$\boldsymbol{V_p}$	Volume of the particle	[m^3]
x, y, z	Cartesian coordinate	

GREEK SYMBOLS

ρ_f	Fluid density	[kg/m^3]
ρ_p	Particle density	[kg/m^3]
ε	Void fraction of bed	[/]

τ_f	Fluid stress tensor	[N/m^2]
τ_p	Particle stress tensor	[N/m^2]
μ	Magnetic permeability of the particle	[kg m/A^{2}s^2]
μ_0	Magnetic permeability of free space ($4\pi \times 10^{-7}$)	[kg m/A^{2}s^2]
μ_b	Magnetic permeability of the bed mixture	[kg m/A^{2}s^2]
μ_f	Viscosity of the fluid phase,	[N s/m^2]
χ	Particle magnetic susceptibility	[/]
β	The friction coefficient defined in equation (2-5)	[/]
ψ	Constant defined in equation (2-9)	[/]
α	Constant defined in equation (4-17)	[/]
γ	Constant defined in equation (4-17)	[/]
λ	Constant defined in equation (4-17)	[m^2/A^2]
π	Constant defined in equation (4-17)	[/]
Φ	Angle of internal friction	[degree]
$K(v)$	Complete elliptic integral of the first kind	[/]
$E(v)$	Complete elliptic integral of the second kind	[/]

THE PREDICTION OF VOIDAGE DISTRIBUTION IN A NON-UNIFORM MAGNETICALLY ASSISTED FLUIDIZED BED: THEORY AND EXPERIMENT

CHAPTER 1
INTRODUCTION

The Magnetically Stabilized Fluidized Bed (MSFB) is one of the most recent and novel chemical engineering developments in the area of fluid-solid contacting operation. It combines some of the best characteristics of fluidized beds, for instance, low pressure drop and the ability to transport solid throughout the system, with the excellent efficiency of the fixed bed in heat transfer, mass transfer, and chemical conversion. Numerous studies have focused on the fluid dynamic characteristics of the MSFB in a **uniform** magnetic field. Rosensweig (1979), Rosensweig *et al.* (1983), and Conan J. Fee (1996) proposed a mathematical model to predict the stability of the MSFB in a uniform magnetic field. Hristov (1996) also studied the effect of field line orientation on the stability of a bed of ferromagnetic particles. In addition, Arnaldos *et al.* (1985) and Wu *et al.* (1997) studied the MSFB containing a mixture of magnetic and non-magnetic particles. Table 1-1 summarizes the most relevant studies of the MSFB.

In our study, the feasibility of using the Magnetically Assisted Fluidized Bed (MAFB) in the microgravity environment is considered. In the absence of gravity, the gravitational force must be substituted with some other force to restore the fluidization conditions. To accomplish this task, the magnetic field inside the fluidization column

Table 1-1 The Summary of The Studies of Magnetically Stabilized Fluidized Bed

Author	Particles	Density (kg/m^3)	Size (μ m)	Fluidization System	Type of Magnetic Field	Type of study
Wu W.Y. *et al.* (1997)	a) Iron b) Copper	7,831 8,920	1,416 935	Gas-Solid	Uniform	Hydrodynamic Characteristics of Magnetic and Non-magnetic Particles
Conan J Fee (1996)	a) Poly-acrylamide-Magnetic (PAM) b) Calcium Alginate-Magnetic (CAM)	1,800 1,200	- -	Liquid-Solid	Uniform	The Stability of The Liquid-Fluidized Magnetically Stabilized Fluidized Bed
Jordan Y. Hristov (1996)	a) Magnetite b) Iron Powder c) Fe Catalyst	5,200 7,800 -	100-400 100-200 200-315	Gas-Solid	Uniform	The Effect of Field Line Orientation on Bed Stability
Qingshan Zhu Hongzhong Li (1995)	a) Reduced iron powder (Fe) b) α-FeO (OH) c) SiO_2	7,810 3,290 2,490	12.92 7.02 13.56	Gas-Solid	Uniform	Study On Magnetic Fluidization Behavior of Group C Powders
S.C. Saxena S. Shrivastava (1991)	a) Steal Shots	7,029	262 624 1,491	Gas-Solid	Uniform	Hydrodynamic Investigation of The MSFB
J.H Siegell (1987)	a) Composite of Non-Magnetic with Stainless Steel b) Stainless Steel	2,700 & 1,900 7,750	- - -	Liquid-Solid	Uniform	Liquid-Fluidized Magnetically Stabilized Beds
J. Arnaldos *et al.* (1985)	a) Steel b) Nickel c) Copper d) Silica	7,500 5,870 8,890 2,670	350-420 177-400 350-420 630-890	Gas-Solid	Uniform	The Stability of The Mixture of Magnetic and Non-magnetic Particles
R.E. Rosensweig *et al.* (1983)	a) Ceramic Ferrite	1,880	-	Gas-Solid	Uniform	The Mechanics of The MSFB
R.E. Rosensweig (1979)	-	-	-	Gas-Solid	Uniform	The Stability of The MSFB

has to be changed from a uniform to a **non-uniform** magnetic field. The magnetic field gradient creates a magnetic force on ferromagnetic particles, replacing the gravitational force, and hence, the fluidization conditions can be restored.

In the MAFB fluidization, forces acting on the particles are composed of the drag force, the gravitational force, the magnetic force, and the buoyancy force. These forces must be in balance to satisfy the fluidization conditions. The gravitational force and the buoyancy force are dependent on the density and the volume of fluidized particles. The drag force is a function of the velocity and the viscosity of fluid, as well as, the diameter of particles and bed voidage. The magnetic force is not only dependent on the magnetic field gradient, but also on the magnetic field intensity and on the magnetic susceptibility of particles. In the experimental operations used in this study, the magnetic field is designed to have a stronger field intensity at the bottom of the bed, and decreases gradually-linearly toward the top of the bed. This change in the magnetic field strength along the fluidization column varies the magnitude of the magnetic force from the bottom to the top of the column. As a result, the particle holdup at any location varies along the column to reflect the equilibrium of the forces.

The magnetic forces in MSFB and MAFB are quite different. In MSFB, the magnetic field intensity in the column is uniform, and the magnetic force that appears in this bed is the only magnetic force between the particles. On the other hand, in MAFB, the magnetic field intensity in the fluidization column varies from the bottom to the top of the bed. Therefore, there are two types of magnetic forces acting on

fluidized particles containing ferromagnetic powder: the magnetic force between particles (as found in MSFB), and the magnetic body force due to the magnetic field gradient.

The main goal of the present work is to demonstrate the effect of the magnetic body force on the fluidized particles and to study the voidage distribution in both 1 g and 0 g experimental conditions. To accomplish this goal, the following objectives have to be realized:

1. design and construct the magnetically assisted fluidized bed with a constant (variable) magnetic field gradient,
2. produce ferromagnetic particles suitable for MAFB demonstration application,
3. measure the variation of the bed porosity at different experimental conditions,
4. develop a mathematical model which can predict the voidage distribution as a function of magnetic field, particle properties, fluid properties, and flow conditions.

The results of the modeling effort will be compared to experimental results.

CHAPTER 2
THEORETICAL BACKGROUND

Fluidization is the process in which a bed of solid particles is transformed into a fluid-like state by suspension in a gas or liquid. When a fluid is passed through a bed of particles at a low flow rate, the fluid will move through the void spaces between particles without affecting the structure of the bed (fixed bed). If the fluid flow increases, the particles will start moving apart with a few vibrations and the height of the bed will increase (expanded bed). At an even higher velocity, a point is reached where the friction forces between the particles and fluid counterbalance the weight of all particles in the bed. This point is referred to as an incipient fluidization (Kunii and Levenspiel, 1991).

Liquid-solid fluidization in the MAFB has limited importance from an industrial point of view. A number of studies and research projects (Burns and Graves (1985,1986), Terranova and Burns (1990), and J.H Siegell (1987)) have been done to improve fluidization operation in various industrial applications. However, no study of liquid-solid fluidization has ever been done in microgravity or variable gravity conditions (Space Station, Moon or Mars). The possibilities for the development of fluidized bed applications in space may include resource recovery (Jovanovic *et al.*, 1999), biochemical reaction processes, and energy conversion. This study, therefore, focuses on: a) liquid-solid fluidization in the MAFB with constant gradient magnetic field, and b) the feasibility of fluidization operation in the absence of the gravitational field. The bed voidage, which is one of the most important fluid dynamic parameters

for predicting performance of the fluidized bed reactor, is the focal point of the experimental and modeling work.

In a conventional fluidized bed, the fluidization conditions result from the interaction of forces acting on fluidized particles. This can be illustrated through a balance of three characteristic forces, the gravitational force, F_g, the buoyancy force, F_b, and the drag force, F_d, as shown in Figure 2-1

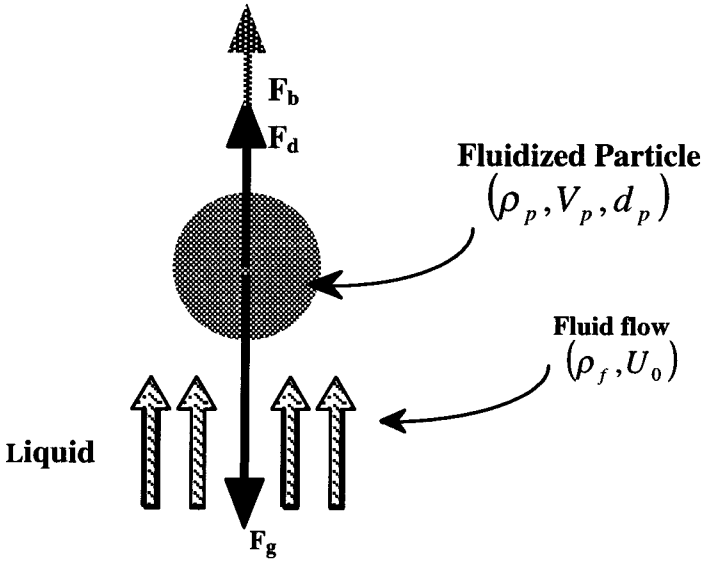

Figure 2-1: A balance of forces acting on a fluidized bed particle in a conventional fluidized bed (liquid media-solid particles)

The equilibrium of forces in Figure 2-1 represents the fluidization condition in the region that is far enough from the distributor plate. At the distributor plate, the water jets will transfer their momentum to the particles, which is eventually distributed throughout the fluidized bed.

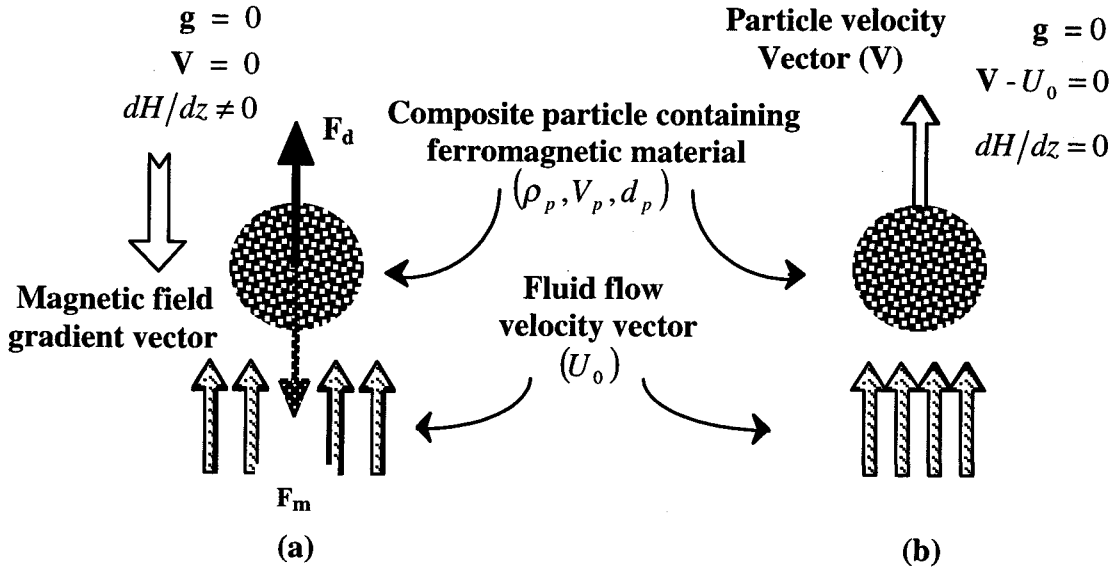

Figure 2-2: A balance of forces acting on a fluidized particle containing ferromagnetic material in, a) magnetically assisted fluidized bed in microgravity, and b) in a fluidized bed in microgravity in the absence of the magnetic field

However, under microgravity conditions where the gravitational force is no longer significant, the drag force still acts on the fluidized particle as shown in Figure 2-2b. It is obvious that the balance of forces no longer exists, and the particles in the fluidized bed reactor will immediately be swept away in the direction of the fluid flow. Fluidization conditions can be restored by introducing an additional force, such as a magnetic force, F_m, to restore the balance of forces on the fluidized particle. The magnetic force acting on the particles can be created simply by placing the particles into a **non-uniform** magnetic field, as shown in Figure 2-2a.

The motion of fluid and particles in the bed can be described by four fundamental equations, namely, the equations of continuity and the equations of motion. These equations describe the motion of the fluid and particles at each point in the column. The fluidized bed is regarded as a two continuous phase flow system. The fluid phase and particle phase are penetrating and interacting with each other. The point mechanical variables, such as the fluid velocity, pressure, and stress components, are interpreted as local average values over a region which is large compared to the particle spacing, but remains small compared to the scale of macroscopic variation from point to point in the system. Anderson and Jackson (1967) are the first researchers to develop the equations of continuity and the equations of motion for a system of fluidized particles. The development of these equations is provided in Appendix A.

2.1 The Mass and Momentum Conservation Equations

The mass conservation equations:

Fluid phase:
$$\frac{\partial \varepsilon}{\partial t} + \nabla \cdot \varepsilon \mathbf{U} = 0 \tag{2-1}$$

Particle phase:
$$\frac{\partial (1-\varepsilon)}{\partial t} + \nabla \cdot (1-\varepsilon)\mathbf{V} = 0 \tag{2-2}$$

The momentum conservation equations:

Fluid phase:
$$\rho_f \varepsilon \left(\frac{\partial \mathbf{U}}{\partial t} + (\mathbf{U} \cdot \nabla)\mathbf{U} \right) = -\varepsilon \nabla P_f - \varepsilon \nabla \cdot \tau_f + \rho_f \varepsilon \mathbf{g} - \varepsilon \boldsymbol{F_1} \tag{2-3}$$

Particle phase: $$\rho_p(1-\varepsilon)\left(\frac{\partial \mathbf{V}}{\partial t}+(\mathbf{V}\cdot\nabla)\mathbf{V}\right)=-(1-\varepsilon)\nabla P_f-(1-\varepsilon)\nabla P_p-(1-\varepsilon)\nabla\cdot\tau_p$$

$$+\rho_p(1-\varepsilon)\varepsilon\mathbf{g}+\varepsilon\boldsymbol{F_I}+\boldsymbol{F_m} \qquad (2\text{-}4)$$

Obviously, the momentum conservation equation for the particle phase is augmented with the magnetic force, $\boldsymbol{F_m}$, which depends on the magnetic field intensity, the magnetization of the particles, and the magnetic field gradient. These sets of the equations cannot be solved unless the expressions for $\boldsymbol{F_I}, \nabla P_P, \nabla\tau_P$ and $\boldsymbol{F_m}$ in terms of the fluid flow and magnetic properties are defined. With the magnetic term coupling in the momentum conservation equation for the particle phase, the magnetic field equations will be reviewed, and then applied in the modeling process.

2.2 Constitutive Relationships

2.2.1 The interaction force between fluid and particles, $\boldsymbol{F_I}$

The main contributors to the interaction between fluid and particles are the buoyancy force, the drag force, and the virtual mass force. The virtual mass force is due to acceleration of the relative velocity (**U-V**) and it relates to the force required to accelerate the surrounding fluid (Crowe *et al.*, 1998). The buoyancy reaction of fluid on the particle is already included in the first term of equation (2-4), $(1-\varepsilon)\nabla P_f$. The expression for the drag force and the virtual mass force, $\boldsymbol{F_I}$, is given by Jackson (1967) as the following:

$$\boldsymbol{F_I} = \beta(\varepsilon)(\mathbf{U}-\mathbf{V}) + \frac{(1-\varepsilon)}{\varepsilon} C(\varepsilon)\rho_f \frac{d(\mathbf{U}-\mathbf{V})}{dt} \tag{2-5}$$

The drag force is assumed to act in the direction of the relative velocity, and depends on the void fraction and on the relative velocity of the two phases. The drag force is proportional to the magnitude of **U-V** and the particle to fluid drag coefficient, β, is assumed to be dependent on the voidage. The form of the coefficient β, for flow through a bed of particles, can be presented as,

$$\beta(\varepsilon) = \frac{150(1-\varepsilon)^2 \mu_f}{d_p^2 \varepsilon^2} + \frac{1.75(1-\varepsilon) U_0 \rho_f}{d_p \varepsilon^2} \tag{2-6}$$

Gidaspow (1994) suggests that Equation (2-6) is valid for fluidized states where $\varepsilon \leq 0.8$. Equation (2-6) is actually an expression proposed by Ergun (1952). Ergun cleverly combined the Kozeny-Carman equation for flow in the viscous regime and the Burke-Plummer equation for the turbulent regime. The characteristic Reynolds number, Re_p, is defined as

$$\mathrm{Re}_p = \frac{d_p U_0 \rho_f}{\mu_f} \tag{2-7}$$

When $\mathrm{Re}_P \langle 20$, the viscous loss term dominates and can be used alone with negligible error. On the other hand, when $\mathrm{Re}_p \rangle 1000$, only the turbulent loss term is needed. The virtual mass coefficient, C, is suggested to be equal to 0.5 for an isolated spherical particle (R.Jackson, 1985).

2.2.2 The magnetic force on the ferromagnetic particles, F_m

The magnetic force is computed with the assumption that the fluidization particles contain a soft ferromagnetic material. The magnetization of the fluidized bed as a whole, $\boldsymbol{M_b}$, is assumed to be collinear with the magnetic field intensity, $\boldsymbol{H}$. Cowley and Rosensweig (1967) define the magnetic body force acting on a fluidized bed in a non-uniform magnetic field as follows:

$$\mathbf{F_m} = \mu_0 M_b \nabla H \tag{2-8}$$

2.2.3 The particle pressure and the particle stress tensor, ∇P_p and τ_p

The effect of interparticle forces, Van der Waals and magnetic interparticle forces, on the fluidized bed are mentioned in many articles. The experimental series named "The Effect of Interparticle Forces on The Stability of Gas-Fluidized Beds"by Rietema *et al.* (1977, 1990 and 1993) demonstrated that the Van der Waals interparticle force has been taken into account as the particle pressure and the particle stress tensor in the momentum conservation equation. In the experiment by Rietema and Muster (1977), a finely dispersed solid was fluidized in a specially designed bed (two dimensions with 10×4 cm horizontal dimensions). The gas flow rate was increased to the condition where the bed was expanded but gas bubbles did not appear. It was shown that the bed could be tilted up to a certain angle without the powder sliding, the surface remaining perpendicular to the direction of flow.

Rosensweig *et al.* (1983) also suggested that the magnetic force between the particles has an effect on the magnetically stabilized fluidized bed. Rosensweig claimed that magnetized particles in MSFB are in close contact with the neighboring particles. Then, the network of contacting particles forms a "magnetic gel" having a measurable yield stress. The yield stress was measured in the MSFB by noting the force required to withdraw a vertical flat plate having surfaces roughened with glued-on bed particles. The experiments have shown that the yield stress becomes higher with increased applied magnetic field intensity, due to magnetization and mutual attraction of particles. In conclusion, the magnetic force between particles can create a mechanical structure that has a certain elasticity. This phenomenon has to be included in the equation of motion in terms of the particle pressure and the particle stress tensor.

Rietema and Mutsers (1977) also suggested a form of the equation of motion for a gas-solid system, considering only the vertical components of velocity. Uniform conditions in the horizontal direction were assumed. Rietema and Mutsers defined the particle pressure and particle stress tensor (z -direction) as following:

If x is the direction perpendicular to the front-face (width by height) of the fluidization column and y is the direction parallel to the front-face (see Figure 2-3), $\tau_{p,yz}$ and $\tau_{p,xz}$ are defined as

$$\frac{\partial \tau_{p,yz}}{\partial z} = 0 \quad \text{and} \quad \frac{\partial \tau_{p,xz}}{\partial z} = 2\psi \frac{c\cos\Phi}{D(1+\sin\Phi)} \tag{2-9}$$

where c is the cohesion constant, Φ is the angle of internal friction, D is the thickness of two-dimensional bed, and the value of ψ is between –1 and 1.

$\nabla P_{p,zz}$ and $\tau_{p,zz}$ are defined as

$$\frac{\partial P_{p,zz}}{\partial z} + \frac{\partial \tau_{p,zz}}{\partial z} = -E\frac{\partial \varepsilon}{\partial z} \tag{2-10}$$

where E is the elastic coefficient of the fluidized bed, and it is depended on the bed voidage. In the MSFB, E is expected to be a function of the field intensity and the magnetization of the particles.

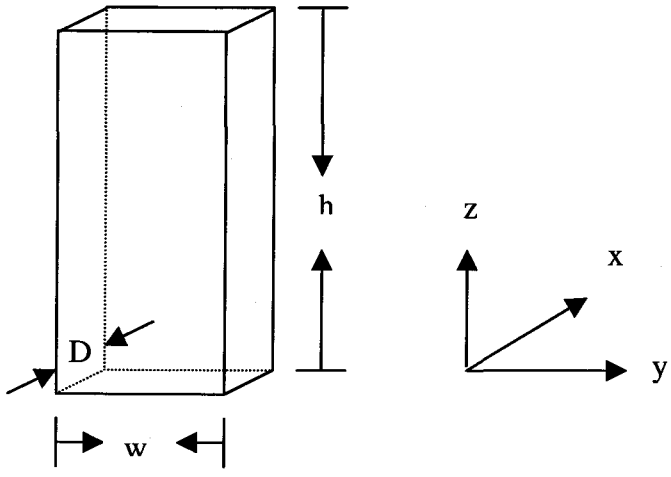

Figure 2-3: Two-dimensional fluidization column

The particle interaction force plays a significant role in cases where particles are relatively small in size (typically below 100 μm). In our studies, the ferromagnetic particles have a comparatively large size (d_p=1500-2500 μm). Therefore, the interparticle force can be ignored when compared to the interaction force between the fluid and the particles and the gravitational force. As a result, the second term, ∇P_p, and the third term, τ_p, in equation (2-4) will be removed from the equation of motion for the particle phase.

2.2.4 Magnetic Equation of State

Rosensweig (1979) was first to propose the magnetic equation of state for a uniformly fluidized bed. He assumed that the magnetization of the bed is collinear with the direction of the magnetic field. In addition, the magnetization of the fluidized bed is proportional to the solid content in the bed.

The magnetic equation of state is expressed as follows:

$$M_b = (1-\varepsilon)\frac{\underline{H}}{H} M_p \quad \text{and} \quad M_p = \chi H \tag{2-11}$$

It should be noted that the magnetization of the bed is also dependent upon the magnitude of the magnetic field intensity and the magnetization of magnetic particles.

CHAPTER 3
EXPERIMENTAL APPARATUS AND MATERIALS

A schematic representation of the experimental apparatus used in this study is shown in Figure 3-1. The experimental apparatus consists of the following elements:

3.1 Fluidization Column

3.2 Magnetic Field Generator (Helmholtz rings)

3.3 Water Supply System

3.4 Instrumentation

3.5 The Ferromagnetic Particles

3.6 Fluidization Column and Magnetic Field Generator (Experiments on Board The NASA KC-135 Plane)

3.7 NASA KC-135 plane

3.1 Fluidization Column

The fluidization column in which the particles are fluidized is made of Plexiglas, allowing visual observation through the wall. The fluidization column is divided into three removable parts: the fluidization section, the calming section, and the overflow box.

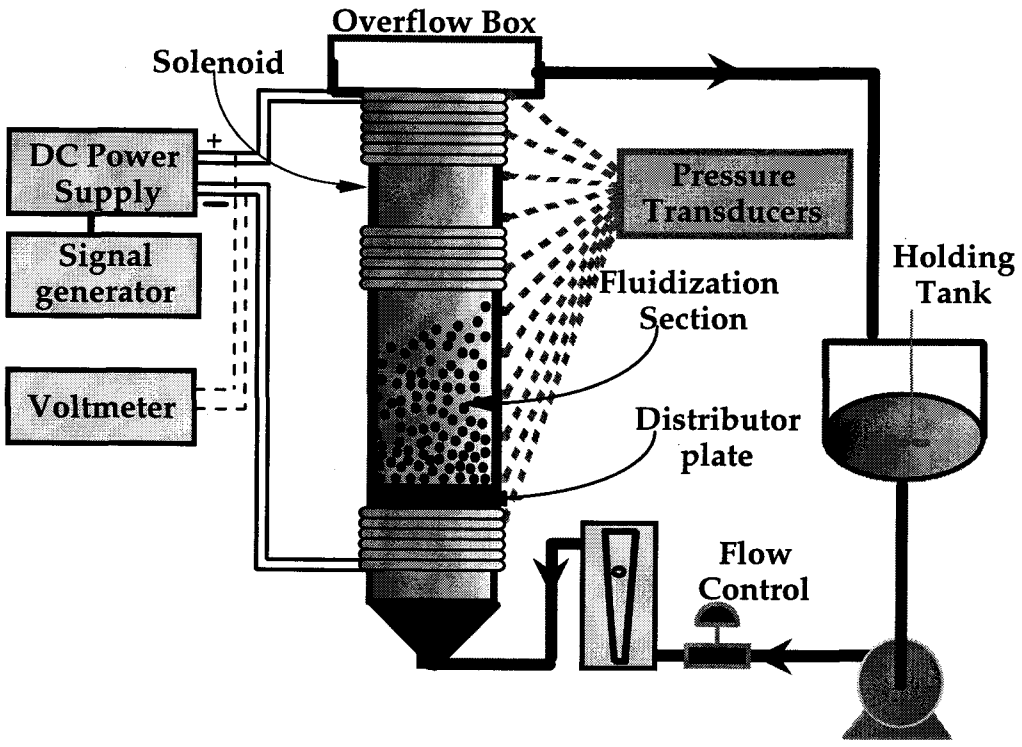

Figure 3-1: Experimental apparatus used in laboratory experiments

The Fluidization Section This section is a 35 cm long clear Plexiglas tube. It has an inside diameter of 4.45 cm and outside diameter of 5.08 cm. A circular distributor plate is located at the bottom of the fluidization section, which can be easily removed or repositioned to any location along the fluidization section. The distributor plate is responsible for evenly distributing the flow over the entire area of the column.

The Calming Section This section is composed of small marbles enclosed under the distributor plate, providing a uniform upward flow to the fluidization section. This section is designed to dissipate large liquid jets which may form at the entrance of the fluidization apparatus. The calming and the fluidization sections are separated by the distributor plate, which is made of a 0.3 mm thick clear plastic plate. The distributor plate is 4.45 cm in diameter and it has one hundred and forty-six, 2 mm circular holes, uniformly distributed throughout the plate. The open area of the distributor plate is about 30% the total area of the distributor plate.

Overflow Box The overflow box is a cylindrical container that is 13 cm in diameter and 16 cm high. The overflow box is mounted on the top of the fluidization section. The outlet from the overflow box is covered with a screen to prevent any particle from leaving from the fluidization section, thus protecting the circulating water supply system.

3.2 Magnetic Field Generator (Helmholtz Rings)

The magnetic field generator is composed of a direct current (DC) power supply connected with ten parallel Helmholtz rings and ten rheostats. The DC power supply can provide 0-5 volts and up to 200 A of current to the system. The output voltage is manually controlled by using a voltage control knob. Each Helmholtz ring consists of 2 layers of 10 turns of 1 mm copper wire, which is fixed around a 2.54 cm long plastic ring with a 5.08 cm outside diameter. The Helmholtz rings can be

positioned at any position along the fluidization column by sliding up and down. The magnetic field is parallel to the direction of the flow, and the magnetic field induction, B, at any given point in space around a single Helmholtz ring is given as the following: (see Figure 3-2 for schematic of a single copper wire).

$$B_z(r,z)=2\times10^{-4}\frac{I}{a}\left[\frac{1}{\left(1+\frac{r}{a}\right)^2+\left(\frac{z}{a}\right)^2}\right]^{\frac{1}{2}}\left[K(v)+\frac{1-\left(\frac{r}{a}\right)^2-\left(\frac{z}{a}\right)^2}{\left(1-\frac{r}{a}\right)^2+\left(\frac{z}{a}\right)^2}E(v)\right] \quad (3\text{-}1)$$

$$B_r(r,z)=2\times10^{-4}\frac{I}{a}\left(\frac{z}{r}\right)\left[\frac{1}{\left(1+\frac{r}{a}\right)^2+\left(\frac{z}{a}\right)^2}\right]^{\frac{1}{2}}\left[\frac{1+\left(\frac{r}{a}\right)^2+\left(\frac{z}{a}\right)^2}{\left(1-\frac{r}{a}\right)^2+\left(\frac{z}{a}\right)^2}E(v)-K(v)\right] \quad (3\text{-}2)$$

where B = magnetic field intensity in Tesla

I = current in amps

r, z, a = displayed in Figure 3-2 with dimensions in mm

$K(v)$ = complete elliptic integral of the first kind

$E(v)$ = complete elliptic integral of the second kind

The elliptic integrals are given by:

$$K(v)=\int_0^{\frac{\pi}{2}}\frac{d\theta}{\sqrt{1-v^2\sin^2\theta}} \quad (3\text{-}3)$$

$$E(v)=\int_0^{\frac{\pi}{2}}\sqrt{1-v^2\sin^2\theta}\,d\theta \quad (3\text{-}4)$$

$$\text{Where} \quad \nu^2 = \frac{4\frac{r}{a}}{\left(1+\frac{r}{a}\right)^2 + \left(\frac{z}{a}\right)^2} \tag{3-5}$$

The rheostats, connected in series with the Helmholtz rings, are used to control the current in each Helmholtz ring. Each rheostat can be maintained at 0-0.5 Ohm and manually controlled by adjusting a control knob. The calibration of rheostat resistance is given in Appendix E. The overall magnetic field intensity within the fluidized bed is the sum of the magnetic field intensity generated from each Heltmoltz ring. In our study, a constant magnetic field gradient is produced by adjusting the currents and the spacing between the ten Helmholtz rings. The magnetic field intensity can be evaluated by either measuring it directly in the fluidization column or calculating it from equations (3-1) to (3-5).

3.3 Water Supply System

The water supply system is composed of a pump driven by a 1/3 Hp, 2600/3000-rpm motor. The pump discharge is connected to a flow rotameter, and it is directed to the fluidization column. The pump suction is jointed with the overflow box through a 3/4 inch inner diameter plastic tube. The fluid flow is regulated by a valve which is mounted upstream of the rotameter. The calibration of the superficial fluid velocity, U_0, corresponding to a rotameter reading is given in Appendix E.

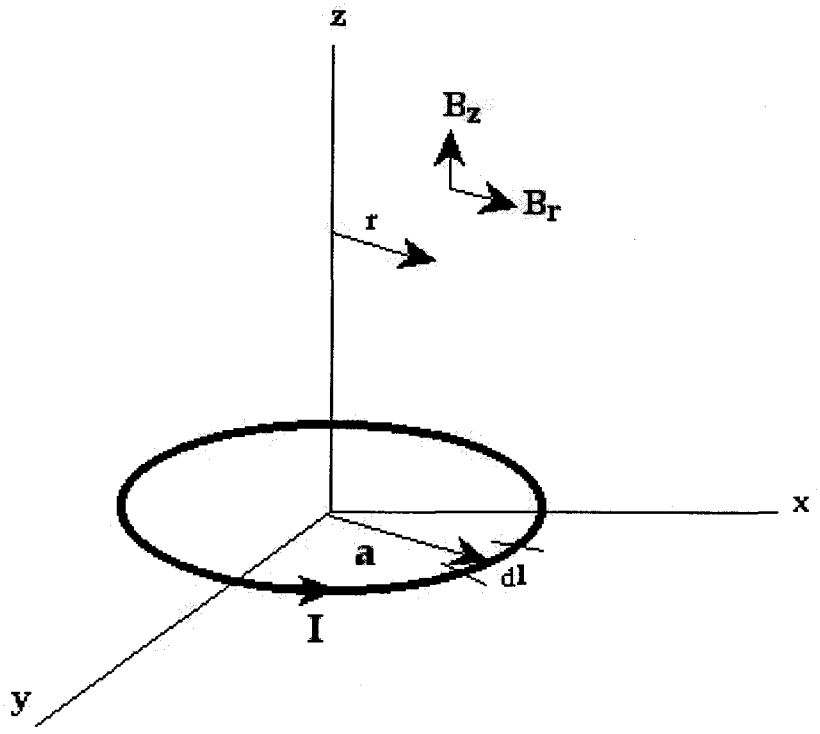

Figure 3-2: A single copper wire and the magnetic induction

3.4 Instrumentation

The Dynamic Pressure Measuring System The pressure measuring system consists of a clear glass tube connected to an aluminum probe. The glass tube has an internal diameter of 2 mm. The aluminum probe is 1 mm in diameter and 80 cm in length. The aluminum probe is inserted into the fluidized column and measures the pressure every 0.5 centimeters from the bottom of the bed. The pressure obtained from this measurement is called the dynamic pressure.

Gaussmeter The magnetic field intensity inside the fluidized bed can be measured directly by using the Gaussmeter, which in this case is a model 410 Gaussmeter by Lake Shore Cryotronics, Inc. It is a hand-held, field-portable unit that provides measurement of AC or DC magnetic fields. Two main parts of the Gaussmeter are the Gaussmeter unit and the axial probe.

a) **Gaussmeter Unit** The Gaussmeter unit has a front panel as shown in Figure 3-3. The probe connector is mounted on top of the unit. The magnetic field intensities can be measured in units of either gauss or Tesla.

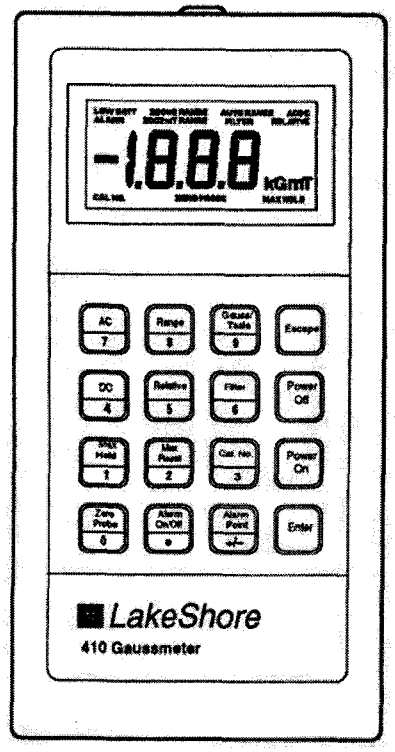

Figure 3-3: The front panel of the Gaussmeter

b) Axial Probe The configuration and dimension of an axial probe are shown in Figure 3-4. The axial probe is connected directly to the Gaussmeter unit by a probe extension cable, which allows the probe to be extended three meters from the unit.

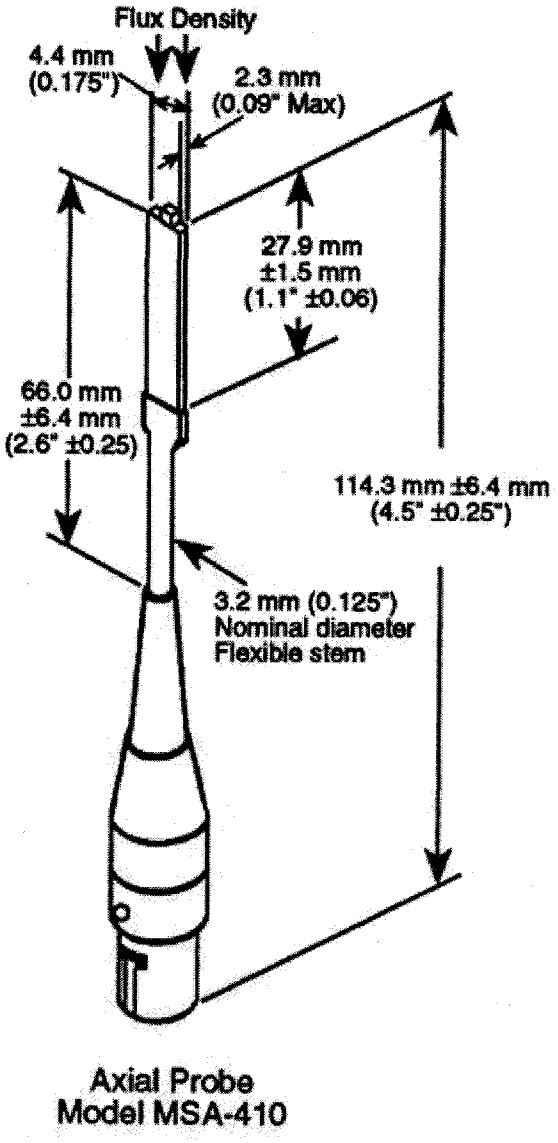

Figure 3-4: Configuration and dimension of an axial probe

3.5 The Ferromagnetic Particles

The ferromagnetic particle consists of a sodium alginate solution, ferromagnetic powder, and microsphere balloons (sodium borosilicate). The ferromagnetic particle is shown in Figure 3-5.

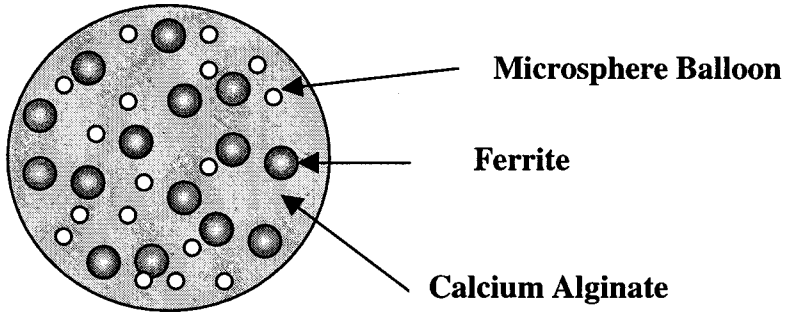

Figure 3-5: The Ferromagnetic particle

The following is the description of the ferromagnetic sodium alginate mixture suspension, the particle generator, and calcium chloride cross-linking, used in our experiments.

Ferromagnetic sodium alginate mixture suspension 1.75 weight % sodium alginate solution is prepared beforehand. The ferromagnetic powder and microsphere balloons are then added to the solution, respectively. The preparation of the sodium alginate

mixture is described in Appendix C. The compositions and properties of ferromagnetic powder and microsphere balloons are given in Appendix D.

The particle generator The schematic diagram of the particle generator is shown in Figure B-1 in Appendix B. The particle generator consists of a nozzle, which is connected to the bottom of a steel column. When the ferromagnetic alginate mixture is poured in at top of the column, it will slowly flow through the nozzle and finally drop into a 1.0 M calcium chloride solution. The particle size can be adjusted by regulating the air pressure at the top of the column, and the airflow at the tip of the nozzle to shear off the particles.

Calcium Chloride Cross-Linking Solution A 1.0 M calcium chloride solution is used to polymerize the ferromagnetic sodium alginate droplets coming out from the nozzle tip. Calcium chloride immediately reacts with sodium alginate, and forms calcium alginate on the surface of the droplets. The chemical reaction can be represented by:

$$2n\ Na(Alg) + n\ Ca^{++} \text{ <----> } n\ Ca(Alg)_2 + 2n\ Na^{+} \qquad (3\text{-}6)$$

At the beginning, only the surface of the sodium alginate droplet reacts with the calcium ion. When the droplet is left in the calcium chloride solution over a period of time, calcium ions will diffuse toward the center of the particle, and form a complete calcium alginate structure throughout the droplet. The particles are rinsed with deionized water, and stored in a low concentration calcium chloride solution at

room temperature. The properties of the ferromagnetic particles used in our studies are listed in Table 3-1.

Table 3-1: The Ferromagnetic Particle Properties

Particle	A	B	C	D
Particle Diameter (mm)	2.16	2.5	2.4	1.5
Density (kg / m^3)	1119	1302	1502	1090
Ferrite	20%	20%	30%	20%
Microsphere Balloon	8%	2%	0%	9%
1.75% Alginate Solution	72%	78%	70%	71%
ε_{mf}	0.43	0.43	0.43	0.43
u_{mf} (m/s)	0.0042	0.0110	0.0151	0.00175
Magnetic Susceptibility, χ	2.79	3.121	5.21	2.75

Particle A and B were used for laboratory experiments. Particle C and D were used for experiments on board the NASA KC-135 plane. The magnetic susceptibility of ferromagnetic powder is measured separately by using Thermal Gravimetric Analysis (TGA), see in Appendix F.

3.6 Fluidization Column, Magnetic Field Generator and Rotameter (Experiment on Board The NASA KC-135 plane)

The schematic flow diagram of the Magnetically Assisted Fluidized Bed used on board the NASA-KC135 plane (zero-g flight) is similar to the MAFB operated in the laboratory (Figure 3-1). The only differences in equipment apparatus are the shape of the fluidization column, the design of the magnetic field generator, and the design of flow rate measuring instrument which has to operate in 0 g.

Fluidization Column The fluidization column used in experiments on the NASA-KC135 is a two dimensional, square cross-section, tapered fluidization column. The design of the fluidization column is unique and we did not find previous reference describing a similar apparatus. The tapered shape of the column is introduced to provide additional stability to the fluidization particles. The stability of the fluidization operation depends on the local intensity of drag and magnetic forces. The tapered shape of the column relates with both forces. The column in which the particles are fluidized is made of Plexiglas, allowing visual observation through the wall. The geometric configuration and dimensions of the fluidization column is shown in Figure 3-6.

Magnetic Field Generator Two short rectangular solenoid coils are used in this experiment. The first solenoid coil has dimensions of 10 cm by 15 cm and the second has dimensions of 10 cm by 20 cm. Both coils have six layers with five turns of wire per layer. The bottom of the fluidization column is located between two solenoid coils where the magnetic field intensity is the highest (see in Figure 3-7).

Rotameter A special flow rotameter is used to measure the liquid flow rate in the absense of gravity. The plastic ball inside the flow rotameter is replaced with a neutrally buoyant magnetic ball called the float. A ring of permanent magnet is located at the top of the flow meter and it is positioned coaxially in such a way that it creates a normal repulsive magnetic force acting on the float, thus pushing the magnetic ball away from the top of the flow meter. As the liquid flow rate increases,

the ball will move closer to the top of the flow meter. The calibration of this unique flow-measuring instrument is given in Appendix E.

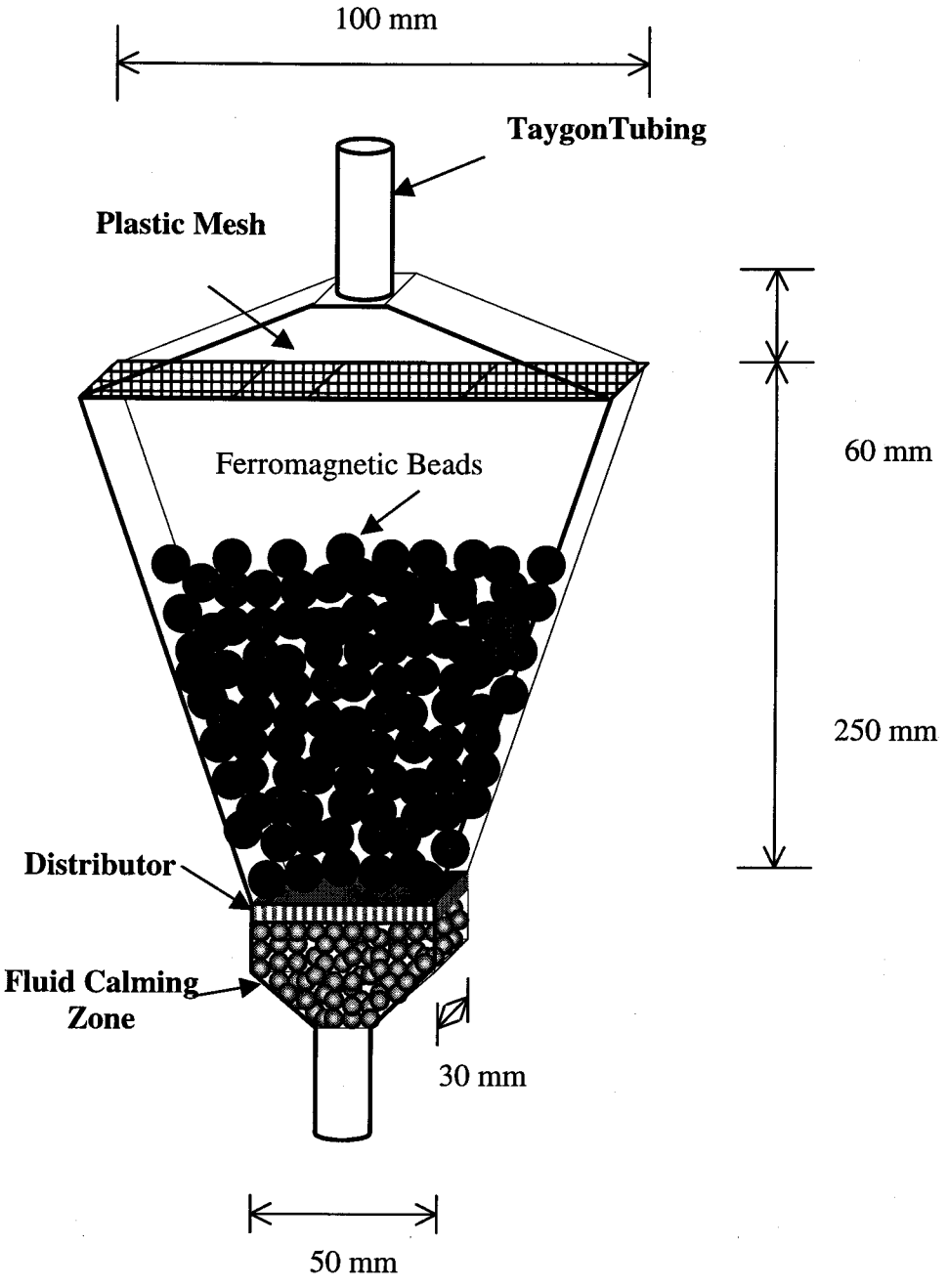

Figure 3-6: The magnetically assisted fluidized bed (experiment on board the NASA KC-135 plane)

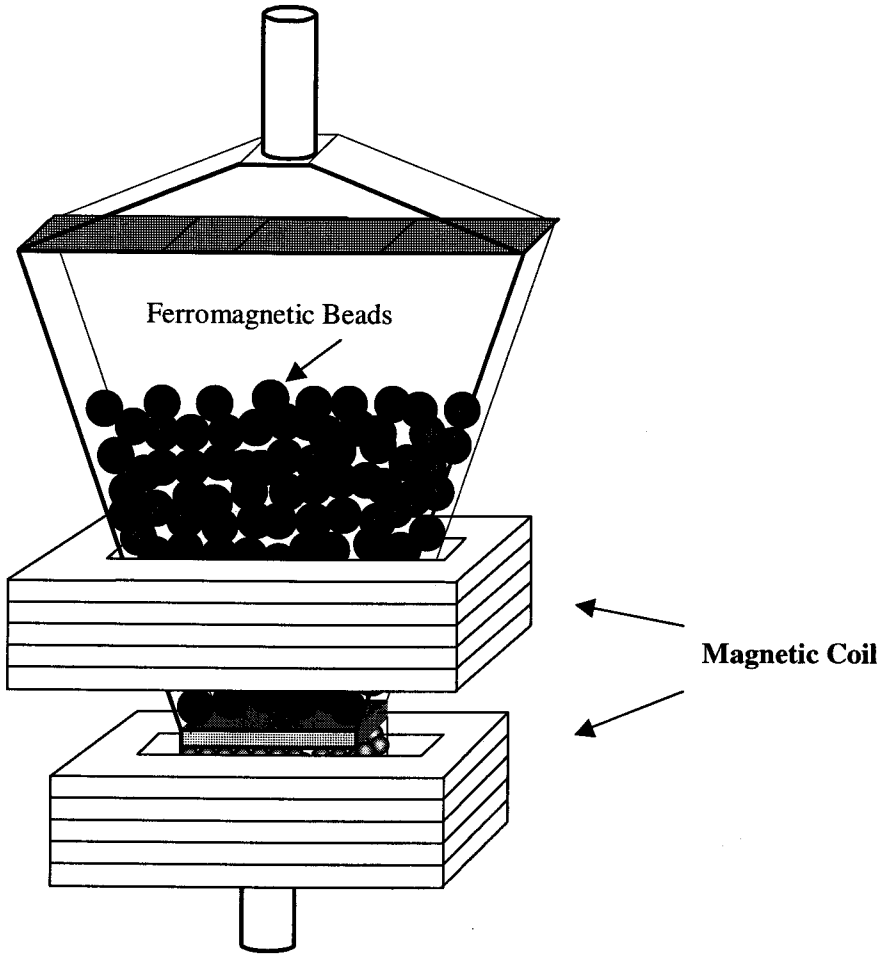

Figure 3-7: The magnetic coils on the magnetically assisted fluidized bed (experiment on board the NASA KC-135 plane)

3.7 The NASA KC-135 Plane

The experiments in the"0" g environment were conducted on board the NASA KC-135 plane. Particle C and D were fluidized in a square two-dimensional fluidization column at different magnetic field intensities and liquid flow rates. The

height of the bed, at any given field intensity and liquid flow rate, is recorded by a video camera.

The Reduced Gravity Student Flight Opportunities program is sponsored by NASA and administered by the Texas Space Grant Consortium and it provides a true three-dimensional "weightless" environment on the Boeing KC-135. This airplane has been used as a platform for testing in reduced-gravity experiments and for the training the US astronauts. The actual trajectory flown on each maneuver provides approximately 25 seconds of zero-gravity condition for experiments. The trajectory is shown in Figure 3-8.

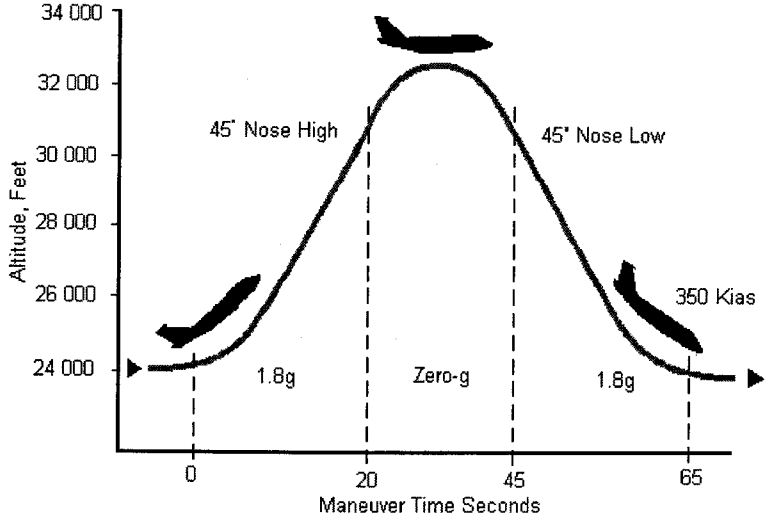

Figure 3-8: The Trajectory of the Boeing NASA KC-135

CHAPTER 4
VOIDAGE DISTRIBUTION MODEL AND EXPERIMENTAL METHOD

4.1 The Voidage Distribution Model

The voidage distribution model in a non-uniform magnetic field fluidization can be derived from the four fundamental equations, namely, equations of continuity and equation of motions for both fluid and particle phases. All the equations presented in Chapter 2 can be summarized as follows:

The Equation of Continuity:

Fluid phase:
$$\frac{\partial \varepsilon}{\partial t} + \nabla \cdot \varepsilon \mathbf{U} = 0 \tag{2-1}$$

Particle phase:
$$\frac{\partial (1-\varepsilon)}{\partial t} + \nabla \cdot (1-\varepsilon)\mathbf{V} = 0 \tag{2-2}$$

The Equation of Motion:

Fluid phase:
$$\rho_f \varepsilon \left(\frac{\partial \mathbf{U}}{\partial t} + (\mathbf{U} \cdot \nabla)\mathbf{U} \right) = -\varepsilon \nabla P_f - \varepsilon \nabla \cdot \tau + \rho_f \varepsilon \mathbf{g} - \varepsilon \boldsymbol{F_I} \tag{2-3}$$

Particle phase:

$$\rho_p (1-\varepsilon) \left(\frac{\partial \mathbf{V}}{\partial t} + (\mathbf{V} \cdot \nabla)\mathbf{V} \right) = -(1-\varepsilon)\nabla P_f - (1-\varepsilon)\nabla P_p - (1-\varepsilon)\nabla \cdot \tau_p$$
$$+ \rho_p (1-\varepsilon)\varepsilon \mathbf{g} + \varepsilon \boldsymbol{F_I} + \boldsymbol{F_m} \tag{2-4}$$

where $\boldsymbol{F_I}$ is the force between fluid and particles and it is defined as

$$\boldsymbol{F_I} = \beta(\varepsilon)(\mathbf{U} - \mathbf{V}) + \frac{(1-\varepsilon)}{\varepsilon} C(\varepsilon) \rho_f \frac{d(\mathbf{U} - \mathbf{V})}{dt} \tag{2-5}$$

Using the Ergun expression, $\beta(\varepsilon)$ is given by

$$\beta(\varepsilon)=\frac{150(1-\varepsilon)^2\mu_f}{d_p^2\varepsilon^2}+\frac{1.75(1-\varepsilon)U_0\rho_f}{d_p\varepsilon^2} \tag{2-6}$$

$\boldsymbol{F_m}$ is the magnetic force acting on the ferromagnetic particles which is defined as follows:

$$\boldsymbol{F_m} = \mu_0(1-\varepsilon)M_p\nabla H \tag{2-8}$$

The magnetization of the particle is collinear with the field intensity and it is given as

$$M_p = \chi H \tag{2-11}$$

This set of equations can also be written in the cylindrical coordinate system as:

The Equation of Continuity:

Fluid Phase:
$$\frac{\partial\varepsilon}{\partial t}+\frac{1}{r}\frac{\partial(r\varepsilon u_r)}{\partial r}+\frac{1}{r}\frac{\partial(\varepsilon u_\theta)}{\partial\theta}+\frac{\partial(\varepsilon u_z)}{\partial z}=0$$

$$\frac{\partial\varepsilon}{\partial t}+\frac{\varepsilon u_r}{r}+u_r\frac{\partial\varepsilon}{\partial r}+\varepsilon\frac{\partial u_r}{\partial r}+\frac{1}{r}u_\theta\frac{\partial\varepsilon}{\partial\theta}+\frac{1}{r}\varepsilon\frac{\partial u_\theta}{\partial\theta}+u_z\frac{\partial\varepsilon}{\partial z}+\varepsilon\frac{\partial u_z}{\partial z}=0 \tag{4-1}$$

Particle Phase:

$$\frac{\partial(1-\varepsilon)}{\partial t}+\frac{1}{r}\frac{\partial(r(1-\varepsilon)v_r)}{\partial r}+\frac{1}{r}\frac{\partial((1-\varepsilon)v_\theta)}{\partial\theta}+\frac{\partial((1-\varepsilon)v_z)}{\partial z}=0$$

$$-\frac{\partial\varepsilon}{\partial t}+\frac{(1-\varepsilon)v_r}{r}-v_r\frac{\partial\varepsilon}{\partial r}+(1-\varepsilon)\frac{\partial v_r}{\partial r}-\frac{v_\theta}{r}\frac{\partial\varepsilon}{\partial\theta}+(1-\varepsilon)\frac{\partial v_\theta}{\partial\theta}-v_z\frac{\partial\varepsilon}{\partial z}+(1-\varepsilon)\frac{\partial v_z}{\partial z}=0$$

(4-2)

The Equation of Motion

Fluid Phase:

$$\rho_f \varepsilon\left(\frac{\partial u_r}{\partial t}+u_r\frac{\partial u_r}{\partial r}+\frac{u_\theta}{r}\frac{\partial u_r}{\partial z}+u_z\frac{\partial u_r}{\partial z}-\frac{u_\theta^2}{r}\right)=-\varepsilon\frac{\partial P}{\partial r}-\frac{\varepsilon}{r}\frac{\partial(r\tau)}{\partial r}-\rho_f\varepsilon g_r-\varepsilon F_{1,r}$$

$$\rho_f \varepsilon\left(\frac{\partial u_\theta}{\partial t}+u_r\frac{\partial u_\theta}{\partial r}+\frac{u_\theta}{r}\frac{\partial u_\theta}{\partial \theta}+u_z\frac{\partial u_\theta}{\partial z}+\frac{u_r u_\theta}{r}\right)=-\frac{\varepsilon}{r}\frac{\partial P}{\partial \theta}-\frac{\varepsilon}{r}\frac{\partial \tau}{\partial \theta}-\rho_f\varepsilon g_\theta-\varepsilon F_{1,\theta}$$

$$\rho_f \varepsilon\left(\frac{\partial u_z}{\partial t}+u_r\frac{\partial u_z}{\partial r}+\frac{u_\theta}{r}\frac{\partial u_z}{\partial \theta}+u_z\frac{\partial u_z}{\partial z}\right)=-\varepsilon\frac{\partial P}{\partial z}-\varepsilon\frac{\partial \tau}{\partial z}-\rho_f\varepsilon g_z-\varepsilon F_{1,z} \qquad (4\text{-}3)$$

Particle Phase:

$$\rho_f(1-\varepsilon)\left(\frac{\partial v_r}{\partial t}+v_r\frac{\partial v_r}{\partial r}+\frac{v_\theta}{r}\frac{\partial v_r}{\partial \theta}-\frac{v_\theta^2}{r}\right)=-(1-\varepsilon)\frac{\partial P}{\partial r}-\rho_p(1-\varepsilon)g_r+\varepsilon F_{1,r}+F_{m,r}$$

$$\rho_f(1-\varepsilon)\left(\frac{\partial v_\theta}{\partial t}+v_\theta\frac{\partial v_\theta}{\partial r}+\frac{v_\theta}{r}\frac{\partial v_\theta}{\partial \theta}+v_z\frac{\partial v_\theta}{\partial z}+\frac{v_r v_\theta}{r}\right)=-\frac{(1-\varepsilon)}{r}\frac{\partial P}{\partial \theta}-\rho_p(1-\varepsilon)g_\theta$$

$$+\varepsilon F_{1,\theta}+F_{m,\theta}$$

$$\rho_f(1-\varepsilon)\left(\frac{\partial v_z}{\partial t}+v_r\frac{\partial v_z}{\partial r}+\frac{v_\theta}{r}\frac{\partial v_z}{\partial \theta}+v_z\frac{\partial v_z}{\partial z}\right)=-(1-\varepsilon)\frac{\partial P}{\partial z}-\rho_p(1-\varepsilon)g_z+\varepsilon F_{1,z}+F_{m,z}$$

(4-4)

Magnetic Force

The magnetic field intensity, $\boldsymbol{H}$, has three components H_r, H_z, H_θ. Therefore, the magnetic force acting on the particles in cylindrical coordinate system can be written as follows.

$$F_{m,z} = \mu_0(1-\varepsilon)\chi\left(H_r \frac{dH_r}{dz} + H_z \frac{dH_z}{dz} + H_\theta \frac{dH_\theta}{dz} \right)$$

$$F_{m,r} = \mu_0(1-\varepsilon)\chi\left(H_r \frac{dH_r}{dr} + H_z \frac{dH_z}{dr} + H_\theta \frac{dH_\theta}{dr} \right)$$

$$F_{m,\theta} = \mu_0(1-\varepsilon)\chi\left(H_r \frac{dH_r}{d\theta} + H_z \frac{dH_z}{d\theta} + H_\theta \frac{dH_\theta}{d\theta} \right) \qquad (4\text{-}5)$$

In order to ease experimental work and to simplify the computation of the bed voidage using the above model, three experimental conditions are introduced and simplifying assumptions are made.

The followings are the specific experimental conditions used in this study.

2. The magnetic field intensity is highest at the bottom of the bed and it decreases linearly with the height of the bed ($\frac{dH}{dz}$ = constant).
3. The system is symmetric in θ direction. Thus, any terms in the θ direction will be neglected.
4. This system is at steady state, $\frac{\partial(\ )}{\partial t} = 0$

The followings are the simplifying assumptions used in this study.

1. The mean particle velocity is assumed to be zero, $V = 0$. With this assumption, all terms that include the particle velocity are negligible.

2. The fluid phase is treated as an inviscid flow except for mutual interaction with the particle phase.
3. The particles phase is regarded as free of mechanical stress at all times. This assumption is based on the fact that the particles are so large that the interparticle forces are small compared to interaction forces between the two phases.
4. The magnetic field intensity in the r and θ directions is much smaller than the field intensity in the z direction. Therefore, the magnetic field intensity in the r and θ directions will be ignored. $(H_r = H_\theta = 0)$
5. The virtual mass force due to the relative acceleration between fluid and particle is small compared to the force due to the gravity so this term will be neglected.
6. The redistribution of flow inside the column is negligible, therefore, the fluid velocity in the r and θ directions is much smaller than the fluid velocity in the z direction. The velocity in r and θ will be neglected. $(u_r = u_\theta = 0)$.
7. The momentum terms due to the change of fluid velocity (fluid acceleration/deceleration term) are small compared to the other forces (the gravitational force, the drag force, and the magnetic force).

With the assumptions and specific experimental conditions listed above, equation (4-1) reduces to,

$$\frac{\partial (\varepsilon\ u_z)}{\partial\ z} = 0 \tag{4-6}$$

Equation (4-2) is automatically satisfied because the mean velocity of the particle is assumed to be equal to zero.

The equation of motion for the fluid and particle phases in the z direction is reduced to

The fluid phase: $$0 = -\varepsilon \frac{\partial P_f}{\partial z} - \rho_f \varepsilon g - \varepsilon F_{1,z} \tag{4-7}$$

The particle phase: $$0 = -(1-\varepsilon)\frac{\partial P_f}{\partial z} - \rho_p (1-\varepsilon) g_z + \varepsilon F_{1,z} + F_{m,z} \tag{4-8}$$

One can rearrange equation (4-7) to obtain,

$$\frac{\partial P_f}{\partial z} = -\rho_f g_z - F_{1,z} \tag{4-9}$$

Substitute equation (4-9) into equation (4-8) and rearrange the terms

$$0 = -(1-\varepsilon)(-\rho_f g_z - F_{1,z}) - \rho_p (1-\varepsilon) g_z + \varepsilon F_{1,z} + F_{m,z}$$

Then, $$0 = (1-\varepsilon)\rho_f g_z + (1-\varepsilon)F_{1,z} - \rho_p (1-\varepsilon) g_z + \varepsilon F_{1,z} + F_{m,z}$$

Finally, $$0 = -(\rho_p - \rho_f)(1-\varepsilon) g_z + F_{1,z} + \mu_0 (1-\varepsilon)\chi H_z \frac{\partial H_z}{\partial z} \tag{4-10}$$

The constitutive expression for the drag force, $F_{1,z}$, is given by the following expressions

$$\boldsymbol{F_1} = \beta(\varepsilon)(\mathbf{U} - \mathbf{V}) + \frac{(1-\varepsilon)}{\varepsilon} C(\varepsilon)\rho_f \frac{d(\mathbf{U} - \mathbf{V})}{dt} \tag{2-5}$$

$$\beta(\varepsilon)=\frac{150(1-\varepsilon)^2\mu_f}{d_p^2\varepsilon^2}+\frac{1.75(1-\varepsilon)U_0\rho_f}{d_p\varepsilon^2} \qquad (2\text{-}6)$$

Then, equation (4-10) can be written as:

$$\frac{d_p^3\rho_f(\rho_p-\rho_f)g_z}{\mu^2}=\frac{1.75}{\varepsilon^3}\left(\frac{d_pU_0\rho_f}{\mu}\right)^2+\frac{150(1-\varepsilon)}{\varepsilon^3}\left(\frac{d_pU_0\rho_f}{\mu}\right)+\frac{\mu_0\rho_f d_p^3}{\mu^2}\chi H_z\frac{dH_z}{dz} \qquad (4\text{-}11)$$

Equation (4-11) is used to determine the corresponding voidage at any given fluid velocity, field intensity and field gradient.

In the absence of gravity, equation (4-11) can be written as

$$0=\frac{1.75}{\varepsilon^3}\left(\frac{d_pU_0\rho_f}{\mu}\right)^2+\frac{150(1-\varepsilon)}{\varepsilon^3}\left(\frac{d_pU_0\rho_f}{\mu}\right)+\frac{\mu_0\rho_f d_p^3}{\mu^2}\chi H_z\frac{dH_z}{dz} \qquad (4\text{-}12)$$

4.2 Experimental Method

The magnetic field intensity will be measured beforehand by using the Gaussmeter. The pressure drop, $\Delta P_{f(d)}$, in the column can be measured by using the pressure probe as described in section 3.4.1. The pressure probe is inserted vertically from the top of the column and moved axially to measure the dynamic pressure every 0.5 centimeters from the bottom upward to the top of the bed.

The dynamic pressure is defined as the total vertical pressure corrected for the hydrostatic head of the fluid. It is expressed as:

$$-\frac{dP_{f(d)}}{dz} = -\frac{dP_f}{dz} - \rho_f g \tag{4-13}$$

The total vertical pressure drop through the bed is strongly related to the individual phase holdups and the magnetic force acting on the particle phase. It is defined as:

$$-\frac{dP_f}{dz} = (\varepsilon\rho_f + (1-\varepsilon)\rho_p)g + \mu_0(1-\varepsilon)\chi H_z \frac{dH_z}{dz} \tag{4-14}$$

In equation (4-14), we assumed that the frictional loss on the wall is negligible. Substituting equation (4-14) into equation (4-13), one obtains

$$-\frac{dP_{f(d)}}{dz} = (1-\varepsilon)(\rho_p - \rho_f)g + \mu_0(1-\varepsilon)\chi H_z \frac{dH_z}{dz} \tag{4-15}$$

and after rearranging of equation (4-15)

$$\varepsilon = 1 - \left(\frac{-\frac{dP_{f(d)}}{dz}}{(\rho_p - \rho_f)g + \mu_0 \chi H_z \frac{dH_z}{dz}} \right) \tag{4-16}$$

By measuring the pressure drop, $\Delta P_{f(d)}$, for a small interval Δz, the corresponding voidage at any location in the bed can be evaluated by with equation (4-16).

The voidage distribution obtained from the experiments is compared with that obtained from the voidage distribution model. The numerical data for the dynamic pressure drop, $\Delta P_{f(d)}$, at any location in the bed, for different flow rates and different magnetic field gradients, are found in Appendix G.

CHAPTER 5
EXPERIMENTAL RESULTS AND DISSCUSSION

The voidage distribution model presented in Chapter 4 is verified by experimental measurements of the voidage distribution obtained both in the laboratory and in the 0 g environment on board the NASA KC-135 plane.

5.1 The Effect of The Magnetic Force on the Magnetically Assisted Fluidized Bed (MAFB)

As mentioned in Chapter 2, the ferromagnetic particles are subjected to a magnetic force when they are placed in a non-uniform magnetic field. In the experiments, the magnetic field is created in such a way that the intensity of the magnetic field is higher at the bottom of the bed and it decreases linearly toward the top of the bed at a constant rate ($\frac{dH_z}{dz} = \text{constant}$). The magnetic field intensities used in the experiments are provided in Appendix E.

Table 5-1, Figure 5-1 and Figure 5-2 report variation of the height of the bed with the magnetic field gradient, and the fluid velocity, for particles A and B.

From Table 5.1, Figure 5.1 and Figure 5-2, we conclude that:

1. at a given magnetic field intensity, H_z and field gradient, $\frac{dH_z}{dz} = \text{constant}$, the height of the bed will increase as the superficial fluid velocity increases,

2. at a given superficial fluid velocity, U_0, the height of the bed, h will decrease as the magnetic field intensity and its gradient increase.

Table 5-1: Bed Height at Different Fluid Flow Rates and Different Magnetic Field Gradients for Particles A and B

Particles	Flow rate (m/s)	dH_z/dz (A/m/m)	H_z at the bottom (A/m)	Initial Bed Height (m)	Final Bed Height (m)
A	0.0176	0	0	0.065	0.145
A	0.0176	-14663	4276.5	0.065	0.130
A	0.0176	-18289	5334.3	0.065	0.120
A	0.0176	-20543	6262.1	0.065	0.110
A	0.0222	0	0	0.095	0.240
A	0.0222	-14663	4276.5	0.095	0.220
A	0.0222	-18289	5334.3	0.095	0.205
A	0.0222	-20543	6262.1	0.095	0.190
B	0.0222	0	0	0.170	0.252
B	0.0222	-14663	4276.5	0.170	0.240
B	0.0222	-18289	5334.3	0.170	0.230
B	0.0222	-20543	6262.1	0.170	0.217

It is clear that the magnetic field intensity and its gradient have a significant effect on the bed height. Experimental observations show that there are three distinct regions appearing in the magnetic fluidized bed.

The first is the region adjacent to the distributor plate. The water coming through the distributor plate has a high velocity, and it creates small jets above the distributor plate. These jets will exchange their momentum with the surrounding fluid and particles. As a result, the particles in this region will be moved vigorously with

visible vibrations. The length of this zone depends on the magnetic field intensity and the field gradient. This zone is longer at a lower magnetic field intensity, and it is can diminish or even disappear if the magnetic field intensity is substantially increased.

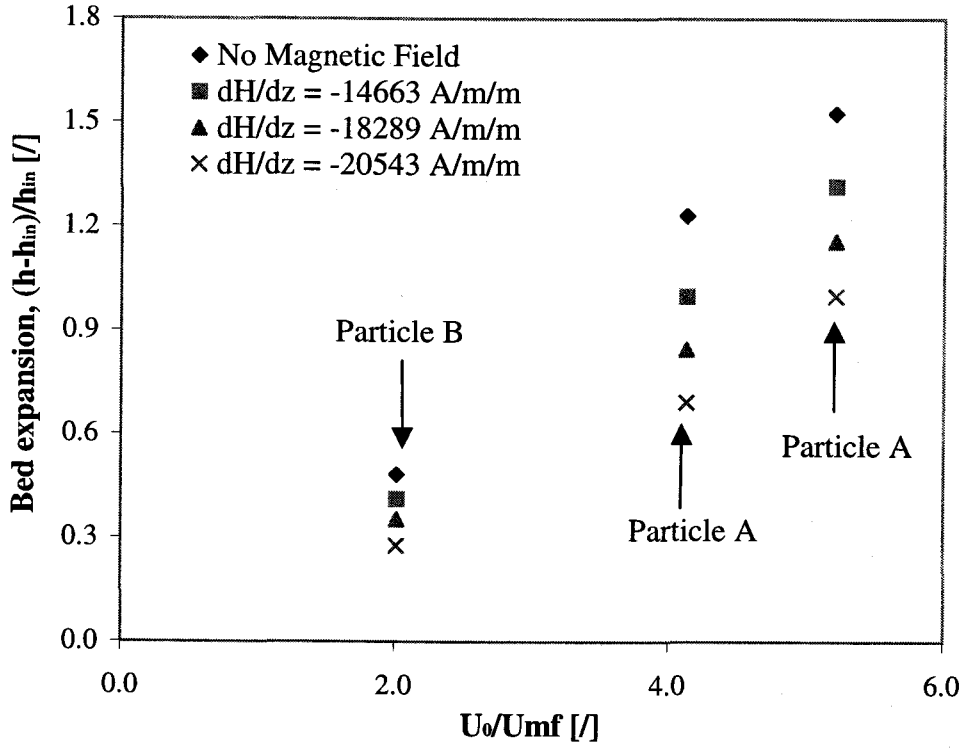

Figure 5-1: Bed expansion as a function of superficial fluid velocity for the different magnetic field intensities and field gradients

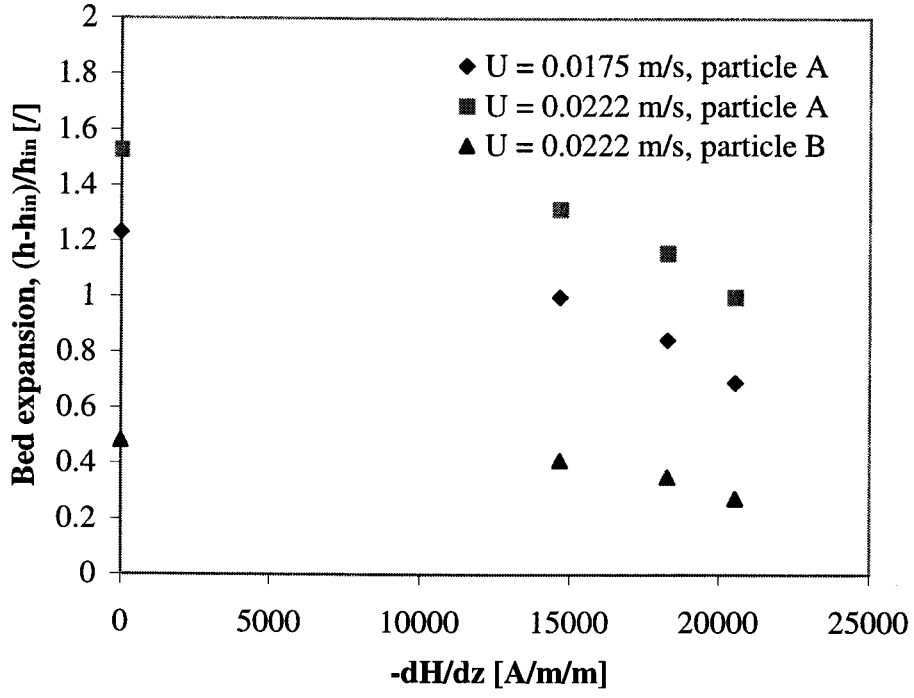

Figure 5-2: Bed expansion as a function of the magnetic field gradient for different superficial fluid velocities

The second is the region where the particles are packed and the jets no longer influence the movement of the particles. This region is established whenever the magnetic forces are stronger than the drag forces acting on the particles. In most of our laboratory studies, this zone is eliminated by carefully choosing the appropriate fluid flow rate and field intensity.

The third region is a part of the fluidized bed where "normal/usual" fluidization is observed. In this region, magnetic forces are well balanced with other forces to allow particulate fluidization.

The influence of the magnetic field and the field gradient on the MAFB observed in the laboratory experiments agrees well with the experiments performed in the zero-gravity environment. These experiments are conducted by the Chemical Engineering Flight Team on board the NASA KC-135 plane. Experimental observations show that the magnetic forces play a major role in keeping the ferromagnetic particles from escaping from the bed. Without the magnetic force, it is not possible to retain the particles in the fluidization column.

5.2 The Voidage Distribution Model and Experimental Results

The voidage distribution obtained from the model presented in Chapter 4 is compared to the voidage distribution obtained from the experiments.

In laboratory experiments, the dynamic pressure, $\Delta P_{f(d)}$, is measured at every 0.5 centimeters from the bottom to the top of the bed. The voidage at any location in the bed is calculated using equation (4-16)

$$\varepsilon = 1 - \left(\frac{-\frac{\Delta P_{f(d)}}{\Delta z}}{(\rho_p - \rho_f) g + \mu_0 \chi H_z \frac{dH_z}{dz}} \right) \qquad (4\text{-}16)$$

On the other hand, the superficial fluid velocity and the magnetic field intensity at any given magnetic field gradient, are the only information needed to predict the voidage distribution in the bed using the model equation (4-16). Once again, the voidage distribution model is represented by;

$$\frac{d_p^3 \rho_f (\rho_p - \rho_f) g_z}{\mu^2} = \frac{1.75}{\varepsilon^3}\left(\frac{d_p U_0 \rho_f}{\mu}\right)^2 + \frac{150(1-\varepsilon)}{\varepsilon^3}\left(\frac{d_p U_0 \rho_f}{\mu}\right) + \frac{\mu_0 \rho_f d_p^3}{\mu^2} \chi H_z \frac{dH_z}{dz} \tag{4-11}$$

Voidage data obtained from the experiments and voidage distribution predicted by the model equation are shown in Figures 5-3 to 5-22. In addition, the calculated total mass of particles in the bed, using both experimental data and calculated voidage is compared with the exact mass of particles in the bed (Figure 5-23). This data provides the insight in the applicability of the model and resolution of our experiments

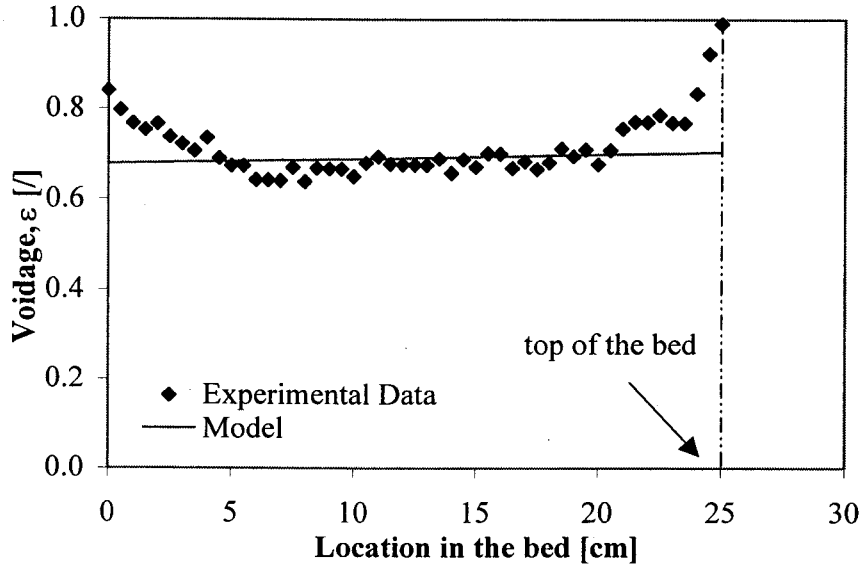

Figure 5-3: The voidage distribution of particle A in the MAFB ($\frac{dH}{dz}$ = -14,663 A/m/m, U_0 = 0.0176 m/s, and the bed height = 0.250 m)

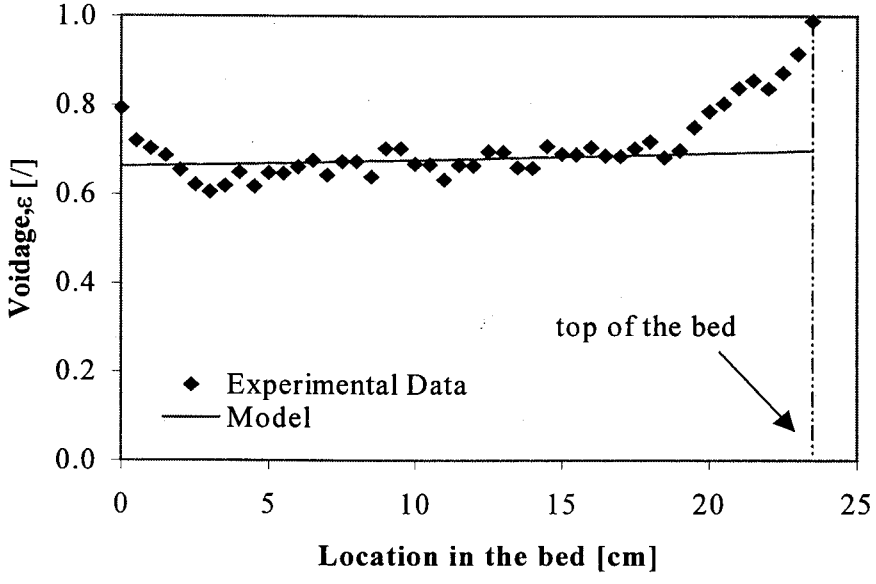

Figure 5-4: The voidage distribution of particle A in the MAFB ($\frac{dH}{dz}$ = -18,289 A/m/m, U_0 = 0.0176 m/s, and the bed height = 0.235 m)

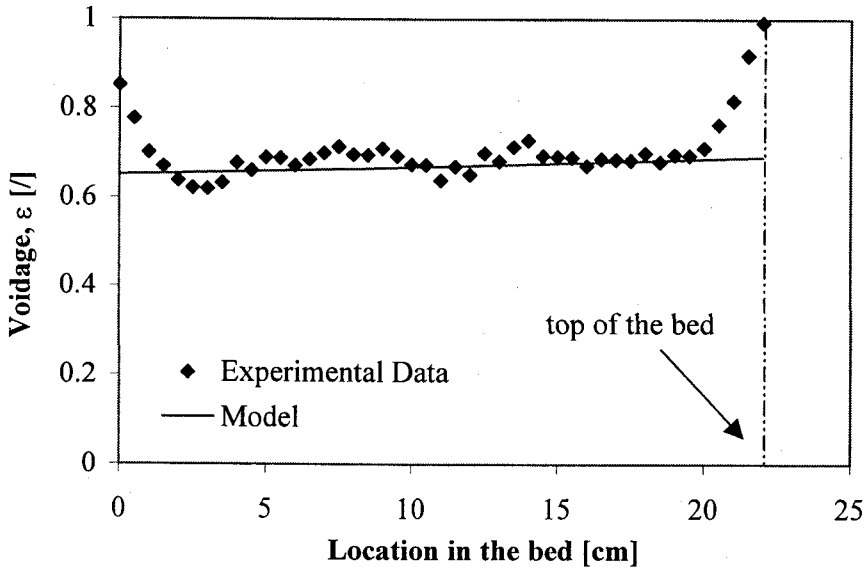

Figure 5-5: The voidage distribution of particle A in the MAFB ($\frac{dH}{dz}$ = -20,543 A/m/m, U_0 = 0.0176 m/s, and the bed height = 0.220 m)

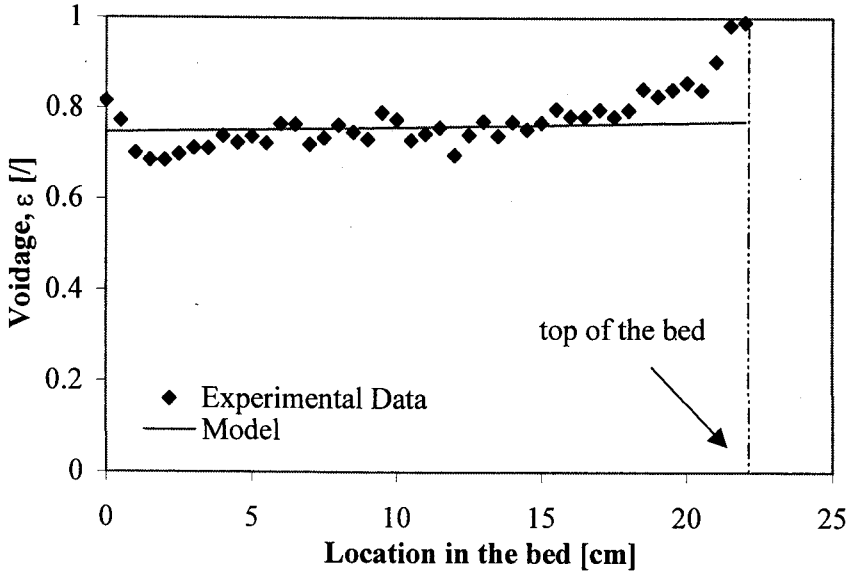

Figure 5-6: The voidage distribution of particle A in the MAFB ($\frac{dH}{dz}$ = - 14,663 A/m/m, U_0 = 0.0222 m/s, and the bed height = 0.220 m)

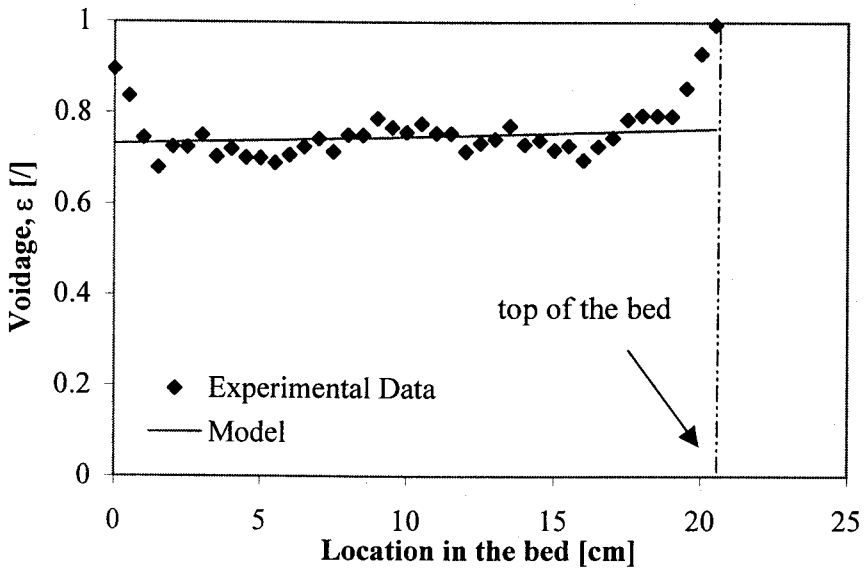

Figure 5-7: The voidage distribution of particle A in the MAFB ($\frac{dH}{dz}$ = - 18,289 A/m/m, U_0 = 0.0222 m/s, and the bed height = 0.205 m)

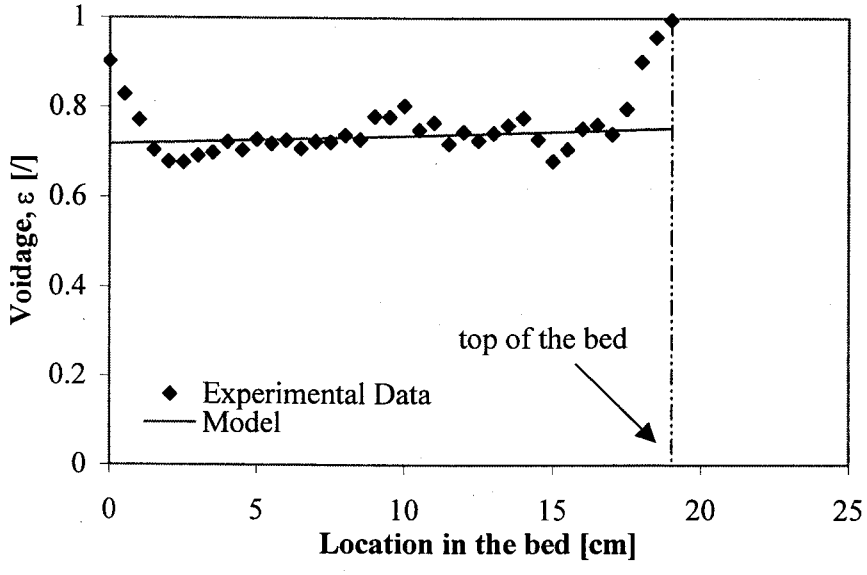

Figure 5-8: The voidage distribution of particle A in the MAFB ($\frac{dH}{dz}$ = - 20,543 A/m/m, U_0 = 0.0222 m/s, and the bed height = 0.190 m)

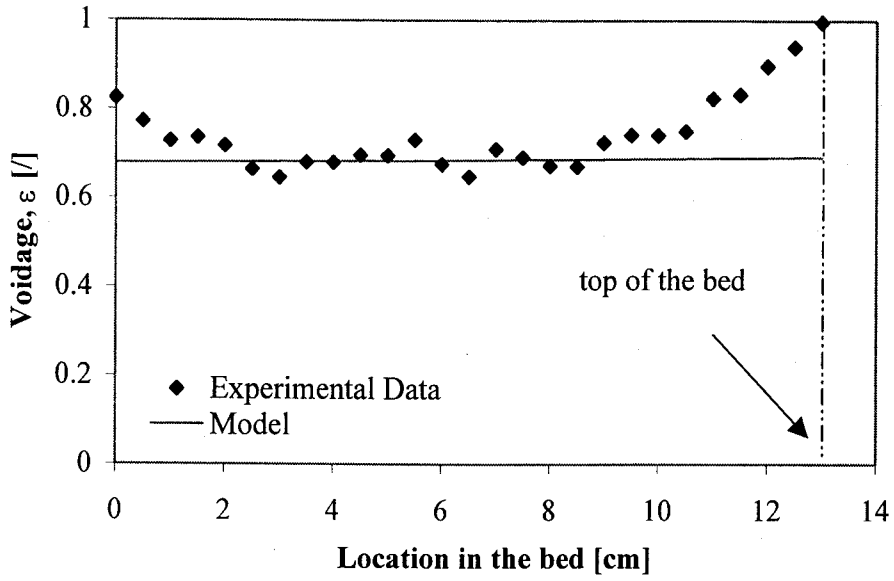

Figure 5-9: The voidage distribution of particle A in the MAFB ($\frac{dH}{dz}$ = - 14,663 A/m/m, U_0 = 0.0176 m/s and the bed height = 0.130 m)

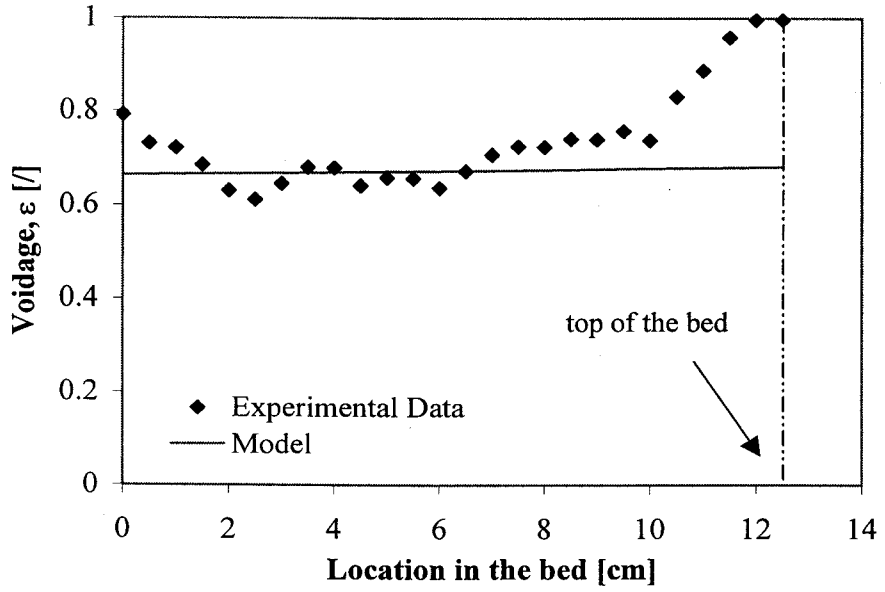

Figure 5-10: The voidage distribution of particle A in the MAFB ($\frac{dH}{dz}$ = - 18,289 A/m/m, U_0 = 0.0176 m/s and the bed height = 0.120 m)

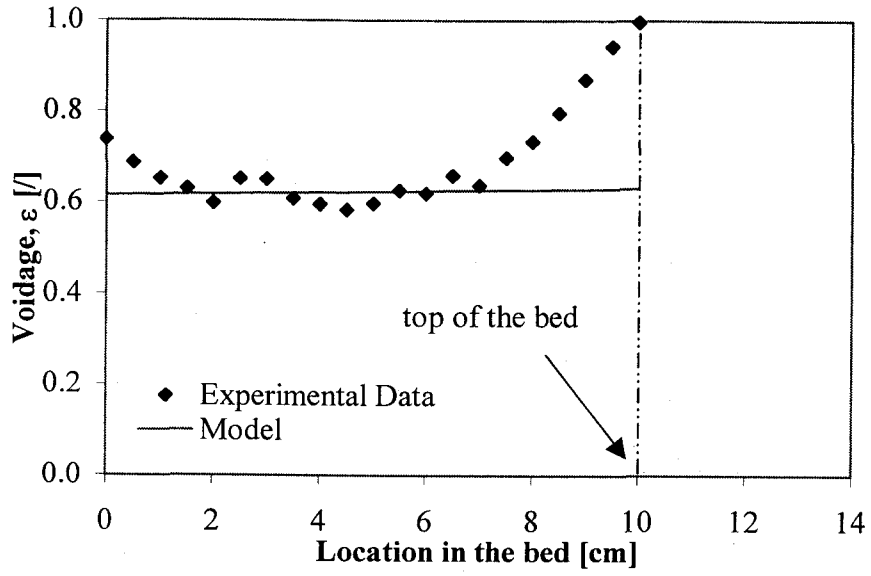

Figure 5-11: The voidage distribution of particle A in the MAFB ($\frac{dH}{dz}$ = - 20,543 A/m/m, U_0 = 0.0153 m/s and the bed height = 0.100 m)

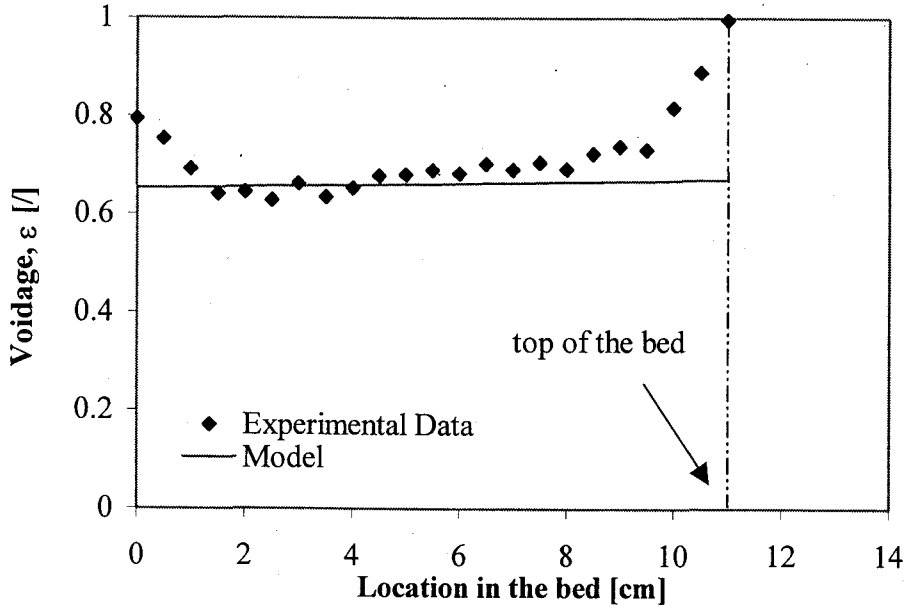

Figure 5-12: The voidage distribution of particle A in the MAFB ($\frac{dH}{dz}$ = - 20,543 A/m/m, U_0 = 0.0176 m/s and the bed height = 0.110 m)

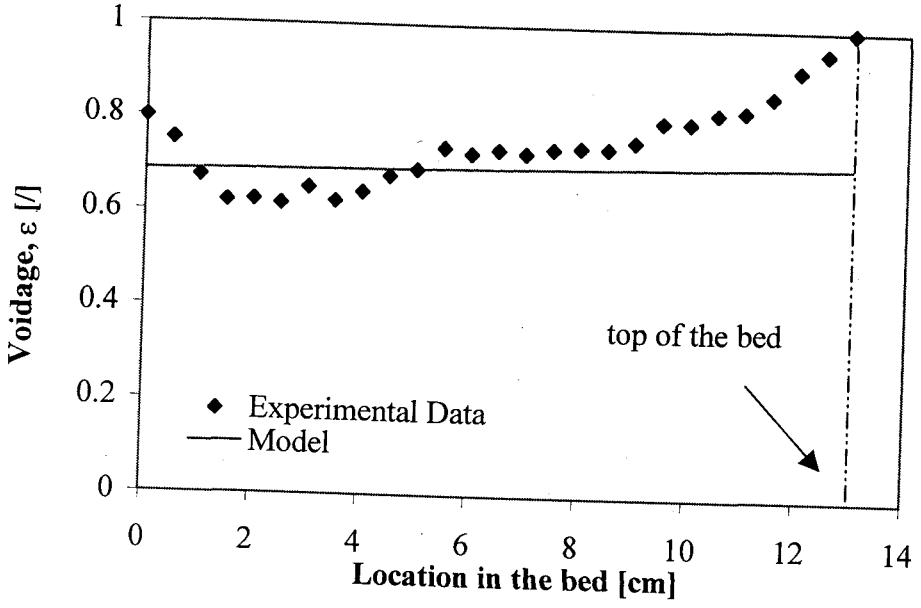

Figure 5-13: The voidage distribution of particle A in the MAFB ($\frac{dH}{dz}$ = - 20,543 A/m/m, U_0 = 0.0199 m/s and the bed height = 0.130 m)

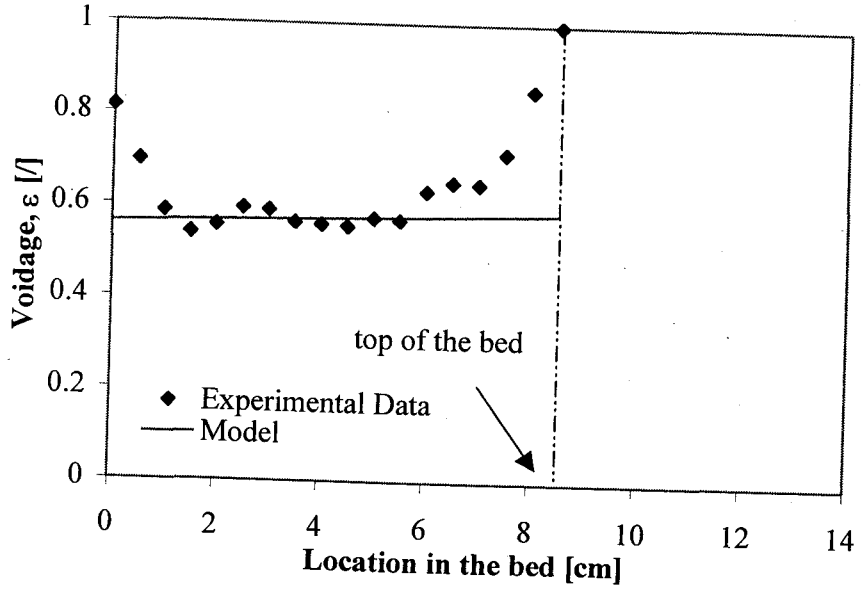

Figure 5-14: The voidage distribution of particle A in the MAFB ($\frac{dH}{dz}$ = - 33,798 A/m/m, U_0 = 0.0153 m/s and the bed height = 0.085 m)

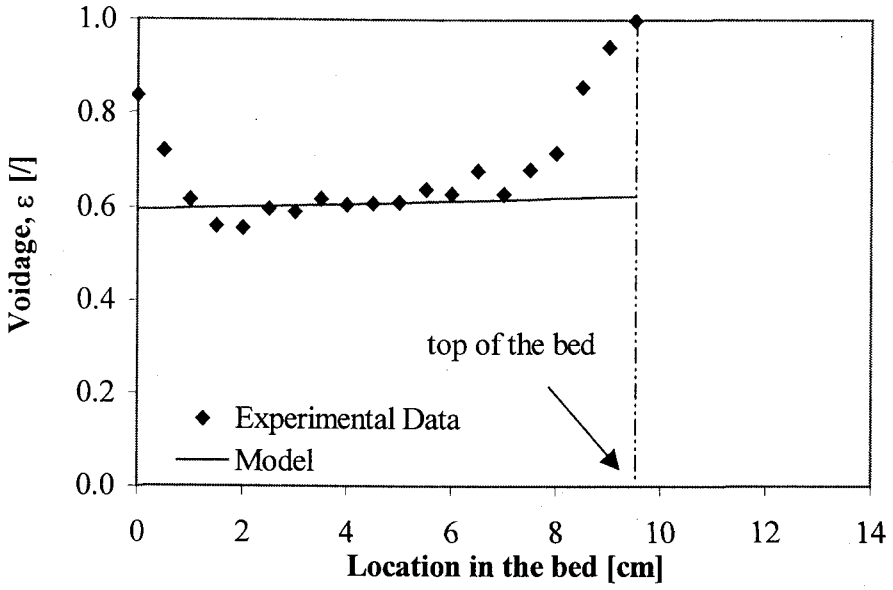

Figure 5-15: The voidage distribution of particle A in the MAFB ($\frac{dH}{dz}$ = - 33,798 A/m/m, U_0 = 0.0176 m/s and the bed height = 0.095 m)

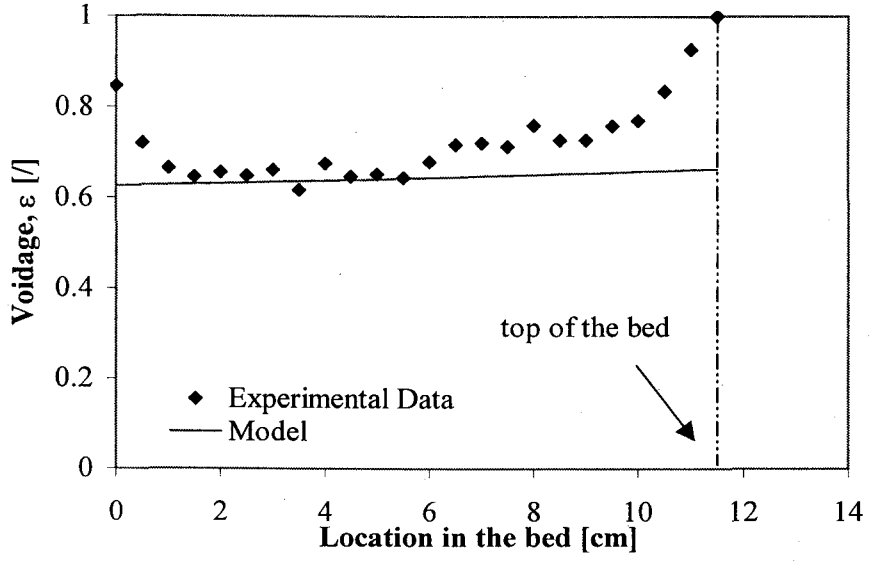

Figure 5-16: The voidage distribution of particle A in the MAFB ($\frac{dH}{dz}$ = - 33,798 A/m/m, U_0 = 0.0199 m/s and the bed height = 0.115 m)

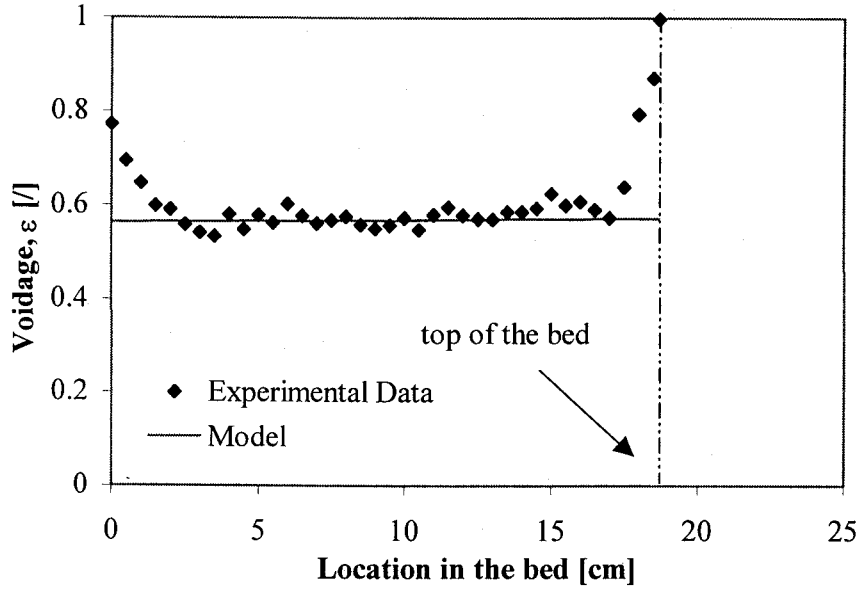

Figure 5-17: The voidage distribution of particle B in the MAFB ($\frac{dH}{dz}$ = - 14,663 A/m/m, U_0 = 0.0222 m/s and the bed height = 0.187 m)

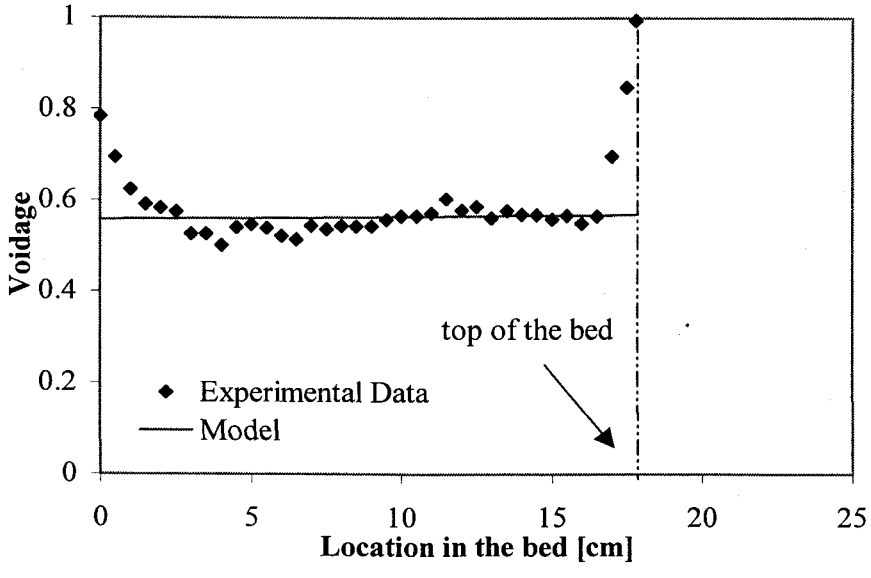

Figure 5-18: The voidage distribution of particle B in the MAFB ($\frac{dH}{dz}$ = - 18,289 A/m/m, U_0 = 0.0222 m/s and the bed height = 0.178 m)

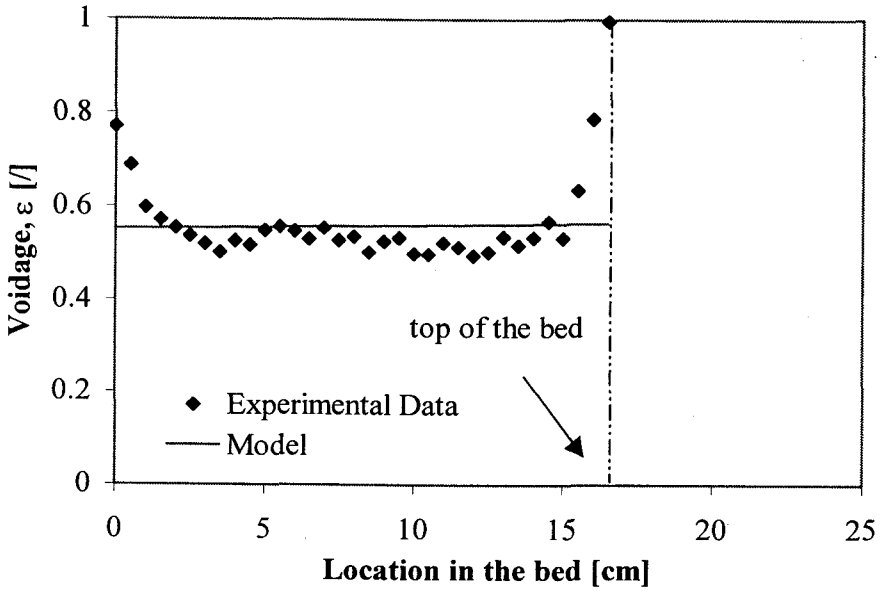

Figure 5-19: The voidage distribution of particle B in the MAFB ($\frac{dH}{dz}$ = - 20,543 A/m/m, U_0 = 0.0222 m/s and the bed height = 0.165 m)

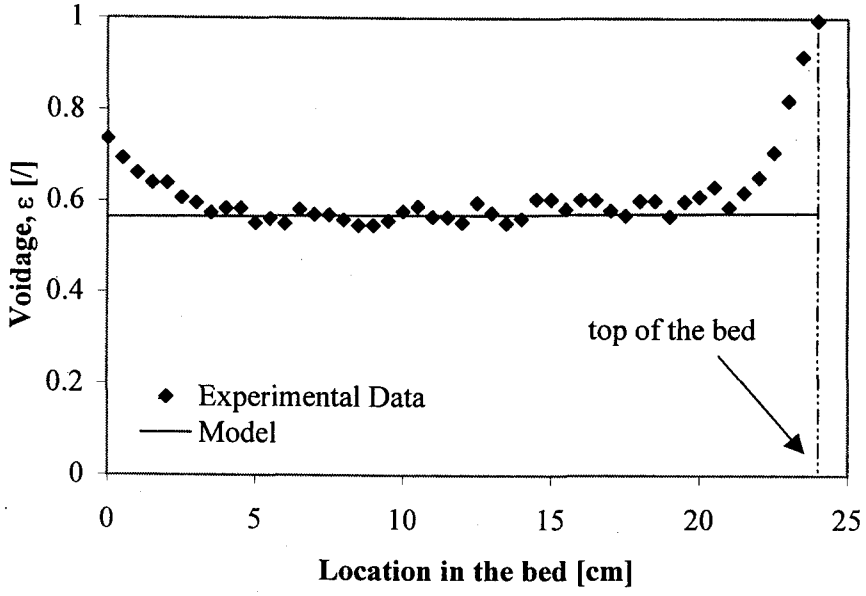

Figure 5-20: The voidage distribution of particle B in the MAFB ($\frac{dH}{dz}$ = - 14,663 A/m/m, U_0 = 0.0222 m/s and the bed height = 0.240 m)

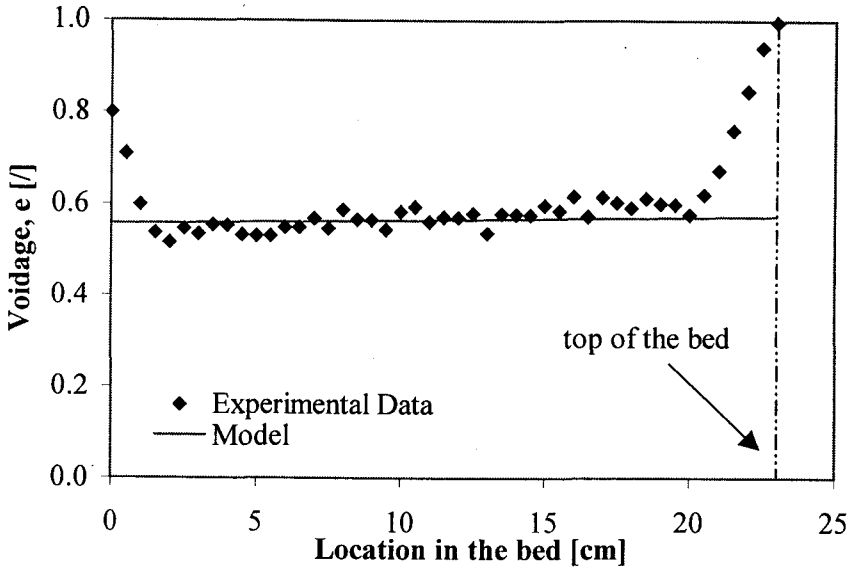

Figure 5-21: The voidage distribution of particle B in the MAFB ($\frac{dH}{dz}$ = - 18,289 A/m/m, U_0 = 0.0222 m/s and the bed height = 0.230 m)

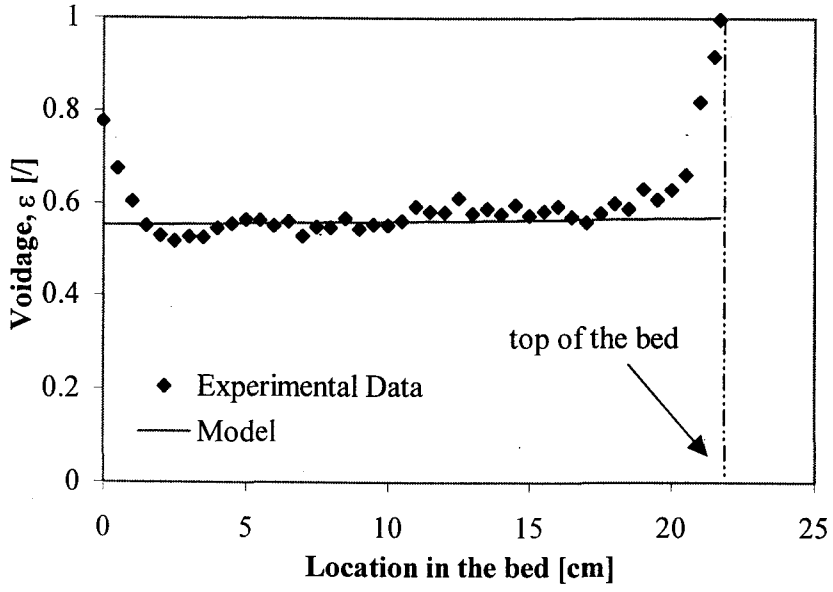

Figure 5-22: The voidage distribution of particle B in the MAFB ($\frac{dH}{dz}$ = - 20,543 A/m/m, U_0 = 0.0222 m/s and the bed height = 0.217 m)

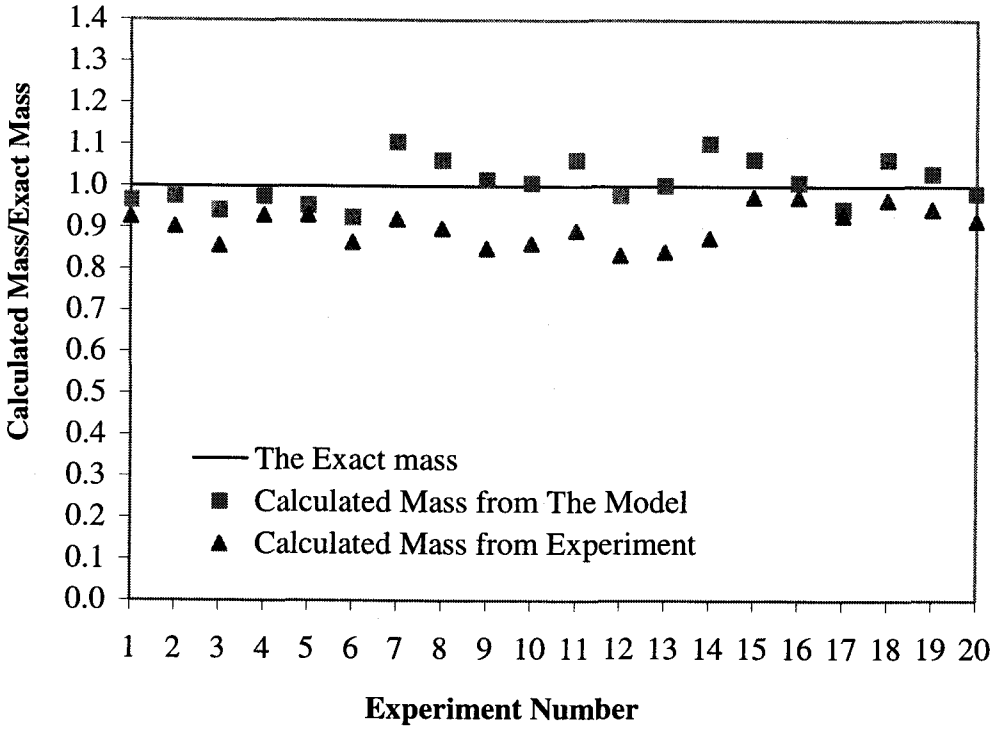

Figure 5-23: The comparison of the calculated mass obtained from the model and experiment with the exact mass

It is noted that the voidage in the region next to the distributor plate (z =0) has a high voidage (roughly 0.8) due to the fact that jets coming through the distributor plate exchange their momentum to the surrounding fluid and particles. Therefore, the particles next to the distributor plate move more vigorously than in other regions, consequently, the voidage is higher than expected. This effect is not captured by the modeling equations, and this is the reason for the difference between experimental observations and the model predictions in this region are observed.

The experiments also show that the voidage distribution at the top of the bed gradually increases and deviates from the model prediction. This phenomenon reflects our inability to determine the exact position of the top of the bed, the boundary between the bed and the particle-void space. Furthermore, at the top of the bed particles are in the vicinity of the level where the magnetic force can no longer equalize the balance of forces. At this "horizon event" level, the compensatory mechanism of the increase of the bed voidage (reduce the interstitial velocity to reduce drag force) is almost depleted, and voidage is close to $\varepsilon \approx 1$. Beyond the horizon event level, fluidization does not exist any more and all particles which are brought in this region are swept away (elutriated).

In addition, at higher values of ε the momentum exchange between particles drop substantially because the number of collision between particles is dramatically reduced. Although the net momentum exchange between adjacent particle layers, according to our model, is assumed to be negligible, this mechanism provides dampening effects on all secondary and tertiary instabilities/disturbances which normally occur in any fluidization bed. Therefore, the random intrusion of secondary and tertiary effects in the top region of the bed are less dampened, and consequently they can be observed as fluctuation of the bed height. At the horizon level, the instability effects are predominant and out of check. Somewhat improved conditions for the suppression of the secondary and tertiary instability can be expected if the geometry of the column is altered like the tapered column in the 0 g experiments. Our modeling equations do not provide terms accommodating for these instabilities and it

is natural to expect that the experimental observations at the top of the bed will deviate from model predictions.

5.3 Experiments on Board The NASA KC-135 Plane

In the experiments performed in the zero-g environment on board the NASA-KC135, the height of the bed is the only measured parameter, for different flow rates and magnetic field strength. The magnetic field intensity used in the zero-g experiment is kept constant for all experiments and it is provided in Appendix E. The fluid flow rate, the field intensity and the field gradient are the only three parameters needed to calculate the voidage distribution using the equation developed earlier,

$$0=\frac{1.75}{\varepsilon^3}\left(\frac{d_p U_0 \rho_f}{\mu}\right)^2+\frac{150(1-\varepsilon)}{\varepsilon^3}\left(\frac{d_p U_0 \rho_f}{\mu}\right)+\frac{\mu_0 \rho_f d_p^3}{\mu^2}\chi H_z \frac{dH_z}{dz} \qquad (4\text{-}12)$$

Notice that there are no empirical adjustable parameters in the model in equation (4-12). Because of the change in cross-sectional area of the bed, the superficial fluid velocity at any location in the bed can be defined as,

$$U_0(z)=\frac{U_0(0)}{\left(1+\frac{2h\tan\theta}{x_0}\right)} \qquad (5\text{-}1)$$

where $\tan\theta$ is the slope of the fluidization column and x_0 is the width of the fluidization column at $h=0$.

The model prediction of the voidage distribution and the bed height in the MAFB in the zero-g condition, including the experimentally observed bed heights is shown in Figure 5-24 to 5-30. The height of the bed obtained from the model prediction is compared to the height of the bed obtained experimentally (Figure 5-31). In addition, the calculated total mass of particles in the bed, using the model predicted voidage distribution, is compared to the exact mass of particles in the bed (Figure 5-32)

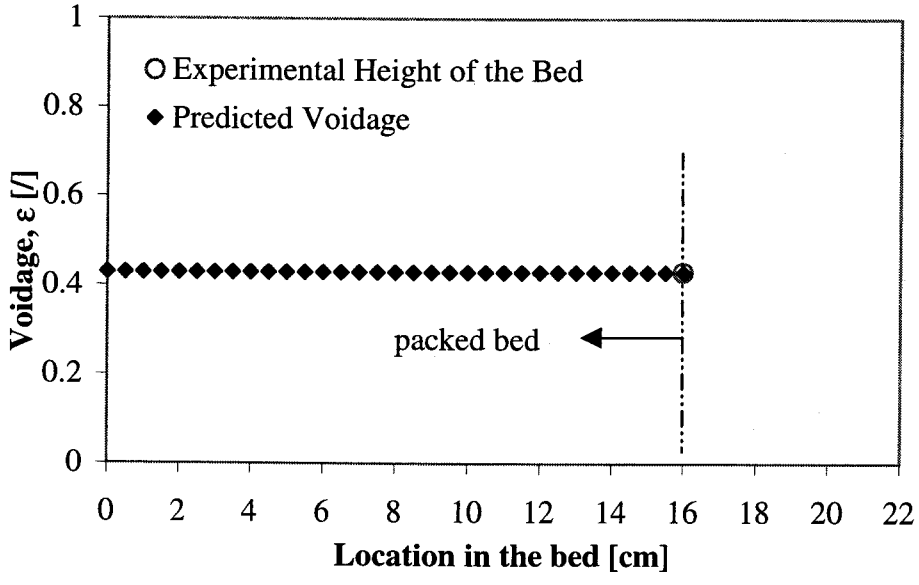

Figure 5-24: The prediction of the voidage distribution of particle C in the zero-g condition ($U_{0(bottom)}$ = 0.0000 m/s, d_p = 0.0024 m, and h = 0.160 m)

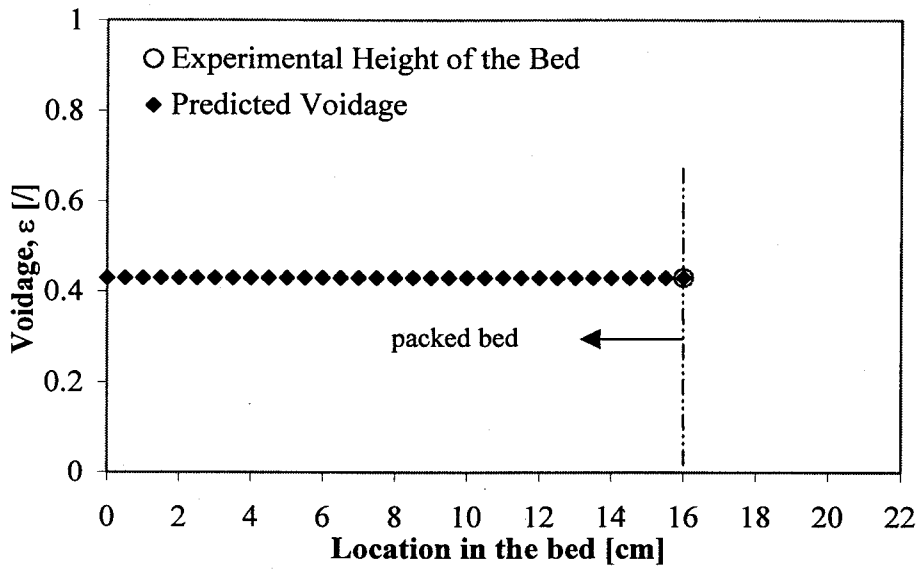

Figure 5-25: The prediction of the voidage distribution of particle C in the zero-g condition ($U_{0(bottom)}$ = 0.0010 m/s, d_p = 0.0024 m, and h = 0.160 m)

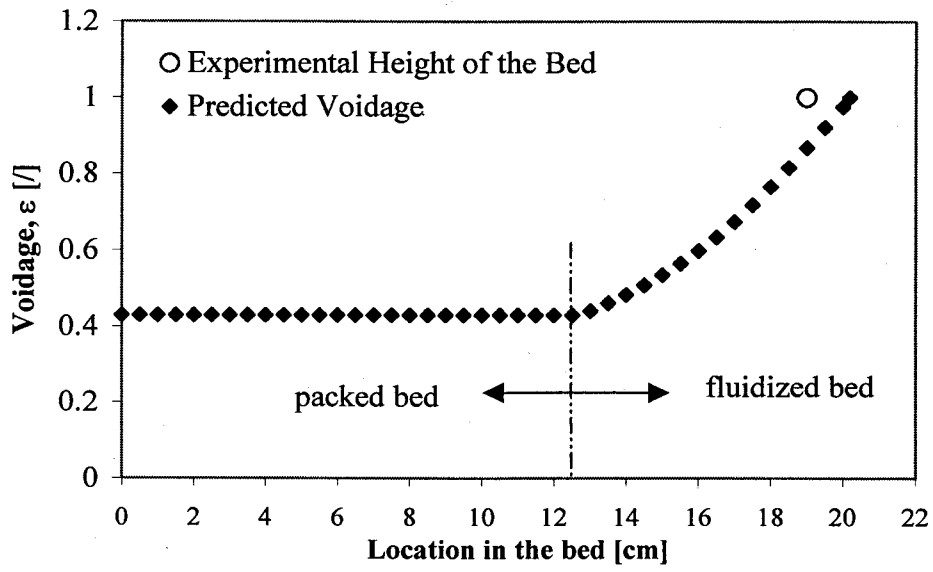

Figure 5-26: The prediction of the voidage distribution of particle C in the zero-g condition ($U_{0(bottom)}$ = 0.0055m/s, d_p = 0.0024 m, and h = 0.202 m)

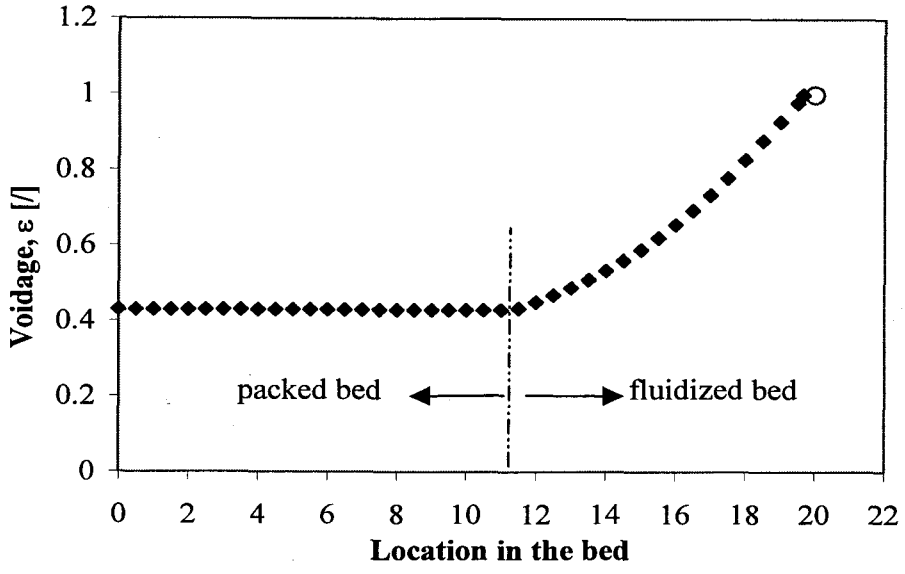

Figure 5-27: The prediction of the voidage distribution of particle C in the zero-g condition ($U_{0(bottom)}$ = 0.0076m/s, d_p = 0.0024 m, and h = 0.197 m)

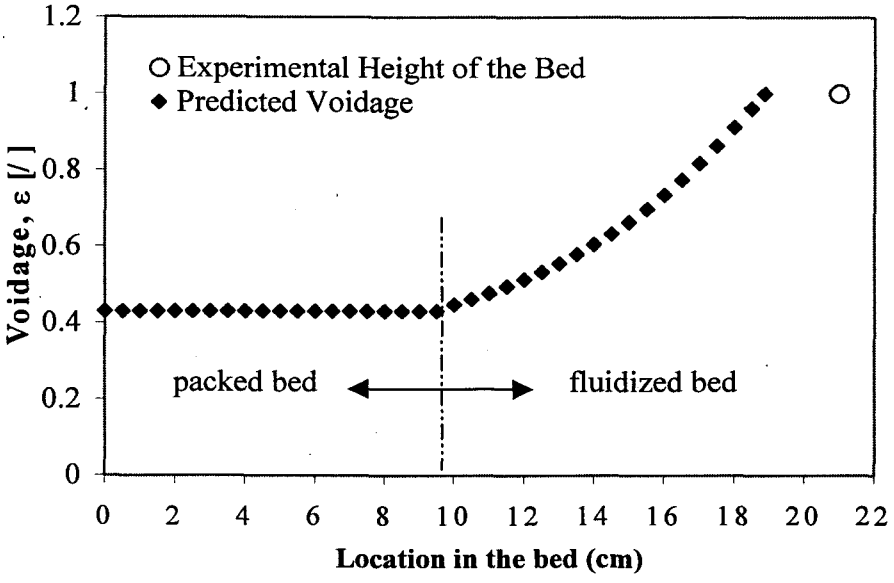

Figure 5-28: The prediction of the voidage distribution of particle C in the zero-g condition ($U_{0(bottom)}$ = 0.0110 m/s, d_p = 0.0024 m, and h = 0.189 m)

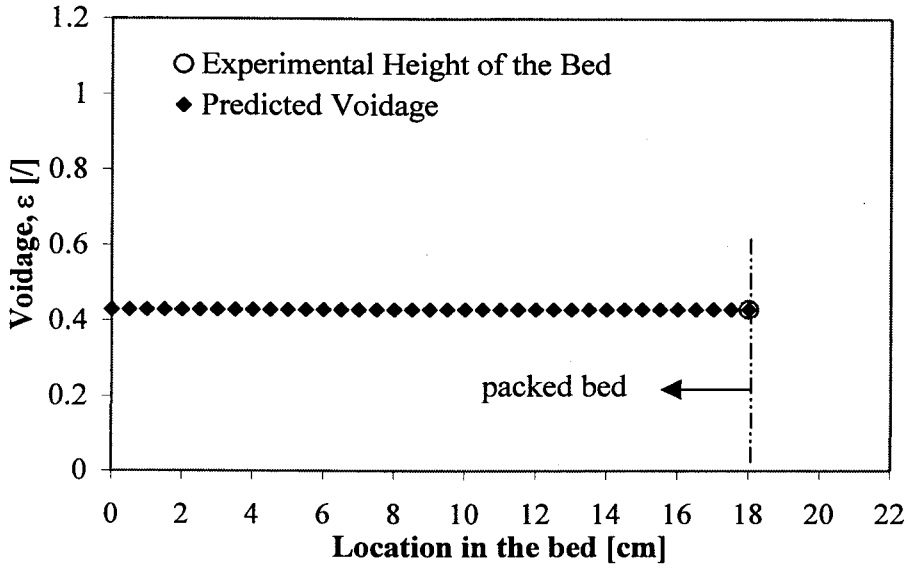

Figure 5-29: The prediction of the voidage distribution of particle D in the zero-g condition ($U_{0(bottom)}$ = 0.0000 m/s, d_p = 0.0015 m, and h = 0.180 m)

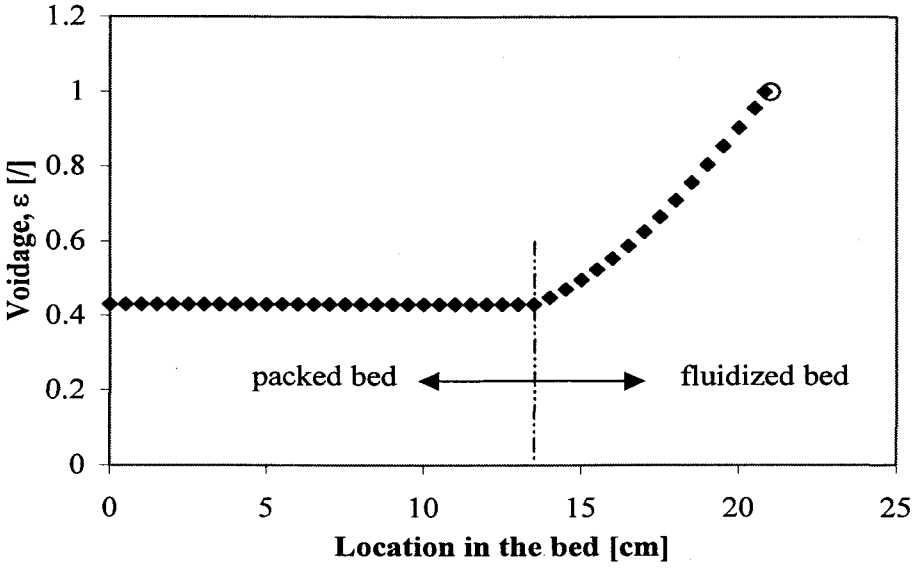

Figure 5-30: The prediction of the voidage distribution of particle D in the zero-g condition ($U_{0(bottom)}$ = 0.0010 m/s, d_p = 0.0015 m, and h = 0.208 m)

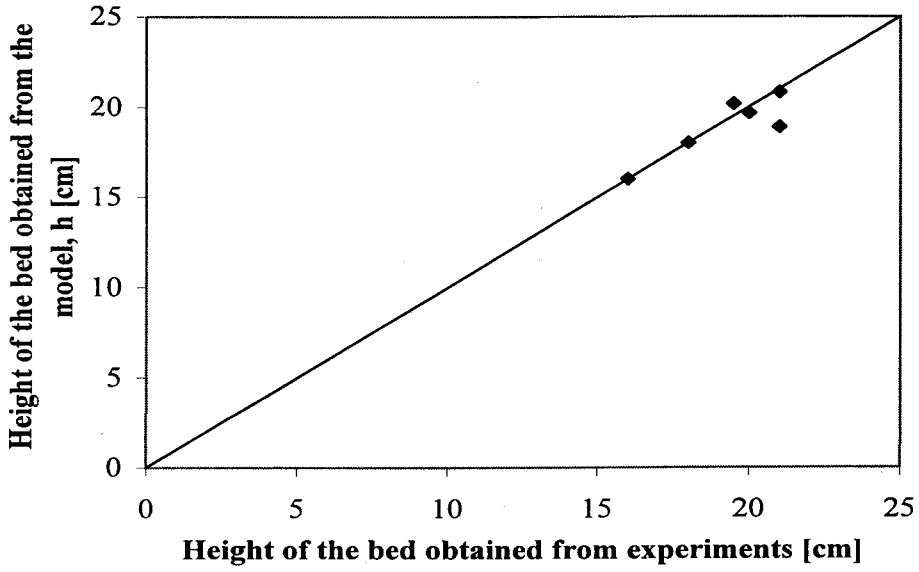

Figure 5-31: The comparison between the height of the bed obtained from the model and the height of the bed obtained from experimental observations

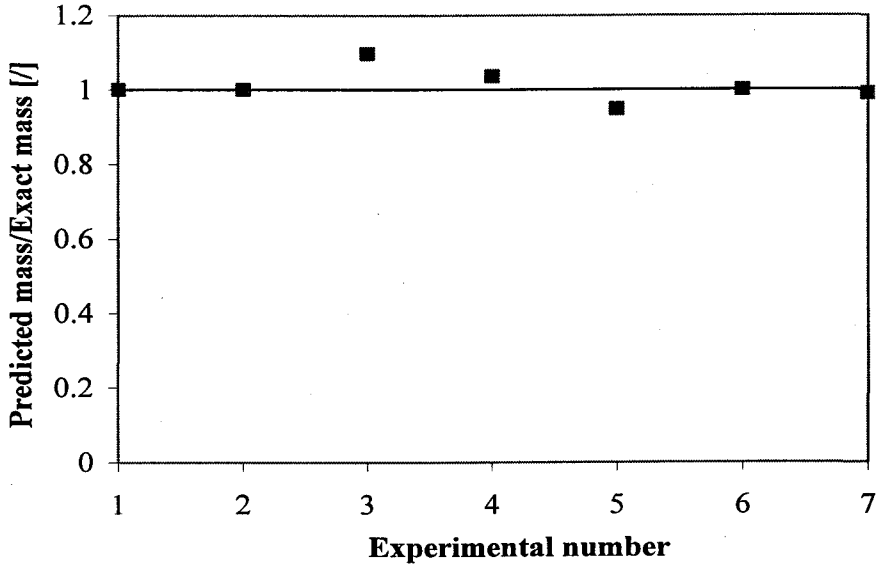

Figure 5-32: The comparison between the predicted mass and the exact mass of particles in the bed

It is noted in the zero-g experiment that all particles are not completely fluidized. Some particles are packed at the bottom of the bed up to a certain height due to the strength of the magnetic force in that region. The magnetic force is stronger than the drag force from the fluid. Particles will start to fluidize at the location where the drag force is in equilibrium with the magnetic force.

5.4 Discussion

From the experimental data and the mathematical model described above, we can conclude the following:

1. The magnetic force due to the gradient of the magnetic field plays a significant role in controlling the height of the fluidized bed. As shown in Figure 5-1, the height of the bed, at any given fluid velocity, decreases as the field intensity and the field gradient increase. As a result, the average bed porosity will decrease as the magnetic field intensity and field gradient increase, for any given superficial fluid velocity. Al-Mulhim (1995) and Rhee (1998) proved that decreasing the bed voidage will result in a better particle-fluid mass transfer. Therefore, based on observed behavior, one may conclude that observed behavior of the magnetically fluidized bed will also enhance the mass transfer rate and improve the chemical conversion.

2. We successfully predicted the voidage distribution in the MAFB in both zero-g condition and in normal 1g conditions. The proposed model describes very

well the experimental data (no experimentally fitted proposed). The overall accuracy of the model is verified by comparing the mass obtained from the voidage distribution predicted by model to the actual mass, and it falls within 11% error. It is noted that the calculated mass from the laboratory experiments is lower than the exact mass. The calculated mass from the laboratory experiment is based on the dynamic pressure drop which is difficult to measure and may involve an error up to 18%. Furthermore, particles exchange momentum with the column wall and the distributor plate. This undoubtedly reduces the dynamic pressure drop. Therefore, the calculated mass from experiment is always lower than the actual mass.

CHAPTER 6
CONCLUSION AND RECOMMENDATIONS

6.1 Conclusion

The experiments with the Magnetically Assisted Fluidized Bed in a non-uniform magnetic field showed that the magnetic force plays an important role in controlling the bed voidage and the height of the bed:

- at a given magnetic field intensity, H_z, and field gradient, $\frac{dH_z}{dz}$ = constant, the height of the bed will increase as the superficial fluid velocity increases,
- at a given fluid superficial velocity, U_0, the height of the bed, h, will decrease as the magnetic field intensity and its gradient increase.

The magnetic force is dependent on the magnetic field intensity and the field gradient. In our experiment, the magnetic field gradient is kept constant and the magnetic field intensity varies from the top to the bottom of the column. The magnetic field intensity is greatest at the bottom of the column and it gradually decreases toward the top of the column. The magnetic force acting on particles, therefore, is highest at the bottom and decreases with the height of the bed. As a result, the particle holdup (voidage) in any location in the bed must change to compensate for the change of magnetic force, which means the voidage at any location in the bed must change as well.

The voidage distribution model developed in this study is based on the four governing equations, namely, the equation of motion and the equation of continuity in both liquid and particle phases.

The resulting expression of the voidage distribution is given as,

$$\frac{d_p^3 \rho_f (\rho_p - \rho_f) g_z}{\mu^2} = \frac{1.75}{\varepsilon^3}\left(\frac{d_p U_0 \rho_f}{\mu}\right)^2 + \frac{150(1-\varepsilon)}{\varepsilon^3}\left(\frac{d_p U_0 \rho_f}{\mu}\right) + \frac{\mu_0 \rho_f d_p^3}{\mu^2} \chi H_z \frac{dH_z}{dz} \tag{4-11}$$

This voidage modeling, which does not contain any adjustable parameter, fit our experimental data very convincingly and the calculated mass of particles from the model deviates from the true mass less than 11%.

The experiemts in zero-g conditions on board the NASA KC-135 plane also proved that the magnetic force has a significant role in keeping the particles from extruding out of the bed. Without the magnetic force, it is impossible to have fluidization in space. The voidage distribution model in zero-g conditions is obtained simply by canceling the g term in equation (4-11). The resulting model is expressed as,

$$0 = \frac{1.75}{\varepsilon^3}\left(\frac{d_p U_0 \rho_f}{\mu}\right)^2 + \frac{150(1-\varepsilon)}{\varepsilon^3}\left(\frac{d_p U_0 \rho_f}{\mu}\right) + \frac{\mu_0 \rho_f d_p^3}{\mu^2} \chi H_z \frac{dH_z}{dz} \tag{4-12}$$

Because of the lack of the pressure drop data measured in 0g environment, only the overall bed height and the calculated mass from the predicted voidage are compared with the experimentally observed height and with the true mass of particles. Both show good agreement with less than 10% error.

The experimental observation of the fluidized bed in laboratory experiments is found to coincide well with the zero-g experiments conducted on the reduced gravity NASA KC-135 plane.

Three fluidization regions are observed in both types of experiments. The first is the region next to the distributor plate where the particles move more vigorously due to the exchange of momentum from the fluid jets to adjacent fluid and particles. The second is the place where the particles are packed and have no movement due to the fact that the magnetic force is higher than the drag force. The third is the region where the particles are fluidized smoothly and all forces are in equilibrium. In most of our laboratory studies, the second region is eliminated by carefully choosing the appropriate fluid flow rate and the magnetic field intensity.

6.2 Recommendations:

For further studies, the following points are recommended:

1. In our modeling development, the particle pressure and particle stress tensor are neglected. In this study, particles are large enough to justify neglecting the influence of the interparticle forces on the voidage distribution. To cover the entire range of particle size and to enhance the correctness of the voidage distribution model, the terms that are omitted in this study, P_p and τ_p, should be also investigated. Although these terms have been neglected in this study, they may have an important role when small particles (below $100\,\mu$ m) are fluidized. Moreover, in the absence of gravity, these terms may have an even more significant effect on the behavior of the bed.
2. In this study, the change of voidage distribution in the r direction due to the change of the magnetic force in that direction is negligible. However, one may want to investigate the variation of voidage in both the r and z directions.
3. To solve the governing equations for the voidage distribution which include other possible terms, including secondary and tertiary effects, one may consider using Computational Fluid Dynamic (CFD) software, which has recently advance to quite a sophisticated level.
4. One may include the modeling of the fluid jets in the equation of motion for the fluid and particle phases.

BIBLIOGRAPHY

Al-Mulhim, Mohammed, "Enchancement of Mass Transfer Coefficient in a Magnetically Stabilized Liquid-Solid Fluidized Bed.", M.S. thesis, Oregon State University, September 1995.

Anderson, T.B.and Roy Jackson, "A Fluid Mechanical Description of Fluidized Bed.", I&EC Fundamentals, Vol 6, No. 4, November 1967.

Arnoldos, J., J. Casal, A. Lucus and L.Puigjaner, "Magnetically Stabilized Fluidization: Modeling and Application to Mixture.", Power Technology, 1985

Burns Mark A. and Graves David J., "Continuous Affinity Chromatography Using a Magnetically Stabilized Fluidized Bed.", Biotechnology Progress, 1 (No.2), 1985

Burns Mark A. and Graves David J., "Structural Studies of A Liquid-Fluidized Magnetically Stabilized Bed.", Chem. Eng. Comm., 67 (1988)

Chemical Engineering Flight Team, Oregon State University, "The Study of Fluidization of Ferromagnetic Beads in The Magnetically Assisted Fluidized Bed in Micro&Variable Gravity.", Final Report, June, 2000

Conan J.Fee, "Stability Of The Liquid-Fluidized Magnetically Stabilized Fluidized Bed", AIChe Journal, Vol. 42, No. 5, May 1996

Cowley, M.D., and Rosensweig, R.E., Journal of Fluid Mech., 1967

Crowe, Clayton, Martin Sommerfeld and Yutaka Tsuji, Multiphase Flows with Droplets and Particles, CRC Press, 1998

Ergun, S., "Fluid Flow through Packed Columns.", Chem. Eng. Prog. 48, (1952)

Giadspow, D.,"Multiphase Flow and Fluidization, Academic Press, San Diego, 1994

Hristov, Jordan Y.,"Fluidization of Ferromagnetic Particles in a Magnetic Field Part 1: The Effect of Field Line Orientation on Bed Stability", Powder Technoloby, No.87, 1996

J.H Segell,"Liquid-Fluidized Magnetically Stabilized Beds.", Powder Technology, No.52, 1987

Jovanovic, Goran, Thana Sornchamni, Seung Yoo, James E. Atwater, James R. Aske , Jeffrey L. DeHart and John W. Fisher, " Magnetically Assisted Gasification of Solid Waste", 29th International Conference on Environmental Systems, Denver, Colorado, 1999, paper 1999-01-2183

Kunii, Daizo and Octave Levenspiel, Fluidization Engineering, second edition, Butterworth-Heinemann, Newton, MA, 1991.

Zhu, Qingshan and Hongzhong Li, "Study on Magnetic Fluidization of Group C Powders", Powder Technology, 86, 1995

R.Jackson, "Hydrodynamic Stability of Fluid-Particles Systems, Fluidization 2nd Edition, edited by J.F. Davidson, R.Clift and D.Harrison, Academic Press, 1985

Rhee, Brian Kanghee,"Enhancement of Mass Transfer Coefficient in A Three-Phase Magnetic Stabilized Fluidized Bed.", M.S. thesis, Oregon State University, February 1998.

Rietema, K and Musters, S.M.D. "The Effect of Interparticle Forces on The Expansion of A Homogeneous Gas-Fluidized Bed.", Powder Technology, Vol 18, 1977

Rietema, K and H.W. Piepers, "The Effect of Interparticle Forces on The Stability of Gas-Fluidized Beds-I. Experimental Evidence.", Chemical Engineering Science, Vol 45, No. 6, 1990

Rietema, K., E.J.E. Cottaar and H.W. Piepers, "The Effect of Interparticle Forces on The Stability of Gas-Fluidized Beds-II Theoretical Derivation of Bed Elasticity on The Basis of Van Der Waals Forces between Power Particles.", Chemical Engineering Science, Vol. 48, No. 9, 1993

Rosensweig, Ronald E., "Magnetic Stabilization of The State of Uniform Fluidization.", Ind. Eng. Chem. Fundam.,Vol 18, No. 3, 1979

Rosensweig, R.E., M. Zahn, W.K. Lee and PS. Hagan, "Theory and Experiments In The Mechanics Of Magnetically Stabilized Fluidized Solids.", 1983

Resensweig, R.E, "Precess Concepts Using Field-Stabilized Two Phase Fluidized Flow.", Journal of Electrostatics, Elsevier Science B.V., 1995

Saxena S.C. and S. Shrivastava. "Some Hydronamic Investigations of A Magnetically Stabilized Air-Fludized Bed of Ferromagnetic Particles", Powder Technology, 64, 1991

Sergeev, Yu. A. and D.A. Dobritsyn, "Linear, Nonlinear Small-Amplitude, Steady and Shock Waves in Magnetically Stabilized Liquid-Solid and Gas-Solid Fluidized Beds.", Int. J. Multiphase Flow, Vol. 21, No.1, 1995

Siegell, J. H,"Liquid-Fluidized Magnetically Stabilized Beds", Powder Technology, 52, 1987

Terranova Brenda E. and Burns Mark A., "Continuous Cell Suspension Processing Using Magnetically Stabilized Fluidized Beds.", Biotechnology and Bioengineering, No.37, 1991

Wu, W.Y., A. Navada and S.C. Saxena, "Hydrodynamic Character of A Magnetically Stabilized Air Fluidized Bed of An Admixture of Magnetic and Non-Magnetic Particles.", Power Technology, 1997

APPENDICES

APPENDIX A
THE DERIVATION OF THE MASS AND MOMENTUM CONSERVATION EQUATIONS FOR THE MAFB

A.1 The mass conservation equations

A.1.1 The mass conservation equation for the fluid phase

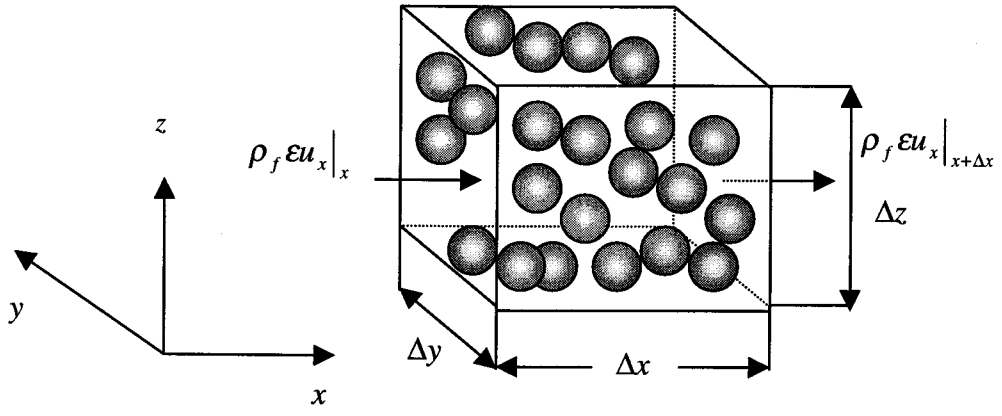

Figure A-1: A stationary volume element $\Delta x \Delta y \Delta z$ through which fluid and particles are flowing

Consider the pair of faces perpendicular to the x-axis. The rate of mass in through the face at x is $(\rho_f \varepsilon u_x)\big|_x \Delta y \Delta z$ and the rate of mass out through the face at $x+\Delta x$ is $(\rho_f \varepsilon u_x)\big|_{x+\Delta x} \Delta y \Delta z$. Similar expressions may be written for the other two pairs of faces.

Hence, a mass balance over a stationary volume element $\Delta x \Delta y \Delta z$ can be presented as the following:

{rate of mass accumulation}={rate of mass input}-{rate of mass output} (A-1)

$$\frac{\partial \rho_f \varepsilon \Delta x \Delta y \Delta z}{\partial t} = \Delta y \Delta z \left[\left(\rho_f \varepsilon u_x \right)_x - \left(\rho_f \varepsilon u_x \right)_{x+\Delta x} \right] + \Delta x \Delta z \left[\left(\rho_f \varepsilon u_y \right)_y - \left(\rho_f \varepsilon u_y \right)_{y+\Delta y} \right]$$

$$+ \Delta y \Delta z \left[\left(\rho_f \varepsilon u_z \right)_z - \left(\rho_f \varepsilon u_z \right)_{z+\Delta z} \right] \quad \text{(A-2)}$$

By dividing Equation A-2 by $\Delta x \Delta y \Delta z$ and taking the limit as these dimensions approach zero, we will get

$$\frac{\partial \rho_f \varepsilon}{\partial t} = -\frac{\partial \rho_f \varepsilon u_x}{\partial x} - \frac{\partial \rho_f \varepsilon u_y}{\partial y} - \frac{\partial \rho_f \varepsilon u_z}{\partial z} \quad \text{(A-3)}$$

If ρ_f is constant, Equation A-2 can be reduced to

$$\frac{\partial \varepsilon}{\partial t} = -\frac{\partial \varepsilon u_x}{\partial x} - \frac{\partial \varepsilon u_y}{\partial y} - \frac{\partial \varepsilon u_z}{\partial z} \quad \text{(A-4)}$$

It may be written in the vector form as

$$\frac{\partial \varepsilon}{\partial t} + \nabla \cdot \varepsilon \mathbf{U} = 0 \quad \text{(A-5)}$$

A.1.2 The mass conservation equation for the particle phase

The particle phase is treated as a continuous phase, therefore, the equation of continuity for the particle phase was obtained in a similar fashion:

$$\frac{\partial (1-\varepsilon)}{\partial t} + \nabla \cdot (1-\varepsilon) \mathbf{V} = 0 \quad \text{(A-6)}$$

A.2 The momentum conservation equations

A.2.1 The momentum conservation equation for the fluid phase

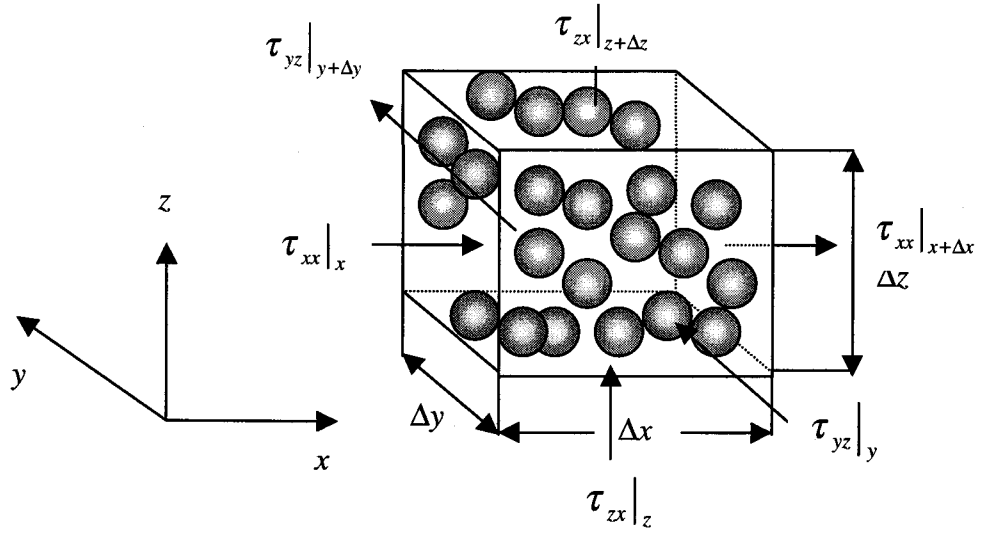

Figure A-2: A stationary volume element $\Delta x\Delta y\Delta z$ in which the x-momentum component is transported through the surface

The equation of motion for the liquid phase can be obtained as follows:

{rate of momentum accumulation}={rate of momentum in}-{rate of momentum out}

+ {sum of forces acting on fluid in the system}

(A-7)

In the x-direction, the momentum flows into and out of the control volume element by two mechanisms: convection (by virtue of the bulk fluid flow) and molecular transfer (by virtue of the velocity gradient)

The rate at which the x- momentum component comes in through the face at x by the convection flow is $\rho_f \varepsilon u_x u_x\big|_x \Delta y \Delta z$, and the rate at which it departs through the face at $x+\Delta x$ is $\rho_f \varepsilon u_x u_x\big|_{x+\Delta x} \Delta y \Delta z$. The rate at which it flows in at y is $\rho_f \varepsilon u_y u_x\big|_y \Delta x \Delta z$. Similar expression may be written for the other three faces.

Therefore, the net convective x-momentum entering into the volume element is

$$\Delta y \Delta z\left(\rho_f \varepsilon u_x u_x\big|_x - \rho_f \varepsilon u_x u_x\big|_{x+\Delta x}\right) + \Delta x \Delta z\left(\rho_f \varepsilon u_y u_x\big|_y - \rho_f \varepsilon u_y u_x\big|_{y+\Delta y}\right) + \Delta y \Delta z\left(\rho_f \varepsilon u_z u_x\big|_z - \rho_f \varepsilon u_z u_x\big|_{z+\Delta z}\right) \tag{A-8}$$

The rate at which the x-component of momentum enters through the face at x by molecular transport is $\tau_{xx}^{(f)}\big|_x \varepsilon \Delta y \Delta x$ and the rate at which the x-component of momentum depart through the face at $x+\Delta x$ is $\tau_{xx}^{(f)}\big|_{x+\Delta x} \varepsilon \Delta y \Delta x$. The rate at which it enters the face at y is $\tau_{yx}^{(f)}\big|_y \varepsilon \Delta x \Delta z$. The x-component of momentum for the remaining three faces can be obtained by similar expressions. The net x-momentum entering the volume element through molecular transported is

$$\varepsilon \Delta y \Delta z\left(\tau_{xx}^{(f)}\big|_x - \tau_{xx}^{(f)}\big|_{x+\Delta x}\right) + \varepsilon \Delta x \Delta z\left(\tau_{yx}^{(f)}\big|_y - \tau_{yx}^{(f)}\big|_{y+\Delta y}\right) + \varepsilon \Delta y \Delta z\left(\tau_{zx}^{(f)}\big|_z - \tau_{zx}^{(f)}\big|_{z+\Delta z}\right) \tag{A-9}$$

The important forces acting on the fluid in the control volume element are fluid pressure, P_f, the gravitational force, g. In addition, the fluid exerts a force on the particles in this control volume element. The sum of these forces is given by

$$\varepsilon\Delta y\Delta z\left(P^{(f)}\Big|_x - P^{(f)}\Big|_{x+\Delta x}\right) + \rho_f g_x \varepsilon\Delta x\Delta y\Delta z - F_{1x}\varepsilon\Delta x\Delta y\Delta z \qquad \text{(A-10)}$$

The rate of x-momentum accumulation within the element is

$$\frac{\partial\left(\rho_f u_x \varepsilon\Delta x\Delta y\Delta z\right)}{\partial t} \qquad \text{(A-11)}$$

Dividing the resulting equation by $\Delta x\Delta y\Delta z$ and taking the limit as Δx, Δy and Δz approach zero, we obtain

$$\frac{\partial\left(\rho_f \varepsilon u_x\right)}{\partial t} = -\left(\frac{\partial\left(\rho_f \varepsilon u_x u_x\right)}{\partial x} + \frac{\partial\left(\rho_f \varepsilon u_y u_x\right)}{\partial y} + \frac{\partial\left(\rho_f \varepsilon u_z u_x\right)}{\partial z}\right) - \varepsilon\left(\frac{\partial \tau_{xx}^{(f)}}{\partial x} + \frac{\partial \tau_{yx}^{(f)}}{\partial y} + \frac{\partial \tau_{zx}^{(f)}}{\partial z}\right)$$

$$-\varepsilon\frac{\partial P_x^{(f)}}{\partial x} + \rho_f \varepsilon g_x - F_{1x}\varepsilon \qquad \text{(A-12)}$$

We can obtain the y and z momentum components by using the same procedure.

$$\frac{\partial\left(\rho_f \varepsilon u_y\right)}{\partial t} = -\left(\frac{\partial\left(\rho_f \varepsilon u_x u_y\right)}{\partial x} + \frac{\partial\left(\rho_f \varepsilon u_y u_y\right)}{\partial y} + \frac{\partial\left(\rho_f \varepsilon u_z u_y\right)}{\partial z}\right) - \varepsilon\left(\frac{\partial \tau_{xy}^{(f)}}{\partial x} + \frac{\partial \tau_{yy}^{(f)}}{\partial y} + \frac{\partial \tau_{zy}^{(f)}}{\partial z}\right)$$

$$-\varepsilon\frac{\partial P_y^{(f)}}{\partial x} + \rho_f \varepsilon g_y - F_{1y}\varepsilon \qquad \text{(A-13)}$$

$$\frac{\partial\left(\rho_f \varepsilon u_z\right)}{\partial t} = -\left(\frac{\partial\left(\rho_f \varepsilon u_x u_z\right)}{\partial x} + \frac{\partial\left(\rho_f \varepsilon u_y u_z\right)}{\partial y} + \frac{\partial\left(\rho_f \varepsilon u_z u_z\right)}{\partial z}\right) - \varepsilon\left(\frac{\partial \tau_{xz}^{(f)}}{\partial x} + \frac{\partial \tau_{yz}^{(f)}}{\partial y} + \frac{\partial \tau_{zz}^{(f)}}{\partial z}\right)$$

$$-\varepsilon\frac{\partial P_z^{(f)}}{\partial x}+\rho_f\varepsilon g_z-F_{1z}\varepsilon \tag{A-14}$$

By combining Equation A-12 with A-14, we obtain the single vector equation

$$\frac{\partial(\rho_f\varepsilon\mathbf{U})}{\partial t}=-\nabla\rho_f\varepsilon UU-\varepsilon\nabla P^{(f)}-\varepsilon\nabla\cdot\tau^{(f)}+\rho_f\varepsilon\mathbf{g}-\varepsilon\boldsymbol{F_1} \tag{A-15}$$

With the aid of the equation of continuity, Equation (A-15) can be written as

$$\rho_f\varepsilon\frac{D\mathbf{U}}{Dt}=-\varepsilon\nabla P^{(f)}-\varepsilon\nabla\cdot\tau^{(f)}+\rho_f\varepsilon\mathbf{g}-\varepsilon\boldsymbol{F_1}$$

$$\rho_f\varepsilon\left(\frac{\partial\mathbf{U}}{\partial t}+(\mathbf{U}\cdot\nabla)\mathbf{U}\right)=-\varepsilon\nabla P_f-\varepsilon\nabla\cdot\tau+\rho_f\varepsilon\mathbf{g}-\varepsilon\boldsymbol{F_1} \tag{A-16}$$

The stress tensors can be written in terms of the velocity gradients and fluid properties as follows:

$$\tau_{xx}^{(f)}=-2\mu\left(\frac{\partial u_x}{\partial x}\right)+\frac{2}{3}\mu(\nabla\cdot\mathbf{U})$$

$$\tau_{yy}^{(f)}=-2\mu\left(\frac{\partial u_y}{\partial y}\right)+\frac{2}{3}\mu(\nabla\cdot\mathbf{U})$$

$$\tau_{zz}^{(f)}=-2\mu\left(\frac{\partial u_z}{\partial z}\right)+\frac{2}{3}\mu(\nabla\cdot\mathbf{U})$$

$$\tau_{xy}^{(f)}=\tau_{yx}^{(f)}=-\mu\left(\frac{\partial u_x}{\partial y}+\frac{\partial u_y}{\partial x}\right)$$

$$\tau_{yz}^{(f)}=\tau_{zy}^{(f)}=-\mu\left(\frac{\partial u_y}{\partial z}+\frac{\partial u_z}{\partial y}\right)$$

$$\tau_{zx}^{(f)} = \tau_{xz}^{(f)} = -\mu\left(\frac{\partial u_z}{\partial x} + \frac{\partial u_x}{\partial z}\right) \tag{A-17}$$

A.2.1 The momentum conservation equation for the particle phase

By using the same analogy as that for the fluid phase, the momentum conservation equation for the particle phase can be given as

$$\rho_p(1-\varepsilon)\left(\frac{\partial \mathbf{V}}{\partial t} + (\mathbf{V}\cdot\nabla)\mathbf{V}\right) = -(1-\varepsilon)\nabla P_f - (1-\varepsilon)\nabla P_p - (1-\varepsilon)\nabla\cdot\tau_p$$
$$+ \rho_p(1-\varepsilon)\varepsilon\mathbf{g} + \varepsilon \boldsymbol{F}_I + \boldsymbol{F}_m \tag{A-18}$$

The term $\boldsymbol{F}_m$ is the magnetic force on the particles, and the term $(1-\varepsilon)\nabla P^{(f)}$ shown in the momentum conservation equation for particle phase is the buoyancy reaction of the fluid on the particles.

APPENDIX B
THE PRODUCTION OF FERROMAGNETIC PARTICLES

The following contents are the procedures for preparing particle A. Particle A is composed of the following materials:

Ferromagnetic Powder	20%
Microsphere Balloons	8%
1.75 % Sodium Alginate Solution	72%

In order to obtain the most uniform distribution of composition in the mixture, 100 g of the suspension is prepared for each production run. The preparation of the ferromagnetic sodium alginate is given by the following instructions:

1. First, weigh 70.74 g of water and pour it into a 250 cm^3 beaker. Place the beaker under the mixer.
2. Weigh 1.26 g of sodium alginate powder. Start mixing the water and slowly add sodium alginate powder into the beaker. Continue mixing until all of the alginate powder is dissolved into the water. This is the 1.75 % sodium alginate solution.
3. Weigh 20 g of ferromagnetic powder and 8 g of microsphere balloons and add them to sodium alginate solution in small increments.
4. Continue mixing all components for about 4 hours. When the suspension is perfectly mixed, pour it into the particle generator.

5. Repeat step 1 to 4 for particle B and C by using the weight percents of microsphere balloon and sodium alginate solution as shown in Table 2-1.

The particle production diagram is shown in Figure B-1

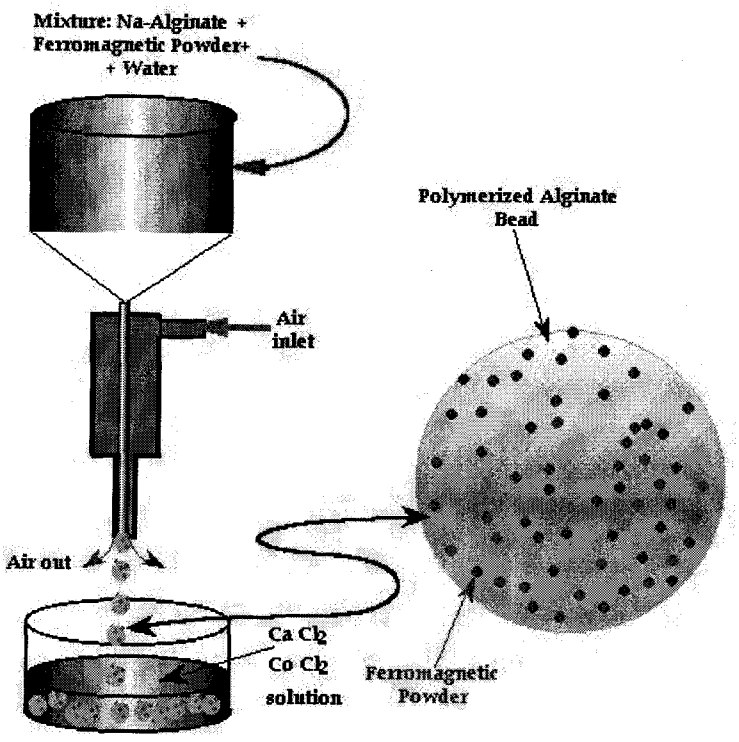

Figure B-1 The particle production schematic diagram

APPENDIX C
PROPERTIES OF MATERIALS

The physical and chemical properties of sodium alginate, ferromagnetic powder and microsphere balloons are tabulated as follows:

Table C-1: The Properties of Sodium Alginate Powder

Chemical Name	Algin (Sodium Alginate)
Chemical Family	Polysaccharide gum
Bulk Density	0.8 g/cm^3
pH 1% Solution	PH $\approx$ 7
Solubility in water	Soluble, forming a viscous solution, becoming a paste at a concentration of about 5%
Molecular Weight	Range from approx. 10,000 to 200,000 depending on viscosity

Table C-2: The Composition and Properties of Ferromagnetic Powder

Chemical Composition	$MnOFe_2O_3$ 45-70% Fe_2O_3 22-55% $FeOFe_2O_3$ 0-0.5%
Density (g/cm^3)	2.2
Median Particle Size (μm)	2
Surface Area (cm^2/g)	2.286
Moister %	0.01
Solubility in water	Negligible
Reactivity in water	Negligible
Melting Point	> 1500 C

Table C-3: The Physical and Chemical Properties of Microsphere Balloons

Chemical Compositions	SiO_2 70% Na_2O 25% B_2O_3 5%
Density (g/cm^3)	0.35
Median Particle Size (μ m)	55

Sodium alginate powder was donated by the NutraSweet Kelco Company and microsphere balloons are obtained from Emerson&Cuming.

APPENDIX D
CALIBRATION CURVES

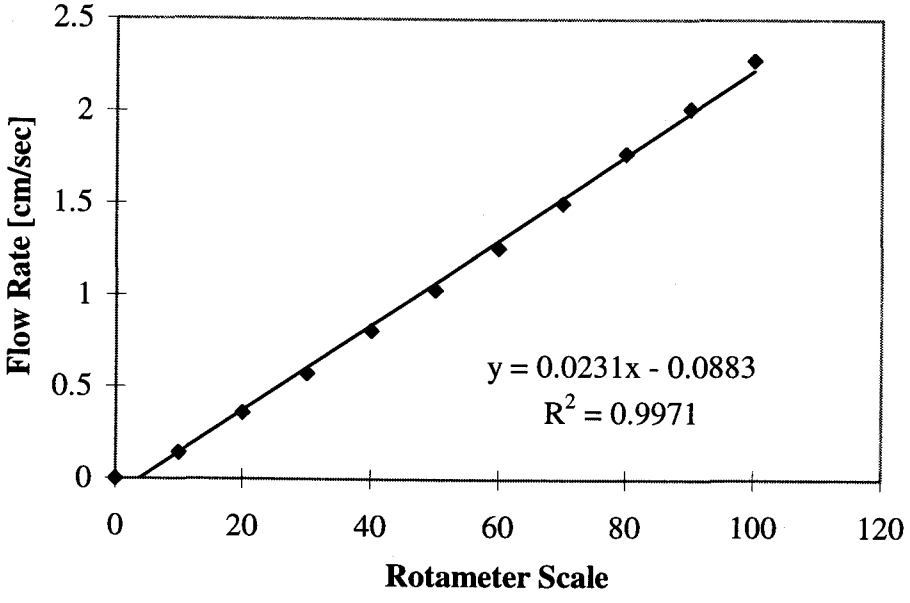

Figure D-1: Flow rotameter calibration curve used in laboratory experiments

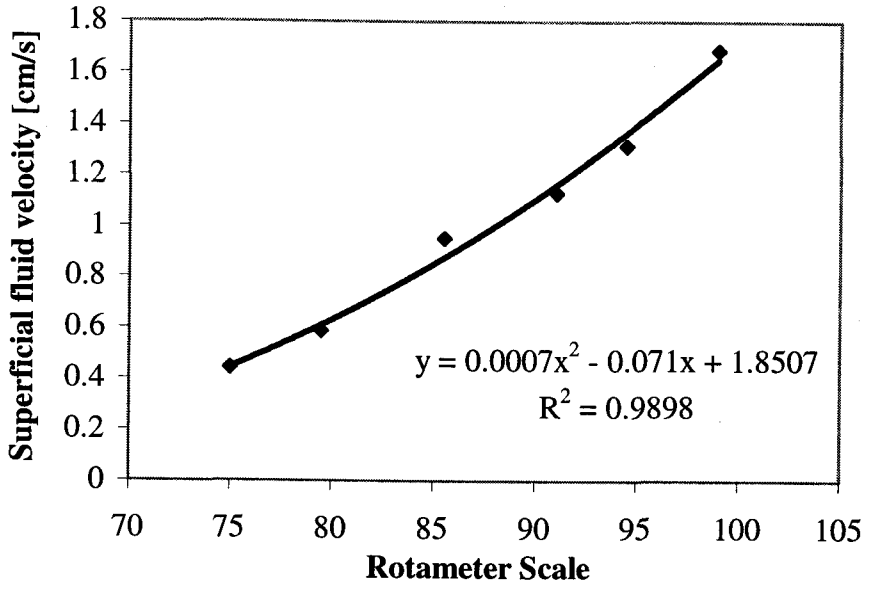

Figure D-2: Flow rotameter calibration curve used on board the NASA KC-135 plane

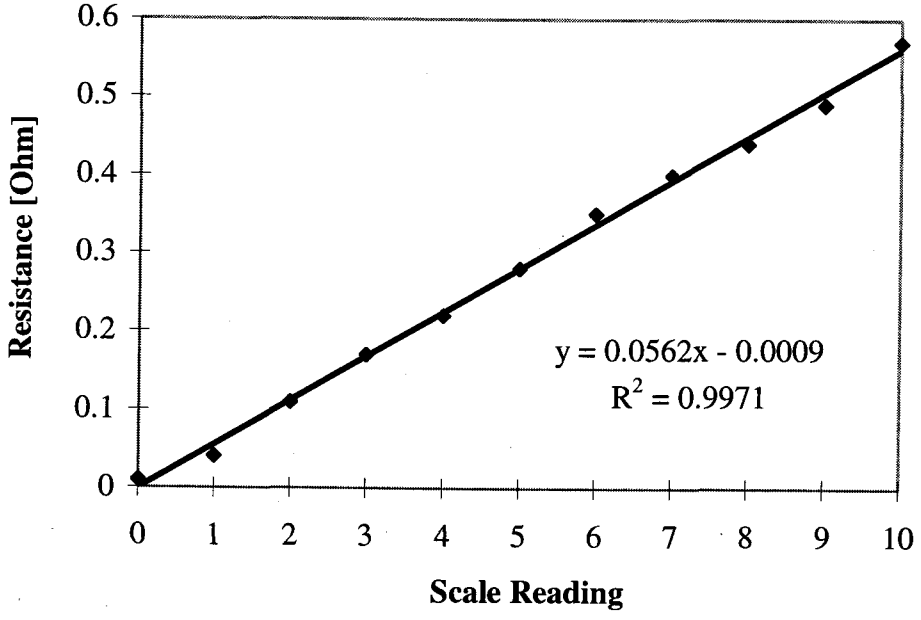

D-3: Rheostat resistance calibration curve

APPENDIX E
MAGNETIC FIELD INTENSITIES

The magnetic field intensities, in the bed, along the center line are measured at different voltages across the power supply.

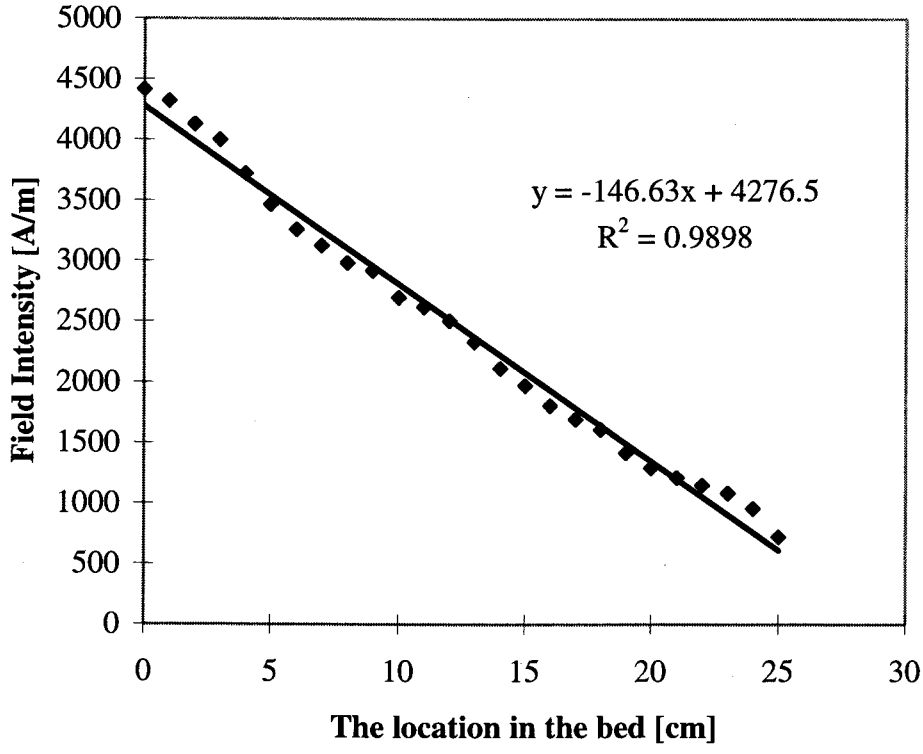

Figure E-1: The Magnetic field intensity in the bed used for the laboratory experiments (voltage setting on the power supply = 1.0 volt)

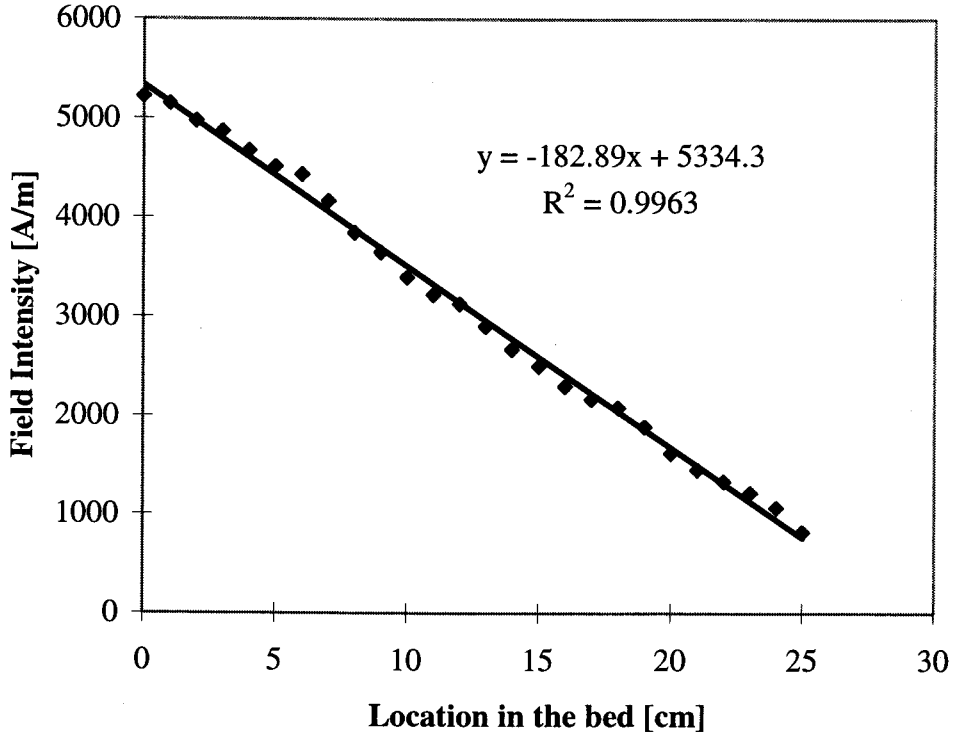

Figure E-2: The magnetic field intensity in the bed used for the laboratory experiments (voltage setting on the power supply = 2.0 volts)

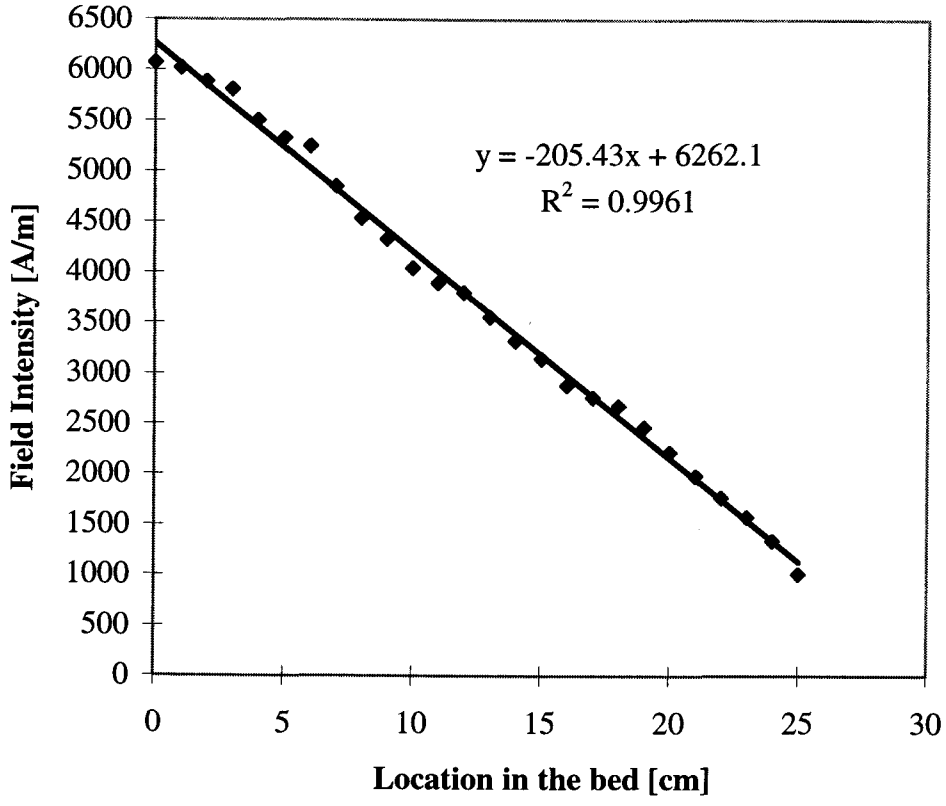

Figure E-3: The magnetic field intensity in the bed in used for the laboratory experiments (voltage setting on the power supply = 3.0 volts)

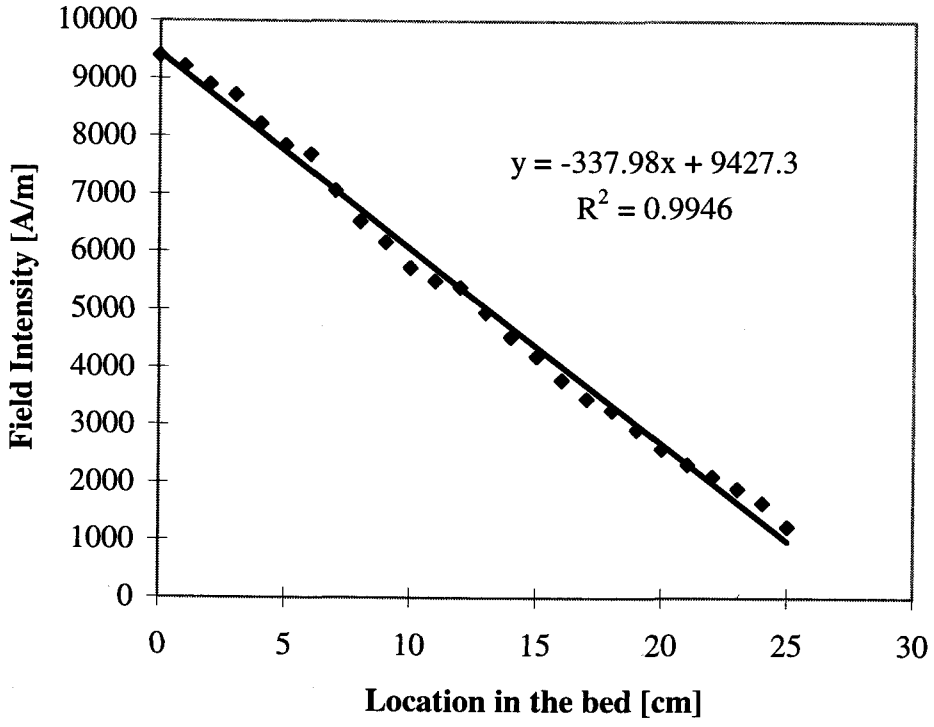

Figure E-4: The magnetic field intensity in the bed used for the laboratory experiments (voltage setting on the power supply = 3.5 volts)

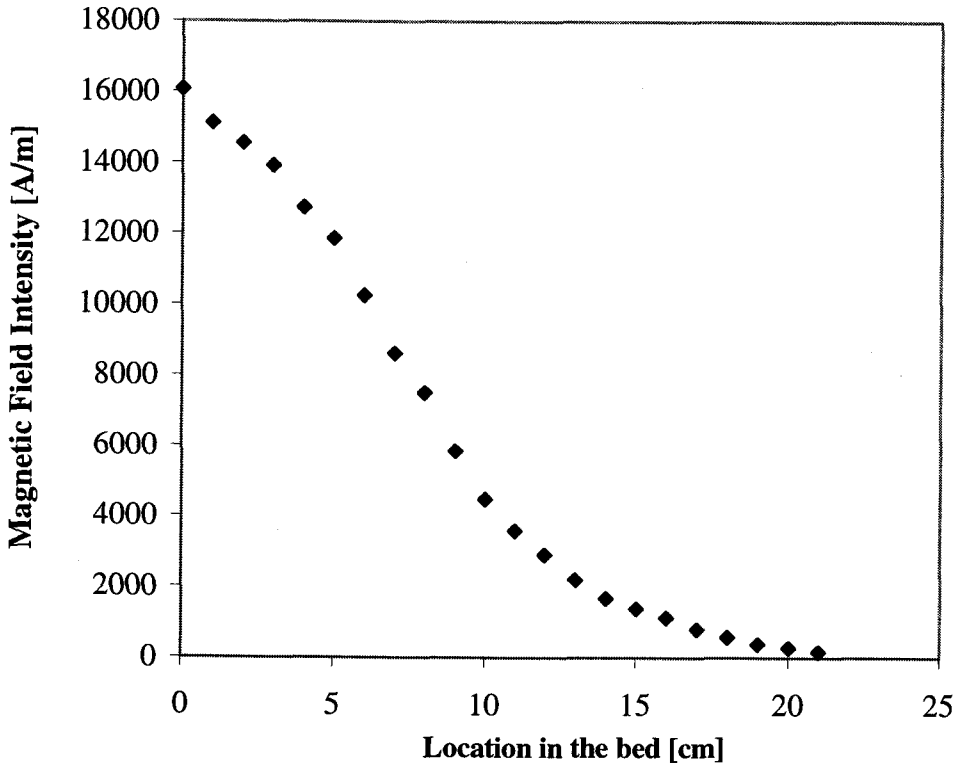

Figure E-5: The magnetic field intensity used for the experiments on board the NASA KC-135 (voltage setting on power supply =1.0 volt)

APPENDIX F
MAGNETIC SUSCEPTIBILITY MEASUREMENT

The magnetic susceptibility of the ferromagnetic powder is measured by using the microbalance in a Thermal Gravimetric Analysis (TGA). The field intensity used in this measurement is shown in Figure F-1.

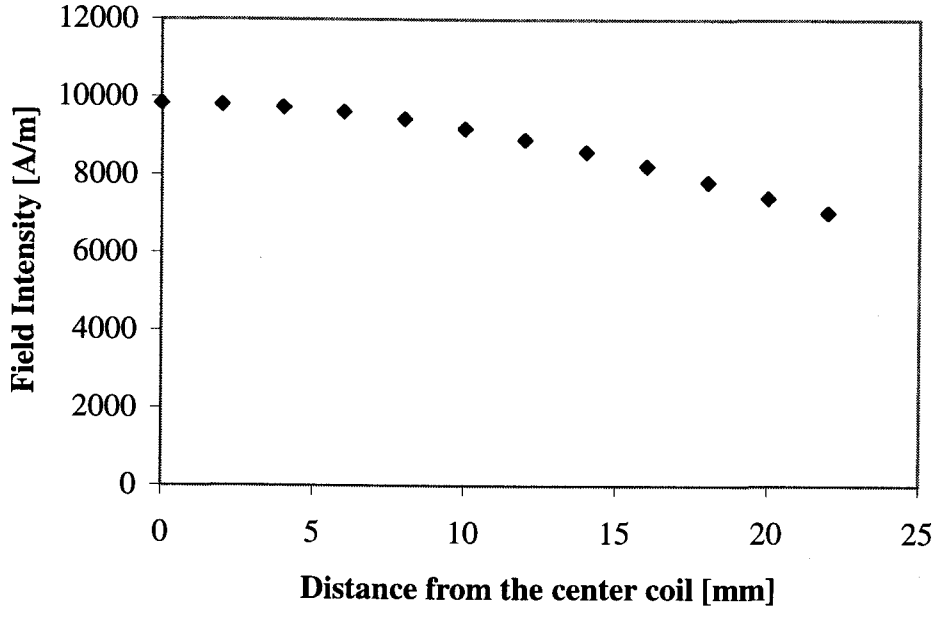

Figure F-1: The magnetic field intensity used for measuring magnetic susceptibility

The magnetic force is calculated by comparing the weight of ferromagnetic particle (d_p = 1 mm, Fe = 20%, Microsphere balloon = 9% and 1.75% alginate solution 71%) inside and outside applied the magnetic field. The calculation of magnetic susceptibility of ferromagnetic particle is shown in Table F-1.

Table F-1: The calculation of magnetic susceptibility of ferromagnetic particle

Number of particles	Axial distance from the center of the coil (mm)	Magnetic Force (N)	Susceptibility, χ
1	4	0.00000755	3.18
1	6	0.00000961	2.71
1	8	0.00001128	2.42
1	10	0.00001285	2.25
3	4	0.00002286	3.21
3	6	0.00003169	2.98
3	8	0.00003659	2.61
3	10	0.00004346	2.54

The average magnetic susceptibility of ferromagnetic particles in this experiment is 2.74 which translates to a ferromagnetic powder susceptibility of 31.98. The magnetic susceptibility of each particle can be obtained by the following equation:

$$\chi_{particle} = \text{volume fraction of ferromagnetic powder} \times \chi_{ferromagneticpowder} \quad \text{(F-1)}$$

The magnetic susceptibility of particles are provided in Table 3-1

APPENDIX G
DYNAMIC PRESSURE DROP AND THE VOIDAGE DISTRIBUTION

Table G-1: Dynamic Pressure Drop, $\Delta P_{f(d)}$, for particle A

at U_0 = 1.76 cm/s, $\frac{dH}{dz}$ = -14,663 A/m/m, h_{in} = 13.5 cm

Height of the bed (cm)	Dynamic Pressure Drop (Pa)	Voidage (Experimental data)	Voidage (Predicted)
0	94.16	0.841	0.678
0.5	93.06	0.798	0.679
1	91.66	0.768	0.679
1.5	90.06	0.753	0.680
2	88.36	0.767	0.680
2.5	86.76	0.737	0.681
3	84.96	0.722	0.681
3.5	83.06	0.706	0.682
4	81.06	0.735	0.682
4.5	79.26	0.690	0.683
5	77.16	0.674	0.683
5.5	74.96	0.673	0.684
6	72.76	0.642	0.684
6.5	70.36	0.641	0.685
7	67.96	0.640	0.685
7.5	65.56	0.669	0.686
8	63.36	0.638	0.686
8.5	60.97	0.668	0.687
9	58.77	0.667	0.687
9.5	56.57	0.666	0.688
10	54.37	0.649	0.688
10.5	52.07	0.679	0.689
11	49.97	0.693	0.689
11.5	47.97	0.677	0.690
12	45.87	0.676	0.690
12.5	43.77	0.675	0.691
13	41.67	0.674	0.691
13.5	39.57	0.689	0.692
14	37.57	0.657	0.692
14.5	35.37	0.687	0.693
15	33.37	0.670	0.693
15.5	31.27	0.701	0.694
16	29.37	0.700	0.694
16.5	27.47	0.667	0.695
17	25.37	0.682	0.695
17.5	23.37	0.665	0.696
18	21.27	0.680	0.696
18.5	19.28	0.712	0.697
19	17.48	0.695	0.697
19.5	15.58	0.710	0.698
20	13.78	0.677	0.699
20.5	11.78	0.708	0.699
21	9.98	0.756	0.700
21.5	8.48	0.772	0.700

Height of the bed (cm)	Dynamic Pressure Drop (Pa)	Voidage (Experimental data)	Voidage (Predicted)
22	7.08	0.771	0.701
22.5	5.68	0.787	0.701
23	4.38	0.769	0.702
23.5	2.98	0.769	0.702
24	1.58	0.834	0.703
24.5	0.58	0.924	0.703
25	0.12	0.990	0.704

Table G-2: Dynamic Pressure Drop, $\Delta P_{f(d)}$, for particle A

at U_0 = 1.76 cm/s, $\frac{dH}{dz}$ = -18,289 A/m/m, h_{in} = 13.5 cm

Height of the bed (cm)	Dynamic Pressure Drop (Pa)	Voidage (Experimental data)	Voidage (Predicted)
0	95.06	0.793	0.664
0.5	94.39	0.721	0.664
1	92.72	0.705	0.665
1.5	90.38	0.688	0.666
2	88.38	0.656	0.666
2.5	86.37	0.623	0.667
3	83.70	0.606	0.668
3.5	81.03	0.621	0.668
4	78.36	0.651	0.669
4.5	75.35	0.618	0.670
5	73.01	0.649	0.670
5.5	71.01	0.648	0.671
6	67.34	0.662	0.672
6.5	65.67	0.677	0.673
7	63.66	0.644	0.673
7.5	60.32	0.675	0.674
8	58.99	0.674	0.675
8.5	56.31	0.640	0.675
9	53.64	0.705	0.676
9.5	52.31	0.704	0.677
10	48.97	0.669	0.678
10.5	47.63	0.668	0.678
11	46.29	0.634	0.679
11.5	42.29	0.666	0.680
12	40.95	0.665	0.681
12.5	38.95	0.697	0.681
13	35.61	0.696	0.682
13.5	34.27	0.661	0.683
14	32.93	0.660	0.684
14.5	29.59	0.710	0.684
15	27.59	0.692	0.685
15.5	26.25	0.691	0.686
16	23.92	0.707	0.687
16.5	21.58	0.688	0.688
17	20.24	0.687	0.688
17.5	18.24	0.704	0.689
18	15.56	0.720	0.690
18.5	14.23	0.684	0.691
19	12.56	0.700	0.691
19.5	10.22	0.752	0.692
20	8.22	0.787	0.693
20.5	6.88	0.804	0.694
21	5.54	0.839	0.695
21.5	4.21	0.856	0.856
22	3.21	0.838	0.838
22.5	2.54	0.873	0.873
23	1.54	0.898	0.898
23.5	0.20	0.971	0.971

Table G-3: Dynamic Pressure Drop, $\Delta P_{f(d)}$, for particle A

at U_0 = 1.76 cm/s, $\frac{dH}{dz}$ = -20,543 A/m/m, h_{in} = 13.5 cm

Height of the bed (cm)	Dynamic Pressure Drop (Pa)	Voidage (Experimental data)	Voidage (Predicted)
0	97.28	0.852	0.652
0.5	96.09	0.777	0.652
1	94.30	0.702	0.653
1.5	91.91	0.671	0.654
2	89.28	0.639	0.655
2.5	86.41	0.622	0.656
3	83.42	0.620	0.656
3.5	80.44	0.634	0.657
4	77.57	0.678	0.658
4.5	75.06	0.661	0.659
5	72.43	0.690	0.660
5.5	70.04	0.689	0.661
6	67.65	0.672	0.661
6.5	65.14	0.686	0.662
7	62.75	0.700	0.663
7.5	60.48	0.715	0.664
8	58.33	0.697	0.665
8.5	56.06	0.696	0.666
9	53.79	0.710	0.666
9.5	51.64	0.693	0.667
10	49.37	0.675	0.668
10.5	46.98	0.673	0.669
11	44.59	0.639	0.670
11.5	41.96	0.670	0.671
12	39.57	0.652	0.672
12.5	37.06	0.700	0.673
13	34.91	0.682	0.673
13.5	32.64	0.714	0.674
14	30.61	0.729	0.675
14.5	28.70	0.694	0.676
15	26.55	0.692	0.677
15.5	24.40	0.690	0.678
16	22.25	0.671	0.679
16.5	19.98	0.687	0.680
17	17.83	0.685	0.681
17.5	15.68	0.684	0.682
18	13.53	0.700	0.683
18.5	11.49	0.680	0.684
19	9.34	0.696	0.685
19.5	7.31	0.695	0.686
20	5.28	0.711	0.687
20.5	3.37	0.764	0.688
21	1.82	0.817	0.689
21.5	0.62	0.919	0.690
22	0.10	0.993	0.691

Table G-4: Dynamic Pressure Drop, $\Delta P_{f(d)}$, for particle A

at U_0 = 2.22 cm/s, $\frac{dH}{dz}$ = -14,663 A/m/m, h_{in} = 9.5 cm

Height of the bed (cm)	Dynamic Pressure Drop (Pa)	Voidage (Experimental data)	Voidage (Predicted)
0	66.28	0.816	0.748
0.5	64.85	0.773	0.748
1	63.02	0.702	0.749
1.5	60.99	0.687	0.749
2	58.77	0.686	0.750
2.5	56.75	0.699	0.750
3	54.66	0.713	0.751
3.5	52.76	0.712	0.751
4	50.87	0.740	0.752
4.5	49.04	0.725	0.753
5	47.28	0.739	0.753
5.5	45.38	0.723	0.754
6	43.81	0.766	0.754
6.5	42.05	0.766	0.755
7	40.48	0.721	0.755
7.5	38.59	0.735	0.756
8	37.02	0.764	0.756
8.5	35.26	0.748	0.757
9	33.69	0.733	0.757
9.5	32.06	0.791	0.758
10	30.62	0.776	0.758
10.5	28.99	0.730	0.759
11	27.35	0.745	0.760
11.5	25.66	0.759	0.760
12	23.89	0.698	0.761
12.5	22.19	0.742	0.761
13	20.50	0.772	0.762
13.5	18.99	0.741	0.762
14	17.43	0.771	0.763
14.5	15.86	0.755	0.764
15	14.42	0.769	0.764
15.5	12.99	0.799	0.765
16	11.68	0.783	0.765
16.5	10.31	0.783	0.766
17	9.00	0.798	0.766
17.5	7.63	0.781	0.767
18	6.39	0.796	0.768
18.5	5.21	0.843	0.768
19	4.17	0.827	0.769
19.5	3.19	0.842	0.769
20	2.21	0.857	0.770
20.5	1.29	0.841	0.770
21	0.57	0.904	0.771
21.5	0.18	0.984	0.772
22	0.08	0.990	0.772

Table G-5: Dynamic Pressure Drop, $\Delta P_{f(d)}$, for particle A

at U_0 = 2.22 cm/s, $\frac{dH}{dz}$ = -18,289 A/m/m, h_{in} = 9.5 cm

Height of the bed (cm)	Dynamic Pressure Drop (Pa)	Voidage (Experimental data)	Voidage (Predicted)
0	68.57	0.896	0.732
0.5	67.79	0.836	0.733
1	66.61	0.745	0.733
1.5	64.78	0.680	0.734
2	62.50	0.725	0.735
2.5	60.54	0.724	0.735
3	58.58	0.750	0.736
3.5	56.81	0.703	0.737
4	54.72	0.721	0.738
4.5	52.76	0.701	0.739
5	50.67	0.700	0.739
5.5	48.58	0.690	0.740
6	46.43	0.708	0.741
6.5	44.40	0.726	0.742
7	42.51	0.744	0.742
7.5	40.74	0.714	0.743
8	38.79	0.751	0.744
8.5	37.09	0.751	0.745
9	35.39	0.788	0.746
9.5	33.95	0.768	0.746
10	32.38	0.758	0.747
10.5	30.75	0.776	0.748
11	29.25	0.756	0.749
11.5	27.62	0.755	0.750
12	25.98	0.715	0.750
12.5	24.09	0.734	0.751
13	22.33	0.743	0.752
13.5	20.63	0.771	0.753
14	19.12	0.731	0.754
14.5	17.36	0.740	0.754
15	15.66	0.719	0.755
15.5	13.83	0.728	0.756
16	12.07	0.696	0.757
16.5	10.11	0.726	0.758
17	8.35	0.745	0.759
17.5	6.71	0.785	0.760
18	5.34	0.795	0.760
18.5	4.04	0.794	0.761
19	2.73	0.793	0.762
19.5	1.42	0.855	0.763
20	0.51	0.931	0.764
20.5	0.08	0.994	0.765

Table G-6: Dynamic Pressure Drop, $\Delta P_{f(d)}$, for particle A

at U_0 = 2.22 cm/s, $\frac{dH}{dz}$ = -20,543 A/m/m, h_{in} = 9.5 cm

Height of the bed (cm)	Dynamic Pressure Drop (Pa)	Voidage (Experimental data)	Voidage (Predicted)
0	70.10	0.903	0.719
0.5	69.31	0.830	0.720
1	67.94	0.772	0.720
1.5	66.11	0.705	0.721
2	63.76	0.679	0.722
2.5	61.22	0.678	0.723
3	58.67	0.693	0.724
3.5	56.25	0.700	0.725
4	53.90	0.723	0.726
4.5	51.74	0.705	0.727
5	49.46	0.729	0.727
5.5	47.37	0.719	0.728
6	45.21	0.727	0.729
6.5	43.12	0.708	0.730
7	40.90	0.724	0.731
7.5	38.81	0.723	0.732
8	36.72	0.739	0.733
8.5	34.76	0.729	0.734
9	32.74	0.780	0.735
9.5	31.10	0.779	0.736
10	29.47	0.805	0.737
10.5	28.03	0.750	0.738
11	26.21	0.767	0.739
11.5	24.51	0.720	0.740
12	22.48	0.746	0.741
12.5	20.65	0.727	0.742
13	18.69	0.743	0.743
13.5	16.86	0.761	0.744
14	15.17	0.778	0.745
14.5	13.60	0.730	0.746
15	11.70	0.682	0.747
15.5	9.48	0.708	0.748
16	7.46	0.754	0.749
16.5	5.76	0.762	0.750
17	4.13	0.742	0.751
17.5	2.36	0.798	0.752
18	0.99	0.903	0.753
18.5	0.34	0.957	0.754
19	0.05	0.996	0.755

Table G-7: Dynamic Pressure Drop, $\Delta P_{f(d)}$, for particle A

at U_0 = 1.76 cm/s, $\frac{dH}{dz}$ = -14,663 A/m/m, h_{in} = 6.5 cm

Height of the bed (cm)	Dynamic Pressure Drop (Pa)	Voidage (Experimental data)	Voidage (Predicted)
0	46.46	0.826	0.678
0.5	45.25	0.773	0.679
1	43.68	0.728	0.679
1.5	41.80	0.736	0.680
2	39.99	0.718	0.680
2.5	38.05	0.664	0.681
3	35.76	0.645	0.681
3.5	33.34	0.680	0.682
4	31.16	0.679	0.682
4.5	28.98	0.696	0.683
5	26.93	0.695	0.683
5.5	24.87	0.730	0.684
6	23.05	0.675	0.684
6.5	20.88	0.647	0.685
7	18.52	0.710	0.685
7.5	16.58	0.691	0.686
8	14.53	0.672	0.686
8.5	12.35	0.671	0.687
9	10.17	0.725	0.687
9.5	8.36	0.743	0.688
10	6.66	0.742	0.688
10.5	4.97	0.750	0.689
11	3.34	0.824	0.689
11.5	2.19	0.833	0.690
12	1.10	0.897	0.690
12.5	0.44	0.940	0.691
13	0.05	0.996	0.691

Table G-8: Dynamic Pressure Drop, $\Delta P_{f(d)}$, for particle A

at U_0 = 1.76 cm/s, $\frac{dH}{dz}$ = -18,289 A/m/m, h_{in} = 6.5 cm

Height of the bed (cm)	Dynamic Pressure Drop (Pa)	Voidage (Experimental data)	Voidage (Predicted)
0	49.00	0.792	0.664
0.5	47.43	0.731	0.664
1	45.41	0.721	0.665
1.5	43.32	0.685	0.666
2	40.97	0.631	0.666
2.5	38.22	0.612	0.667
3	35.35	0.646	0.668
3.5	32.74	0.680	0.668
4	30.39	0.678	0.669
4.5	28.03	0.641	0.670
5	25.42	0.658	0.670
5.5	22.94	0.656	0.671
6	20.46	0.637	0.672
6.5	17.84	0.672	0.673
7	15.49	0.707	0.673
7.5	13.40	0.724	0.674
8	11.44	0.723	0.675
8.5	9.48	0.741	0.675
9	7.66	0.739	0.676
9.5	5.83	0.757	0.677
10	4.13	0.737	0.678
10.5	2.30	0.830	0.678
11	1.12	0.886	0.679
11.5	0.34	0.958	0.680
12	0.05	0.996	0.681

Table G-9: Dynamic Pressure Drop, $\Delta P_{f(d)}$, for particle A

at U_0 = 1.53 cm/s, $\frac{dH}{dz}$ = -20,543 A/m/m, h_{in} = 6.5 cm

Height of the bed (cm)	Dynamic Pressure Drop (Pa)	Voidage (Experimental data)	Voidage (Predicted)
0	51.54	0.739	0.616
0.5	50.59	0.688	0.617
1	47.48	0.652	0.617
1.5	45.21	0.631	0.618
2	43.06	0.599	0.619
2.5	39.12	0.652	0.620
3	36.37	0.651	0.620
3.5	33.50	0.608	0.621
4	30.87	0.596	0.622
4.5	28.13	0.584	0.623
5	24.30	0.598	0.624
5.5	21.44	0.627	0.624
6	18.45	0.620	0.625
6.5	14.98	0.660	0.626
7	12.83	0.637	0.627
7.5	9.73	0.699	0.627
8	7.22	0.734	0.628
8.5	4.59	0.797	0.629
9	2.92	0.871	0.630
9.5	1.24	0.944	0.631
10	0.05	0.998	0.632

Table G-10: Dynamic Pressure Drop, $\Delta P_{f(d)}$, for particle A

at U_0 = 1.76 cm/s, $\frac{dH}{dz}$ = -20,543 A/m/m, h_{in} = 6.5 cm

Height of the bed (cm)	Dynamic Pressure Drop (Pa)	Voidage (Experimental data)	Voidage (Predicted)
0	50.21	0.793	0.652
0.5	48.54	0.753	0.652
1	46.55	0.692	0.653
1.5	44.08	0.641	0.654
2	41.21	0.644	0.655
2.5	38.39	0.627	0.656
3	35.44	0.661	0.656
3.5	32.77	0.634	0.657
4	29.90	0.653	0.658
4.5	27.19	0.677	0.659
5	24.69	0.680	0.660
5.5	22.22	0.689	0.661
6	19.83	0.682	0.661
6.5	17.40	0.702	0.662
7	15.13	0.690	0.663
7.5	12.78	0.704	0.664
8	10.55	0.692	0.665
8.5	8.24	0.722	0.666
9	6.17	0.737	0.666
9.5	4.21	0.730	0.667
10	2.22	0.816	0.668
10.5	0.87	0.888	0.669
11	0.05	0.997	0.670

Table G-11: Dynamic Pressure Drop, $\Delta P_{f(d)}$, for particle A

at U_0 = 1.99 cm/s, $\frac{dH}{dz}$ = -20,543 A/m/m, h_{in} = 6.5 cm

Height of the bed (cm)	Dynamic Pressure Drop (Pa)	Voidage (Experimental data)	Voidage (Predicted)
0	51.81	0.798	0.686
0.5	50.18	0.752	0.687
1	48.18	0.674	0.688
1.5	45.57	0.621	0.688
2	42.55	0.625	0.689
2.5	39.57	0.618	0.690
3	36.55	0.652	0.691
3.5	33.81	0.625	0.692
4	30.87	0.644	0.693
4.5	28.09	0.679	0.693
5	25.60	0.693	0.694
5.5	23.24	0.740	0.695
6	21.24	0.728	0.696
6.5	19.15	0.737	0.697
7	17.15	0.730	0.698
7.5	15.11	0.740	0.699
8	13.15	0.744	0.700
8.5	11.23	0.743	0.700
9	9.32	0.758	0.701
9.5	7.52	0.801	0.702
10	6.05	0.800	0.703
10.5	4.58	0.821	0.704
11	3.27	0.826	0.705
11.5	2.01	0.859	0.706
12	0.99	0.915	0.707
12.5	0.38	0.952	0.708
13	0.03	0.998	0.709

Table G-12: Dynamic Pressure Drop, $\Delta P_{f(d)}$, for particle A

at U_0 = 1.53 cm/s, $\frac{dH}{dz}$ = -33,798 A/m/m, h_{in} = 6.5 cm

Height of the bed (cm)	Dynamic Pressure Drop (Pa)	Voidage (Experimental data)	Voidage (Predicted)
0	66.88	0.814	0.562
0.5	64.75	0.697	0.563
1	61.32	0.586	0.564
1.5	56.68	0.541	0.566
2	51.57	0.558	0.567
2.5	46.70	0.594	0.569
3	42.26	0.590	0.570
3.5	37.83	0.565	0.571
4	33.17	0.561	0.573
4.5	28.50	0.556	0.574
5	23.84	0.575	0.576
5.5	19.40	0.570	0.577
6	14.97	0.635	0.579
6.5	11.24	0.654	0.580
7	7.74	0.651	0.582
7.5	4.24	0.718	0.583
8	1.44	0.856	0.585
8.5	0.03	0.999	0.587

Table G-13: Dynamic Pressure Drop, $\Delta P_{f(d)}$, for particle A

at U_0 = 1.53 cm/s, $\frac{dH}{dz}$ = -33,798 A/m/m, h_{in} = 6.5 cm

Height of the bed (cm)	Dynamic Pressure Drop (Pa)	Voidage (Experimental data)	Voidage (Predicted)
0	66.98	0.837	0.595
0.5	65.11	0.720	0.596
1	61.94	0.615	0.597
1.5	57.62	0.559	0.599
2	52.73	0.555	0.600
2.5	47.83	0.596	0.602
3	43.42	0.590	0.603
3.5	38.99	0.617	0.605
4	34.88	0.605	0.606
4.5	30.68	0.607	0.608
5	26.55	0.610	0.609
5.5	22.49	0.638	0.611
6	18.76	0.628	0.613
6.5	14.96	0.677	0.614
7	11.69	0.627	0.616
7.5	7.96	0.680	0.618
8	4.79	0.715	0.619
8.5	1.99	0.856	0.621
9	0.59	0.941	0.623
9.5	0.02	0.999	0.624

Table G-14: Dynamic Pressure Drop, $\Delta P_{f(d)}$, for particle A

at U_0 = 1.99 cm/s, $\frac{dH}{dz}$ = -33,798 A/m/m, h_{in} = 6.5 cm

Height of the bed (cm)	Dynamic Pressure Drop (Pa)	Voidage (Experimental data)	Voidage (Predicted)
0	69.90	0.846	0.626
0.5	68.40	0.721	0.628
1	66.77	0.666	0.629
1.5	64.61	0.646	0.631
2	58.93	0.656	0.632
2.5	55.53	0.649	0.634
3	52.79	0.662	0.635
3.5	47.56	0.618	0.637
4	44.04	0.676	0.638
4.5	41.82	0.648	0.640
5	35.28	0.653	0.642
5.5	33.72	0.646	0.643
6	30.71	0.680	0.645
6.5	24.44	0.718	0.647
7	22.74	0.722	0.648
7.5	20.91	0.715	0.650
8	15.89	0.760	0.652
8.5	14.38	0.729	0.654
9	12.42	0.728	0.655
9.5	8.83	0.760	0.657
10	6.48	0.771	0.659
10.5	4.59	0.836	0.661
11	1.97	0.929	0.663
11.5	0.01	1.000	0.665

Table G-15: Dynamic Pressure Drop, $\Delta P_{f(d)}$, for particle B

at U_0 = 2.22 cm/s, $\frac{dH}{dz}$ = -14,663 A/m/m, h_{in} = 13.5 cm

Height of the bed (cm)	Dynamic Pressure Drop (Pa)	Voidage (Experimental data)	Voidage (Predicted)
0	236.10	0.773	0.565
0.5	232.45	0.694	0.565
1	227.56	0.647	0.565
1.5	221.90	0.599	0.565
2	215.50	0.591	0.565
2.5	208.97	0.559	0.566
3	201.93	0.542	0.566
3.5	194.65	0.534	0.566
4	187.23	0.581	0.566
4.5	180.58	0.548	0.567
5	173.42	0.580	0.567
5.5	166.76	0.563	0.567
6	159.85	0.602	0.567
6.5	153.57	0.578	0.567
7	146.91	0.561	0.568
7.5	140.01	0.569	0.568
8	133.22	0.576	0.568
8.5	126.56	0.560	0.568
9	119.66	0.551	0.569
9.5	112.62	0.558	0.569
10	105.71	0.574	0.569
10.5	99.06	0.549	0.569
11	92.02	0.581	0.569
11.5	85.49	0.596	0.570
12	79.21	0.580	0.570
12.5	72.68	0.571	0.570
13	66.02	0.570	0.570
13.5	59.36	0.586	0.570
14	52.96	0.585	0.571
14.5	46.55	0.593	0.571
15	40.27	0.625	0.571
15.5	34.49	0.600	0.571
16	28.34	0.608	0.572
16.5	22.31	0.591	0.572
17	16.03	0.574	0.572
17.5	9.50	0.639	0.572
18	3.97	0.795	0.572
18.5	0.83	0.872	0.573
18.7	0.05	0.997	0.572

Table G-16: Dynamic Pressure Drop, $\Delta P_{f(d)}$, for particle B

at U_0 = 2.22 cm/s, $\frac{dH}{dz}$ = -18,289A/m/m, h_{in} = 13.5 cm

Height of the bed (cm)	Dynamic Pressure Drop (Pa)	Voidage (Experimental data)	Voidage (Predicted)
0	237.18	0.785	0.558
0.5	233.66	0.694	0.558
1	228.76	0.623	0.559
1.5	222.73	0.591	0.559
2	216.20	0.583	0.559
2.5	209.54	0.574	0.560
3	202.76	0.526	0.560
3.5	195.22	0.526	0.560
4	187.69	0.501	0.561
4.5	179.77	0.540	0.561
5	172.49	0.548	0.561
5.5	165.33	0.539	0.561
6	158.04	0.523	0.562
6.5	150.51	0.514	0.562
7	142.84	0.545	0.562
7.5	135.68	0.537	0.563
8	128.40	0.544	0.563
8.5	121.24	0.544	0.563
9	114.08	0.543	0.564
9.5	106.92	0.558	0.564
10	100.01	0.566	0.564
10.5	93.23	0.565	0.565
11	86.44	0.573	0.565
11.5	79.79	0.604	0.565
12	73.63	0.580	0.566
12.5	67.10	0.587	0.566
13	60.69	0.562	0.566
13.5	53.91	0.578	0.567
14	47.38	0.569	0.567
14.5	40.72	0.569	0.567
15	34.07	0.560	0.568
15.5	27.28	0.567	0.568
16	20.63	0.550	0.568
16.5	13.72	0.566	0.569
17	7.06	0.697	0.569
17.5	2.41	0.849	0.569
17.8	0.10	0.995	0.570

Table G-17: Dynamic Pressure Drop, $\Delta P_{f(d)}$, for particle B

at U_0 = 2.22 cm/s, $\frac{dH}{dz}$ = -20,543 A/m/m, h_{in} = 13.5 cm

Height of the bed (cm)	Dynamic Pressure Drop (Pa)	Voidage (Experimental data)	Voidage (Predicted)
0	237.35	0.771	0.552
0.5	233.54	0.688	0.553
1	228.37	0.597	0.553
1.5	221.70	0.572	0.553
2	214.62	0.555	0.554
2.5	207.27	0.537	0.554
3	199.65	0.520	0.555
3.5	191.76	0.502	0.555
4	183.60	0.526	0.555
4.5	175.84	0.517	0.556
5	167.95	0.550	0.556
5.5	160.60	0.557	0.557
6	153.39	0.548	0.557
6.5	146.04	0.530	0.557
7	138.42	0.555	0.558
7.5	131.21	0.529	0.558
8	123.59	0.536	0.558
8.5	116.10	0.502	0.559
9	108.07	0.526	0.559
9.5	100.45	0.534	0.560
10	92.97	0.499	0.560
10.5	84.94	0.498	0.560
11	76.91	0.523	0.561
11.5	69.29	0.513	0.561
12	61.53	0.495	0.562
12.5	53.51	0.503	0.562
13	45.61	0.536	0.562
13.5	38.27	0.518	0.563
14	30.64	0.535	0.563
14.5	23.30	0.568	0.564
15	16.49	0.533	0.564
15.5	9.14	0.636	0.565
16	3.43	0.788	0.565
16.5	0.11	0.997	0.565

Table G-18: Dynamic Pressure Drop, $\Delta P_{f(d)}$, for particle B

at U_0 = 2.22 cm/s, $\frac{dH}{dz}$ = -14,663 A/m/m, h_{in} = 17.0 cm

Height of the bed (cm)	Dynamic Pressure Drop (Pa)	Voidage (Experimental data)	Voidage (Predicted)
0	291.11	0.737	0.565
0.5	286.93	0.694	0.565
1	282.07	0.662	0.565
1.5	276.71	0.640	0.565
2	271.02	0.640	0.565
2.5	265.32	0.608	0.566
3	259.13	0.596	0.566
3.5	252.76	0.575	0.566
4	246.06	0.585	0.566
4.5	239.53	0.584	0.567
5	233.00	0.552	0.567
5.5	225.96	0.562	0.567
6	219.10	0.550	0.567
6.5	212.06	0.582	0.567
7	205.53	0.571	0.568
7.5	198.83	0.570	0.568
8	192.13	0.559	0.568
8.5	185.27	0.547	0.568
9	178.23	0.547	0.569
9.5	171.20	0.557	0.569
10	164.33	0.578	0.569
10.5	157.80	0.588	0.569
11	151.44	0.566	0.569
11.5	144.74	0.565	0.570
12	138.04	0.554	0.570
12.5	131.17	0.597	0.570
13	124.97	0.574	0.570
13.5	118.44	0.552	0.570
14	111.58	0.562	0.571
14.5	104.88	0.606	0.571
15	98.85	0.605	0.571
15.5	92.82	0.582	0.571
16	86.45	0.604	0.572
16.5	80.42	0.603	0.572
17	74.39	0.581	0.572
17.5	68.03	0.569	0.572
18	61.50	0.602	0.572
18.5	55.47	0.601	0.573
19	49.44	0.567	0.573
19.5	42.91	0.600	0.573
20	36.88	0.611	0.573
20.5	31.02	0.632	0.574
21	25.49	0.587	0.574
21.5	19.29	0.620	0.574
22	13.60	0.653	0.574
22.5	8.41	0.709	0.574
23	4.05	0.820	0.575
23.5	1.37	0.917	0.575
24	0.13	0.995	0.575

Table G-19: Dynamic Pressure Drop, $\Delta P_{f(d)}$, for particle B

at U_0 = 2.22 cm/s, $\frac{dH}{dz}$ = -18,289 A/m/m, h_{in} = 17.0 cm

Height of the bed (cm)	Dynamic Pressure Drop (Pa)	Voidage (Experimental data)	Voidage (Predicted)
0	292.56	0.801	0.558
0.5	289.25	0.710	0.558
1	284.45	0.599	0.559
1.5	277.84	0.538	0.559
2	270.23	0.517	0.559
2.5	262.29	0.547	0.560
3	254.85	0.536	0.560
3.5	247.25	0.555	0.560
4	239.97	0.554	0.561
4.5	232.70	0.533	0.561
5	225.09	0.532	0.561
5.5	217.48	0.531	0.561
6	209.88	0.550	0.562
6.5	202.60	0.550	0.562
7	195.32	0.569	0.562
7.5	188.38	0.548	0.563
8	181.10	0.588	0.563
8.5	174.49	0.567	0.563
9	167.54	0.566	0.564
9.5	160.60	0.544	0.564
10	153.32	0.585	0.564
10.5	146.71	0.594	0.565
11	140.26	0.562	0.565
11.5	133.31	0.572	0.565
12	126.53	0.571	0.566
12.5	119.75	0.580	0.566
13	113.14	0.537	0.566
13.5	105.86	0.579	0.567
14	99.25	0.578	0.567
14.5	92.63	0.577	0.567
15	86.02	0.597	0.568
15.5	79.74	0.586	0.568
16	73.29	0.617	0.568
16.5	67.33	0.573	0.569
17	60.72	0.615	0.569
17.5	54.77	0.604	0.569
18	48.65	0.592	0.570
18.5	42.37	0.613	0.570
19	36.41	0.601	0.570
19.5	30.29	0.600	0.571
20	24.18	0.578	0.571
20.5	17.73	0.620	0.571
21	11.94	0.674	0.572
21.5	6.98	0.760	0.572
22	3.34	0.847	0.572
22.5	1.03	0.941	0.573
23	0.13	0.996	0.573

Table G-20: Dynamic Pressure Drop, $\Delta P_{f(d)}$, for particle B

at U_0 = 2.22 cm/s, $\frac{dH}{dz}$ = -20,543 A/m/m, h_{in} = 17.0 cm

Height of the bed (cm)	Dynamic Pressure Drop (Pa)	Voidage (Experimental data)	Voidage (Predicted)
0	292.90	0.777	0.552
0.5	289.07	0.675	0.553
1	283.49	0.603	0.553
1.5	276.70	0.551	0.553
2	269.04	0.529	0.554
2.5	261.03	0.518	0.554
3	252.84	0.527	0.555
3.5	244.83	0.526	0.555
4	236.81	0.545	0.555
4.5	229.15	0.555	0.556
5	221.66	0.564	0.556
5.5	214.35	0.563	0.557
6	207.03	0.551	0.557
6.5	199.54	0.561	0.557
7	192.22	0.528	0.558
7.5	184.39	0.548	0.558
8	176.90	0.547	0.558
8.5	169.41	0.567	0.559
9	162.27	0.545	0.559
9.5	154.78	0.554	0.560
10	147.46	0.553	0.560
10.5	140.14	0.562	0.560
11	133.00	0.593	0.561
11.5	126.38	0.582	0.561
12	119.59	0.581	0.562
12.5	112.80	0.612	0.562
13	106.53	0.578	0.562
13.5	99.74	0.588	0.563
14	93.12	0.576	0.563
14.5	86.32	0.597	0.564
15	79.88	0.574	0.564
15.5	73.09	0.584	0.565
16	66.47	0.594	0.565
16.5	60.02	0.571	0.565
17	53.23	0.559	0.566
17.5	46.26	0.580	0.566
18	39.64	0.601	0.567
18.5	33.37	0.588	0.567
19	26.93	0.632	0.567
19.5	21.18	0.609	0.568
20	15.08	0.630	0.568
20.5	9.34	0.663	0.569
21	4.11	0.820	0.569
21.5	1.32	0.919	0.570
21.7	0.07	0.998	0.570